ELSEVIER

Physics Reports 374 (2003) 385–481

PHYSICS REPORTS

www.elsevier.com/locate/physrep

Optical pulse shaping approaches to coherent control

Debabrata Goswami*

Tata Institute of Fundamental Research, Homi Bhabha Road, Mumbai 400 005, India

Accepted 1 September 2002
editor: J. Eichler

Abstract

The last part of the twentieth century has experienced a huge resurge of activity in the field of coherent light–matter interaction, more so in attempting to exert control over such interactions. Birth of coherent control was originally spurred by the theoretical understanding of the quantum interferences that lead to energy randomization and experimental developments in ultrafast laser spectroscopy. The theoretical predictions on control of reaction channels or energy randomization processes are still more dramatic than the experimental demonstrations, though this gap between the two is consistently reducing over the recent years with realistic theoretical models and technological developments. Experimental demonstrations of arbitrary optical pulse shaping have made some of the previously impracticable theoretical predictions possible to implement. Starting with the simple laser modulation schemes to provide proof-of-the-principle demonstrations, feedback loop pulse shaping systems have been developed that can actively manipulate some atomic and molecular processes. This tremendous experimental boost of optical pulse shaping developments has prospects and implications into many more new directions, such as quantum computing and terabit/sec data communications. This review captures certain aspects and impacts of optical pulse shaping into the fast developing areas of coherent control and other related fields. Currently available reviews focus on one or the other detailed aspects of coherent control, and the reader will be referred to such details as and when necessary for issues that are dealt in brief here. We will focus on the current issues including control of intramolecular dynamics and make connections to the future concepts, such as, quantum computation, biomedical applications, etc.

PACS: 42.50.−p; 32.80.−t; 33.80.−b

Keywords: Control of atomic and molecular processes; Multiphoton processes; Population inversion; Selective bond breaking; Molecular relaxation; Optical pulse shaping

* Corresponding author. Tel.: +91-22-215-2971; fax: +91-22-215-2110/2118.
E-mail address: debu@tifr.res.in (D. Goswami).

0370-1573/03/$ - see front matter
PII: S0370-1573(02)00480-5

Contents

1. Introduction

The desire to manipulate and control quantum-mechanical phenomena is quite old, ever since the days of early quantum mechanics in the 1930s. In the 1960s, this desire translated to an enormous effort in dumping energy into specific chemical bonds with the development of the high-power pulsed lasers. The basic approach was simply to deposit enough energy on the local mode frequency of the targeted bond with an intense laser, tuned to that frequency, until the bond broke [1]. However, in essentially every large molecule, energy can be deposited in a specific bond only for a short period. The energy then randomizes due to the typically strong coupling amongst the molecular degrees of freedom [2]. This behaviour, known as intramolecular vibrational redistribution (IVR), is simply explained in quantum mechanical terms: the states that carry the oscillator strength are not eigenstates. These developments doomed the attempts to do "laser selective chemistry", and the decades old dream of using photons as "reagents" in chemical reaction lost much of its allure by the end of the 1970s.

Nevertheless, understanding of IVR has been an important step towards the knowledge of more complex chemical reactions and ultimately towards controlling reactivity. The fact that all quantum mechanical processes are wave phenomena and are subject to constructive and destructive interferences has lead to the recognition that actively manipulating these interferences is the essential step towards the success of this field. This has spurred a resurgence of activity in both theoretical and experimental fronts. Development of ultrafast lasers with pulses as short as a trillionth of second (i.e., 10^{-12} s or picosecond (ps)) or even thousand times shorter (i.e., 10^{-15} s or femtosecond (fs)) has also been key to the active manipulation of IVR. An ultrafast laser pulse can be represented as a coherent superposition of many monochromatic light waves within a range of frequencies that is inversely proportional to the duration of the pulse. The short temporal duration of the ultrafast pulses results in a very broad spectrum quite unlike the notion of monochromatic wavelength property of continuous wave (CW) lasers. Thus, a 10 fs pulse at 800 nm that is available commercially has a spectrum as broad as 94 nm. In fact, the leaps and bounds of the present day technological developments even allows access to the subfemtosecond pulses (currently demonstrated pulsewidths are as short as 0.65 fs) [3], which are bursts of light so short that more than a million billion ($> 10^{15}$) of them would fit within a second.

Historically, reliable generation of pulses with widths below 100 fs occurred for the first time in 1981 with the invention of the colliding pulse modelocked (CPM) ring dye laser [4]. These sub-100 fs pulses from the CPM laser were further compressed with non-linear techniques to a series of even shorter pulses by the mid-1980s, culminating in pulses as short as 6 fs in the visible, which corresponds to only three optical cycles. Such pulse durations are approaching the fundamental single optical cycle limit. In the 1990s, further rapid progress occurred following the demonstration

of femtosecond pulse generation from solid-state laser media. Solid-state femtosecond lasers bring in substantially improved output power, stability, and new physical mechanisms for pulse generation that is advantageous for production of extremely short pulses in comparison to their liquid dye laser counterparts. Such advances in laser technology now allow the generation of pulses below 6 fs directly from the laser. The use of solid-state gain media has also led to simple, turnkey femtosecond lasers that are practical and low cost, suitable for real-world applications. Current status on the details of the femtosecond laser technology can be found in several recent journal special issues [5], books [6], and in some recent review articles [7]. However, such pulses are all identical in their amplitude profile being Gaussian (or hyperbolic sechant) and equally spaced temporally without any distinct phase relationship. Possibilities of manipulating such an ultrafast coherent broadband source have opened up the exciting field of "ultrafast pulse shaping".

1.1. What is pulse shaping

Pulse shaping essentially involves control over the amplitude, phase, frequency and/or inter-pulse separation. Complex pulse shaping aims to control one or more of the above-mentioned parameters in a programmable manner, such that the user has complete control. In other words, complex pulse shaping allows generation of complicated ultrafast optical waveforms according to user specification. Application of pulse shaping technology has essentially revolutionized nuclear magnetic resonance spectroscopy (NMR). In fact, the many successful applications of complex NMR pulse sequences suggest future directions for optical spectroscopy, which some believe might even revolutionize chemistry. A practical issue, however, is that implementing useful pulse shaping or multiple pulse sequences with lasers is much more difficult than in the NMR case. Phrased in the language of optical spectroscopists, all proton NMR transitions have the same dipole moment, all samples are optically thin and exhibit no propagation effects, NMR transmitters are perfectly stable monochromatic radiation sources, and the entire spectrum has a small bandwidth. None of these assumptions is generally true for laser spectroscopy. The ability to selectively excite a single transition or part of a transition frequently becomes important, as does the ability to correct for laser imperfections and spectral complexity. Largely for this reason, programmable pulse shaping with temporal resolution of 50–100 fs and high powers has played a central role in the recent resurgence of interest in laser selective chemistry and quantum control. Even the simplest pulse shaping (matching bandwidth to a specific transition or generating rectangular pulses for multiphoton excitation) is valuable and broadly applicable.

The first experiments, which used non-overlapping nanosecond (10^{-9} s = 1 ns) pulses with a completely controlled phase, came in 1981. Later in the 1980s, the phase shifting technology rapidly evolved into the femtosecond time domain. At about the same time, optical pulse shaping capabilities evolved from nanosecond resolution with pieces chopped out of a continuous laser to less than 100 fs time resolution with amplified pulses and programmability. Today's technological breakthroughs also permit arbitrarily amplitude modulated laser pulses with 20–30 fs resolution and 10^7 peak powers limited by only the amplifying lasers—either in the time domain or in the frequency domain, and a tremendous range of applications can be readily envisioned. Such schemes, coupled with the recent advances in femtosecond pulse characterization techniques [8], have demonstrated a strong impact as an experimental tool providing unprecedented control over ultrafast laser waveforms for ultrafast spectroscopy, non-linear fibre optics, and high-field physics. Continuous efforts are in

progress [9] to extend the technology to wider wavelength ranges (all the way from the X-rays to the far-IR and terahertz regions) and towards shorter and shorter pulse widths. Pulse shaping technology with which, one can manipulate the individual constituents of the pulse to have a desired shape both in the time and frequency domain has lead to a spurt of activity in "coherent control".

1.2. What is coherent control

Coherent control is the ability to control the dynamics at various stages of a process as it evolves under the effect of a coherent source. Many of the frequencies constituting the ultrafast pulse can simultaneously excite many coherent transitions to the excited states, and a capability to manipulate them with the shaped pulses lead to the interesting results. In fact, the recent advances in pulse shaping technology have been linked with the growth of the coherent control studies.

The introduction of control theory concepts has put the subject of active manipulation of quantum phenomena on a firm theoretical footing. It has become clear that not only the dynamics of the probability distribution of wavefunctions are important but also the phase difference of the initial and final wavefunctions, which is the concept of quantum "coherence", is critical. The importance of the coherent nature of laser radiation in manipulating electronic and nuclear motion was recognized and "coherent control" was born. The term "coherent control" refers to the idea of manipulating molecular states coherently and thus avoids the issue of uncertainty principle for situations involving ultrafast timescales. The ability to monitor chemical reactions in real ultrafast timescale, which honoured Zewail with the 1999 Nobel Prize, and the technological and theoretical developments in optical pulse shaping schemes have been some of the key contributors towards this rapid progress. Thus, while reviews of this field till even the 1980s focussed on the validity of idea and called it more of a dream, the 1990s and later have seen the reviews [10–18] to focus more on the timeline of realistically achieving the dream.

The renewed vigour was triggered in the late 1970s and early 1980s when coherent laser spectroscopy started flourishing, mainly with the clever use of pulse sequences which were extremely insensitive to their shape or phase shifts. Coherent spectroscopy—the use of radiation fields with well-defined phase properties to extract information about atoms and molecules—began around 1950 with the demonstration of "spin echo" in NMR: A simple two-pulse sequence which separated inhomogeneous from homogeneous line broadening. In the ensuing decades literally hundreds of different NMR pulse sequences (often with shaped radiofrequency pulses) have been developed, and are now in routine use by organic chemists to unravel molecular structure. In 1957, Feynman, Vernon and Hellwarth published a landmark paper [19] pointing out that all two-level systems are mathematically identical, and that if coherent light fields were ever created, it would be possible to use these same methods on optical transitions. Not surprisingly, then, the invention of the *laser* in 1960 was followed quickly by demonstration of the "photon echo"—the optical analogue of "spin echo". Virtually all laser experiments use one or two laser pulses, and make the pulses non-collinear or use multiple colours—thus intrinsically averaging the optical phase over a distance comparable to a wavelength. Such sequences (particularly with "ultrafast" laser pulses, which can probe dynamics on a femtosecond time scale) have significantly enhanced our understanding of reaction dynamics and energy transfer.

Successful approaches towards coherent control have resulted from essentially two independent dimensions: One that relies on the choice of appropriate molecules (passive control), while the other involves manipulating the environment such that exerting control becomes feasible (active control).

1.3. Passive versus active control

The passive control approach relies on the ability to produce a certain superposition of eigenstates that would evolve on its own to result in a unique set of products. This control is passive since the *time evolution* of the initially prepared superposition-state is not under the control of the experimentalist—control is only possible in the *preparation* of the initial superposition-state. For the success of this scheme, stress is on the choice of appropriate molecule, so that one is not confronted with problem of energy leakage due to IVR, and one can excite a particular vibrational mode selectively. Unfortunately, only a few molecules possess such decoupled systems where no couplings between various possible modes exist.

Nevertheless, using this approach of choosing appropriate molecules, bond selective photodissociation have been demonstrated in some molecules where the local mode picture is prevalent. Thus, in case of CH_2IBr [20] and CH_3SH [21], the state selection has been controlled by the wavelength of the exciting radiation and selective bond breaking has been achieved. Crim et al. [22] and Zare et al. [18,23] have demonstrated the bond selective photodissociation in water and its isotopes (D_2O and HOD), while Anderson and coworkers [24] have demonstrated such selectivity in acetylene (C_2H_2). In the H + HOD reaction, vibrational excitation of a particular bond leads to a large enhancement in the reactive cleavage of that bond, while the other bond OH or OD acts as a spectator. The stretching vs. bending mode excitation in $H + D_2O$ reaction has also been compared. The asymmetric stretch in D_2O enhances the reaction rate by a factor of 5, whereas bending does not affect the reaction rate. This observation is explained by considering the D_2O stretch as superposition of localized stretches and the vibrational branching ratio simply reflects the relative reactivity of excited vs. unexcited OD bonds in D_2O.

In Anderson's experiment, which shows selectivity in the reaction of $C_2H_2^+$ with methane, there are three major low-energy product channels. The cross-section of direct reaction channel corresponding to the formation of $C_2H_3^+$ was studied for stretching and bending mode excitations of carbon–carbon triple bond, rather than exciting the C–H bond on methane that was to be broken. The results showed that the direct reaction cross-section was essentially unaffected for stretch, whereas the bend-mode excitation surmounted the activation barrier easily, leading to the reaction-enhancement by a factor of 30 at low collision energies. The explanation for such bending enhancement is simple: Adding the third hydrogen on acetylene requires a change in geometry from simple linear shape and the bending mode does just that. Crim and coworkers [25] also have discussed the mode and bond selective reaction of chlorine atoms with H_2O and HOD in high vibrational states. All of these are nice demonstrations of selectivity, but the fact remains that the choice is essentially limited to simple and small molecules where IVR is not an issue, and thus not a generally applicable approach.

A more active manipulation of the atomic and molecular states requires modifying the experimental environment and is the basis of the active control approaches. Typical experiments involve a control of the nuclear and electronic motion within an atom or molecule by manipulating the properties on an external electromagnetic field. Such manipulations could involve optical interference techniques with single frequency lasers and polarization variations, or could involve concepts

that are more sophisticated, such as, optical pulse shaping in time and frequency. The approach of active manipulation is a very general approach, but has required strict technological developments and only recently, some experimental demonstrations have become possible. Active control uses the coherence of light to steer reactions into the desired products. Such processes may be classified according to the type of target-state to be populated. In the order of increasing complexity, this may be a single bound eigenstate, a superposition of bound eigenstates (i.e. a wavepacket), and one or more continuum states that may decay to form chemical products. Active control can also be subdivided according to the approaches involved in controlling the outcome of a reaction, and we will be discussing them in this review. One approach is the frequency domain control involving CW lasers while the other one is control in the time domain with pulsed lasers. In the frequency domain, Elliott demonstrated the controlled modulation of fluorescence yield based on the phase of the overlapping CW lasers [26]. Brumer and Shapiro developed a theoretical quantum-mechanical interference approach with CW-laser sources [27]. In the time domain, Rice and Tannor developed the wavepacket modulation approach [28] towards coherent control while Rabitz and coworkers [29] used the optimal control theory to get the best optical pulse sequences for control. Similarly, several research groups [30,31] have developed pulse-shaping schemes to experimentally illustrate coherent control. Unfortunately, the typical problems in experimental design of the optimized pulse shapes persist due to the inappropriate knowledge of molecular Hamiltonian, laser inhomogeneity, etc. Over the recent years, clever concepts of experimental feedback schemes are increasingly being used to circumvent these inherent difficulties to ensure robustness. Some recent reviews [12,13] have discussed some of these techniques in detail, which also illustrates the importance of the optimal control theory.

1.4. Centre-of-mass versus internal degrees of freedom motion control

Control processes may also be classified according to whether the centre-of-mass or internal degrees of freedom of the target are manipulated. Manipulation of the internal degrees of freedom has been the more commonly used "coherent control" strategy, and several approaches have been proposed: Controlling electronic wavepacket motion, nuclear wavepacket motion, multiphoton processes, selective photodissociation of molecules by favouring specific reaction channels, etc. Examples of control of the centre-of-mass motion type are the use of optical tweezers to move a DNA molecule around on a microscope slide, and the spatial confinement of atoms in a magneto-optic trap to produce Bose–Einstein condensate (laser cooling), etc. In these cases, the control is on the overall motion of molecules, i.e. the control of external degrees of freedom, and the momentum of the coherent laser beam is used to guide or trap various types of objects. The first work with optical tweezers was done by Ashkin et al. [32]. They successfully demonstrated trapping of small particles, atoms and living biological cells, etc. The optical tweezers can be used non-destructively for repositioning small structures inside the living cell and in combination with other techniques like laser scalpel; it can also be used for micro-manipulations like cutting small DNA segments inside cells. However, the most interesting application of this type of control is in manipulating single molecules. Mehta et al. [33] have discussed the application of various laser techniques to study single molecules biomechanics, e.g. the motion of single proteins.

S. Chu, C. Cohen-Tannoudji and W.D. Phillips were awarded the 1997 Nobel Prize for demonstrating methods to cool and trap atoms. Using sub-recoil laser cooling technique with three pairs of

laser beams, atoms have been cooled down to a temperature of 180 nK [34]. Such manipulation of external degrees of freedom can also lead to selective chemistry. A recent experiment by Stapelfeldt and coworkers [35] is an example of this, where they demonstrate control over branching ratio of photodissociation of iodine (I_2) molecules by aligning them in the field of intense linearly polarized laser pulse. The branching ratio of I + I and I + I* is controlled by a factor of 26 by selective photoexcitation of two potential curves, each of which adiabatically correlate to one of the product channels. This selectivity is obtained by irradiating the aligned molecules with light polarized parallel or perpendicular to the polarization axis of the aligning laser. Attempts are also on-way that are trying to combine the manipulation of the centre-of-mass or internal degrees of freedom of the target to achieve molecule-specific coherent control in liquids that is of relevance to biology [36].

Since the original inception of control over quantum phenomenon as a goal, the potential applications have broadened out beyond chemical reactivity. In principle, quantum phenomena of any variety could become amenable to control with the choice of appropriate parameters. In fact, in recent years the aim of coherent control is no longer solely limited to bond-selective chemistry, but to find applications in various fields of science and technology. To quote a few of such efforts [11]: Controlling electrons in solid state multiple quantum wells; encoding or decoding information in the wavepacket of moving electrons in semiconductors; the possible use of active manipulation of molecular dynamics to extract information on underlying Hamiltonian; and the possible creation of quantum computers [37].

1.5. Structure of this review

A number of approaches for ultrafast pulse shaping have been advanced, among which fast and programmable optical pulse shaping is of most interest and has been achieved by the spatial pulse shaping techniques. In this review, we will concentrate on the most successful and widely adopted method, in which waveform synthesis is achieved by spatial masking of the spatially dispersed optical frequency spectrum and it does not require any ultrafast modulators. A recent review by Weiner [38] provides a broad account of femtosecond pulse shaping as well as related pulse processing techniques. Other useful reviews [39,40] describe early results on femtosecond pulse shaping using fixed masks and related experiments.

This review would cover experimental and theoretical applications and developments that have become possible in the recent years, which would show how optical pulse shaping has been a key contributor to the fast developing area of coherent control. However, it will be impossible to discuss all the theoretical recipes and experimental concepts that are in use in coherent control, and we will stress on areas that have not been reviewed extensively before. For issues that are dealt in brief here, the reader will be referred to the other details. Our overall effort would be to elucidate the importance of coherent control efforts with pulse shaping techniques that are bursting with immense activity now and many more new exciting and upcoming research is on the way, just waiting to happen.

2. Theory behind pulse shaping

NMR scientists have extensively used pulse shaping in the radio-frequency (RF) domain, where the pulse lengths are on the order of microseconds and conventional microwave electronic circuits

can be used. Such pulse shaping approach is based on the linear, time-invariant filtering scheme, a common electrical engineering concept, where linear filtering is used to process electrical signals ranging from low frequencies (audio and below) to very high frequencies (microwave). The boons of such techniques are evident from the tremendous applications of NMR available today. The natural desire is to extend this technique into the optical domain. However, when one extends the concept to the optical domain, the hardware needed for programmable linear filtering of femtosecond laser pulses look very different from the familiar resistors, capacitors, and inductors used for linear filtering of conventional signals. Conceptually, linear filtering can be described either in the time or in the frequency domain.

2.1. Time domain pulse shaping

In the time domain, the filter is characterized by a time response function $g(t)$. The output of the filter $E_{\text{out}}(t)$ in response to an input pulse $E_{\text{in}}(t)$ is given by the convolution of $E_{\text{in}}(t)$ and $g(t)$, such that, $E_{\text{out}}(t) = E_{\text{in}}(t) \otimes g(t)$, where $\otimes$ denotes convolution. If the input is a delta function, the output is simply $g(t)$, and so for a sufficiently short input pulse, the problem of generating a specific output pulse shape is equivalent to the task of fabricating a linear filter with the desired time response. Shaping ultrafast pulses in the picosecond (ps) or subpicosecond (sub-ps) range is non-trivial since there are no electronic devices that can work on these timescales. If the optical pulse that we wish to shape has a temporal duration of fs or ps, then we need a modulator that works on this time scale. The idea of shaping a pulse by sending it through a modulator, such as a Mach–Zehnder, is referred to as direct pulse shaping. Current modulators can operate at 60 GHz, which is much slower than necessary to shape a femtosecond pulse, and hence indirect schemes are sought after.

2.2. Fourier domain pulse shaping

A creative solution to the problem of slow modulators is the technique of indirect pulse shaping in the frequency domain. In the frequency domain, the filter is characterized by its frequency response $G(\omega)$. The output of the linear filter $E_{\text{out}}(\omega)$ is the product of the input signal $E_{\text{in}}(\omega)$ and the frequency response $G(\omega)$, i.e.,

$$E_{\text{out}}(\omega) = E_{\text{in}}(\omega) \otimes G(\omega) \ , \tag{1}$$

where $E_{\text{in}}(t), E_{\text{out}}(t)$, and $g(t)$ and $E_{\text{in}}(\omega)$, $E_{\text{out}}(\omega)$, and $G(\omega)$, respectively, are Fourier transform pairs–i.e., $G(\omega) = \int \mathrm{d}t\, g(t)\mathrm{e}^{-\mathrm{i}\omega t}$ and $g(t) = (1/2\pi) \int \mathrm{d}t\, G(\omega)\mathrm{e}^{\mathrm{i}\omega t}$. With a delta function input pulse, the input spectrum $E_{\text{in}}(\omega)$ is equal to unity, and the output spectrum is equal to the frequency response of the filter, and thus, due to the Fourier transform relations, generation of a desired output waveform can be accomplished by implementing a filter with the required frequency response. This concept is shown in Fig. 1. A grating spreads the pulse, so that each different spectral component maps onto a different spatial position. The collimating lenses and anti-parallel grating pair are set up in a $4F$ configuration (F being the focal length of the collimating lenses), and in the centre of the 4-F system, an element is placed that modulates the spectrum. The individual frequency components contained within the incident ultrashort pulse are angularly dispersed by the first diffraction grating, and then focussed to small diffraction limited spots at the back focal plane of the first lens,

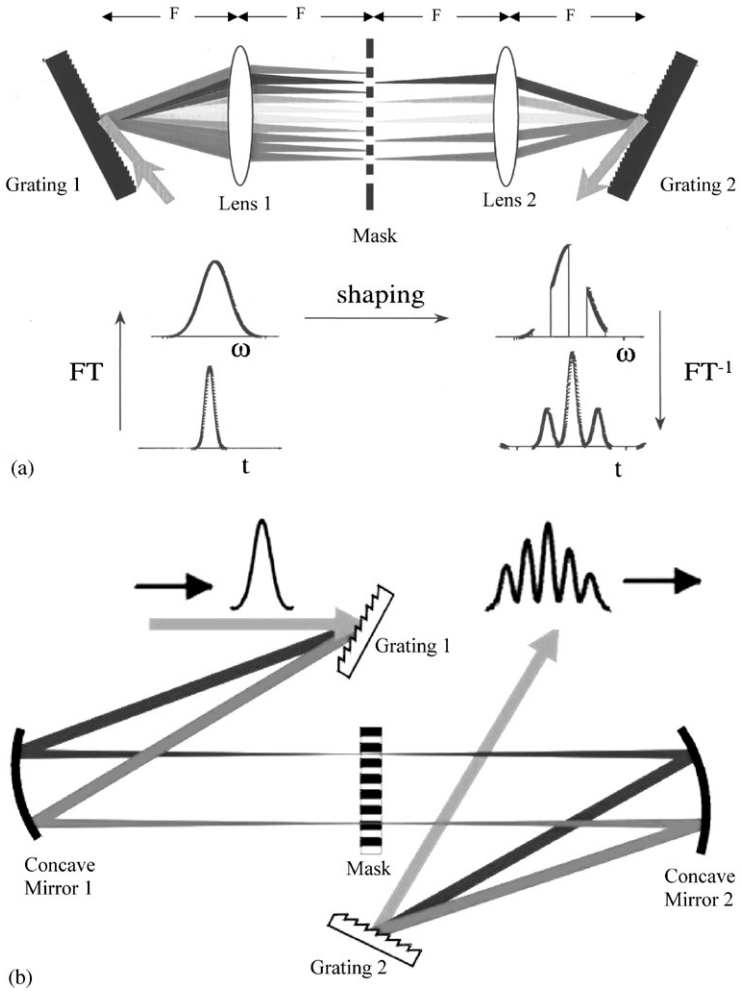

Fig. 1. Principle of Fourier domain pulse shaping: (a) A pair of grating and a pair of lens is arranged in 4*F* configuration (*F* is the lens focal length). The gratings spread and collect the spectral components while the lenses perform the forward and reverse Fourier transforms, respectively. The Spatial Mask at the focal point imparts the pulse modulation that is static in time. (b) Using curved mirrors instead of lenses can further the dispersion-free arrangement for the Fourier domain pulse shaping as shown in (a) for really short pulses ($\leqslant 20$ fs).

where the frequency components are spatially separated along one dimension. Essentially the first lens performs a Fourier transform, which converts the angular dispersion from the grating to a spatial separation at the back focal plane. Spatial modulators are placed in this focal plane to manipulate the spatially dispersed optical Fourier components. At a focal distance from the spatial modulator, the second lens performs an inverse Fourier transform but the frequencies are still dispersed. Finally, the second grating placed at a focal distance from the second lens recombines all the frequencies into a single collimated beam resulting in a shaped output pulse (Fig. 1a). The Fourier transform of the pattern transferred by the spatial modulator onto the spectrum is the output pulse

shape. There are four distinct programmable spatial pulse shaping devices that have been demonstrated to date, viz., Liquid-Crystal Modulator arrays [39], Acousto-Optic Modulator [41], deformable mirror [42] and Holographic patterns [43,44].

In fact, with this approach, it is not even necessary to have modulators in the system to shape the ultrafast pulse and the first demonstration of such indirect pulse shaping used a fixed spatial mask [38], a technique that does not have programmability. The spatial mask can be created using lithographic techniques as in semiconductor processing. The fact that the spatial mask cannot be changed in real time limits the utility of this technique. This approach does have the advantage that it is simple, and requires no pulse picker. In order for this technique to work as desired, one requires that in the absence of a pulse-shaping mask, the output pulse should be identical to the input pulse. Therefore, the grating and lens configuration must be truly free of dispersion. This can be guaranteed if the lenses are set up as a unit magnification telescope, with the gratings located at the outside focal planes of the telescope. The dispersion-free condition also depends on several approximations, e.g., that the lenses are thin and free of aberrations, that chromatic dispersion in passing through the lenses or other elements which may be inserted into the pulse shaper is small, and that the gratings have a flat spectral response. For very short pulses, especially in the 10–20 fs range, more care must be taken to satisfy these approximations. For example, both the chromatic aberration of the lenses in the pulse shaper and the dispersion experienced in passing through the lenses can become important effects. However, by using spherical mirrors instead of lenses [45], these problems can be avoided and dispersion-free operation has been obtained (Fig. 1b).

3. Theoretical concepts in coherent control

Let us start the discussion with the basic concepts in population inversion and dynamics for simple systems interacting with lasers. While most of the coherent control issues have focussed on single photon resonances, one of the recent developments in the field have been in extending it to the multiphoton resonances and we will cover both. We will start with simple two-level system for a single photon resonance condition and generalize it to the multilevel case and to the multiphoton case with the use of the density matrix concepts and wavepacket dynamics.

3.1. Two-level system

The simplest model describing a molecular system is an isolated two-level system or ensemble without relaxation or inhomogeneities. This simple model often turns out to be a very practical model for most systems interacting with ultrashort laser pulses as the magnitude of the relaxation processes (typically in nanoseconds) are immensely large as compared to the light–matter interaction time. Let us consider a linearly polarized laser pulse is being applied to the $|1\rangle \rightarrow |2\rangle$ transition, where $|1\rangle$ and $|2\rangle$ represent the ground and excited eigenlevels, respectively, of the field-free Hamiltonian (Fig. 2). In the laboratory-frame of reference, the general form for the scalar component of the linearly polarized electromagnetic field $E(t)$ (due to the laser) along the direction of the $|1\rangle \rightarrow |2\rangle$ transition can be classically represented as

$$E(t) = \varepsilon(t)e^{i[\omega(t)t+\phi(t)]} + c.c. = \varepsilon(t)e^{i[\omega+\dot{\phi}(t)]t} + c.c. \ , \tag{2}$$

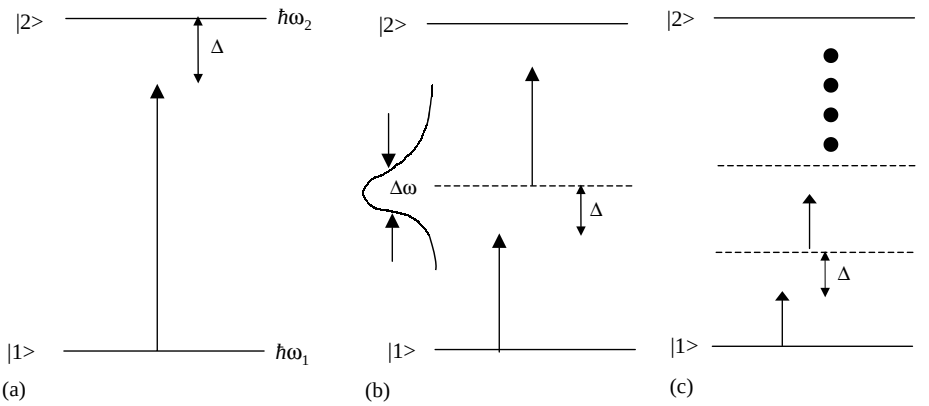

Fig. 2. Schematic of ultrafast pulse laser excitation for a two level system through (a) single-photon, (b) two-photon, and (c) multi-photon process, respectively. Symbols and notations are defined in the text.

where $\varepsilon(t)$, $\phi(t)$, and $\dot{\phi}(t)$ as the instantaneous amplitude, phase and frequency-sweep, respectively; and ω is the carrier frequency or the centre laser frequency in case of the pulsed lasers. The form with a cosine wave instead of a complex exponential can also be used, but this form is mathematically simpler because it permits transformation to the rotating frame of reference easily.

In case of single photon interactions (Fig. 2a), the total laboratory-frame Hamiltonian for such two-level system under the effect of the applied laser field in Eq. (2), can be written as [46]

$$H = \begin{pmatrix} E_1 & V_{12} \\ V_{21} & E_2 \end{pmatrix} = \begin{pmatrix} \hbar\omega_1 & \dfrac{\mu.E}{2} \\ \dfrac{\mu.E^*}{2} & \hbar\omega_2 \end{pmatrix} = \frac{\hbar}{2} \begin{pmatrix} -\omega_R & \dfrac{\mu.\varepsilon}{\hbar}\, e^{i(\omega t+\phi)} \\ \dfrac{\mu.\varepsilon^*}{\hbar}\, e^{-i(\omega t+\phi)} & \omega_R \end{pmatrix} , \tag{3}$$

where $\omega_R = \omega_2 - \omega_1$ is resonance frequency, V_{12} and V_{21} are the negative interaction potentials and $h\omega_1, h\omega_2$ are the energies of ground (E_1) and excited state (E_2), respectively, and μ is the transition dipole moment of the $|1\rangle \rightarrow |2\rangle$ transition. Solving an eigenvalue problem with such a formidable Hamiltonian can be simplified greatly by transforming it into a different frame of reference. A time-dependent transformation operator, T transforms the *Schrödinger* equation as follows:

$$\begin{aligned} & T\left(i\hbar \frac{\partial}{\partial t}\Psi = H\Psi\right) , \\ & i\hbar \frac{\partial}{\partial t}(T\Psi) - i\hbar \frac{\partial}{\partial t}(T^{-1}T)\Psi = TH(T^{-1}T)\Psi , \\ & i\hbar \frac{\partial}{\partial t}(T\Psi) = \left[THT^{-1} + i\hbar \frac{\partial}{\partial t}T^{-1}\right](T\Psi) . \end{aligned} \tag{4}$$

This results in the following transformation equation:

$$H^{\text{Transformed}} = THT^{-1} + i\hbar T^{-1}\frac{\partial T}{\partial t} . \tag{5}$$

Using the above transformation relation, there are two different ways to transform the elements of the laboratory frame Hamiltonian, H, into a rotating frame of reference. One of them is the frame of reference that rotates at ω and is known as the phase-modulated frame (PM). This is derived from H by the transformation [47]:

$$T^{\mathrm{PM}} = \begin{pmatrix} \mathrm{e}^{-\mathrm{i}\frac{\omega t}{2}} & 0 \\ 0 & \mathrm{e}^{\mathrm{i}\frac{\omega t}{2}} \end{pmatrix} \tag{6}$$

and is given below with an additional zero-point energy shift of $\Delta/2$ as

$$H^{\mathrm{PM}} = \hbar \begin{pmatrix} \Delta & \frac{\mu\varepsilon}{2\hbar}\,\mathrm{e}^{\mathrm{i}\phi} \\ \frac{\mu\varepsilon^*}{2\hbar}\,\mathrm{e}^{-\mathrm{i}\phi} & 0 \end{pmatrix} = \hbar \begin{pmatrix} \Delta & \frac{\mu\varepsilon}{2\hbar}\,\mathrm{e}^{\mathrm{i}\phi} \\ \frac{\Omega_1^*}{2}\,\mathrm{e}^{-\mathrm{i}\phi} & 0 \end{pmatrix} , \tag{7}$$

where $\Omega_1(t) = \mu \cdot \varepsilon(t)/\hbar$ and $\Omega_1^*(t) = \mu \cdot \varepsilon^*(t)/\hbar$ are complex conjugate pairs and is known as the Rabi frequency and $\Delta = \omega_R - \omega$ is the time-independent detuning. This is the usual frame of reference used in NMR. However, in order to investigate the off-resonance behaviour of continuously modulated pulses it is useful to instead perform a rotating-frame transformation to a frequency modulated (FM) frame [47] by the transformation

$$T^{\mathrm{FM}} = \begin{pmatrix} \mathrm{e}^{-\mathrm{i}\frac{\omega t+\phi}{2}} & 0 \\ 0 & \mathrm{e}^{\mathrm{i}\frac{\omega t+\phi}{2}} \end{pmatrix} .$$

of Eq. (3). This results in a transformed Hamiltonian with an additional energy shift of $(\Delta - \dot{\phi})/2$:

$$H^{\mathrm{FM}} = \hbar \begin{pmatrix} \Delta - \dot{\phi}(t) & \frac{\Omega}{2} \\ \frac{\Omega^*}{2} & 0 \end{pmatrix} . \tag{8}$$

The time derivative of the phase function $\dot{\phi}(t)$, i.e., frequency modulation, appears as an additional resonance offset over and above the time-independent detuning Δ, while the direction of the field in the orthogonal plane remains fixed. The time evolution of the unrelaxed two-level system can then be evaluated by integrating the Liouville equation:

$$\frac{\mathrm{d}\rho(t)}{\mathrm{d}t} = \frac{\mathrm{i}}{\hbar}\,[\rho(t), H^{\mathrm{FM}}(t)] , \tag{9}$$

where $\rho(t)$ is a 2×2 density matrix whose diagonal elements represent populations in the ground and excited states and off-diagonal elements represent coherent superposition of states. This approach has been very successful in solving most single-photon processes beyond perturbation limits for arbitrarily shaped amplitude and frequency-modulated pulses.

3.2. Adiabatic passage and adiabatic half-passage

Excitation exactly on resonance creates a complete population inversion when the "pulse area" (the time integral of the Rabi frequency, Ω_1) equals π [48]. Such "π pulses" were first practically employed in magnetic resonance, where the Rabi frequency is usually fairly uniform and generally exceeds both the overall spectral width and the width of the individual resonance. Unfortunately, these conditions are often difficult, and sometimes impossible, to achieve in laser spectroscopy of real molecules. Effects such as inhomogeneous broadening, Rabi frequency distribution and multiple levels prevent 100% population transfer to the excited state. In fact, on an average only 50% population transfer can be achieved at best with CW or pulsed laser sources, given the degree of inhomogeneity that practically exists under every experimental condition. In an effort to overcome such unfavourable conditions, sequences of π pulses have been attempted that have "packets" of simultaneous π pulses; each tuned to an appropriate Bohr frequency ("Cooke–Shore" pulses) [46]. In general, however, a more robust approach is to use pulse shaping, usually including frequency-swept (chirped) laser pulses [49,50].

If we expand the instantaneous phase function of $E(t)$ of Eq. (2) as a Taylor series with constants b_n, we have [51]

$$\begin{aligned}
\phi(t) &= b_0 + b_1 t + b_2 t^2 + b_3 t^3 + b_4 t^4 + b_5 t^5 + \cdots \ , \\
\dot{\phi}(t) &= b_1 + 2b_2 t + 3b_3 t^2 + 4b_4 t^3 + 5b_5 t^4 + \cdots \ , \\
\dot{\phi}(t) &= \sum_{n=1} n b_n t^{(n-1)} \ . \qquad (10)
\end{aligned}$$

Establishing this generalization for the continuously frequency modulated ("chirped") pulses enables us to treat all possible chirped pulse cases by exploring the effects of each of the terms in Eq. (10) initially for a simple two-level system and then extend it to the multilevel situation.

These modulated pulses can be generated to sweep from far above resonance to far below resonance (blue-to-red sweeps) or alternatively, from far below resonance to far above resonance (red-to-blue sweeps). If the frequency sweep is sufficiently slow, the transitions it induces in the molecular system are said to be "adiabatic". The chirped-pulse adiabatic rapid passage (ARP) method is insensitive to pulse-shape and area [52–54]. The term "rapid" in ARP signifies that the adiabatic process has to be fast compared to the characteristic relaxation time of the system. ARP can be described using the optical Bloch (Feynman psuedopolarization) vector model [55], which is illustrated herein as Fig. 3. In this picture, the effective field ε (Eq. (2)) exerts a torque $\mu \times \varepsilon$ on the oscillating dipole moment μ, forcing μ to precess around ε. The vector components of μ and ε are just the elements of ρ and H, respectively:

$$\mu_x = \frac{\rho_{12} + \rho_{21}}{2}; \quad \mu_y = \frac{\rho_{12} - \rho_{21}}{2\mathrm{i}}; \quad \mu_z = (\rho_{11} - \rho_{22}) \ , \qquad (11)$$

$$\varepsilon_x = \frac{H_{12} + H_{21}}{2} = \mathrm{Re}(\Omega_1(t)); \quad \varepsilon_y = \frac{H_{12} - H_{21}}{2\mathrm{i}} = \mathrm{Im}(\Omega_1(t)); \quad \varepsilon_z = H_{11} - H_{22} = \Delta(t) \ . \qquad (12)$$

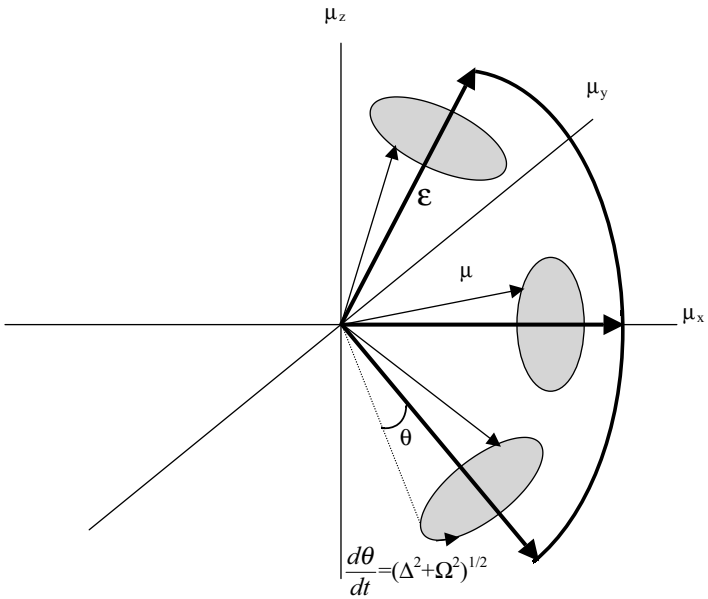

Fig. 3. Feynman–Vernon–Helworth vector description of adiabatic rapid passage (ARP). As the rotation axis ε changes slowly from large and positive (far above resonance) to large and negative (far below resonance), the magnetization or pseudopolarization vector follows and generates inversion.

A system initially in the thermal equilibrium has its moment pointing in the z direction ($\mu_z = 1,\ \mu_x = \mu_y = 0$). If the radiation field is applied near resonance such that $\Omega_1 \gg \Delta$, then $\varepsilon \approx \varepsilon_x$, causing μ to oscillate in the yz-plane with an angular frequency Ω_1. Such an excitation process is called "non-adiabatic" and common $\pi/2$ and π pulses are familiar examples. In an adiabatic process, on the other hand, μ precesses with a small angle about ε and remains nearly parallel to ε as ε changes in time. Sweeping the frequency changes the direction of the rotating axis. If the sweep is done rapidly compared to the inverse of the relaxation times, but slowly compared to the rate of precessing of μ, the vector will follow the rotation axis from the $+z$ to the $-z$ direction, thus generating complete inversion (ARP). Qualitatively this works because the "vector average position" of a magnetization vector that is initially close to the rotation axis, and which has time to precess through a large angle, lies on top of the rotation axis. More quantitatively [47], the instantaneous inclination of ε above the xy-plane is

$$\theta(t) = \tan^{-1}\left(\frac{\Delta(t)}{\Omega_1(t)}\right) \tag{13}$$

and the constraints for adiabatic inversion are

$$\frac{\mathrm{d}\theta(t)}{\mathrm{d}t} \ll \sqrt{\Omega_1^2 + \Delta^2}\ , \tag{14}$$

$$\theta(t_0) = \pm\frac{\pi}{2} \text{ or } \mp\frac{\pi}{2}\ , \tag{15}$$

where $\pm t_0$ is the time at the beginning and the end of the pulse. Eq. (14) implies that the radiation field must initially be far below resonance or far above resonance for $\mu \| \varepsilon$, and must end up far enough above or below resonance for the $\mu \| \varepsilon$ criterion to be maintained, which results in perfect inversion. As the carrier frequency is tuned close to resonance, ε rotates towards x. On resonance $\varepsilon \| x$, and if μ adiabatically follows ε, it is also brought into alignment with x (Fig. 3). Continuing the frequency sweep to the other side of resonance, the reverse process takes place and ε and μ tilt back toward $-z$. The complete process of inverting μ from $+z$ to $-z$ (from $\Delta \gg 0$ to $\Delta \ll 0$, or vice versa) is called adiabatic passage. Analogously, the process of sweeping μ from z to x (from $\Delta \gg 0$ to $\Delta = 0$ or resonance) is termed "adiabatic half-passage".

The exact shape of the envelope and the chirping functions are not critical as long as Eqs. (14) and (15) are fulfilled. A related feature is that above a certain threshold Ω_1 value, the process is insensitive to the magnitude of Ω_1. The first results to be derived assumed an infinitely long linear frequency sweep with constant amplitude. Obviously, such a sweep is impractical, and in fact quite wasteful of energy. Eq. (14) shows that, for a given Rabi frequency, a much more rapid frequency sweep is permissible far below or far above resonance than is permitted near resonance. Thus, a tangent frequency sweep is readily derived to be the optimum frequency sweep for constant amplitude. Another possibility is to decrease the amplitude Ω_1 near the beginning and the end of the sweep, which again is permissible because of the resonance offset Δ in Eq. (14). Thus, for example, a Gaussian envelope with a linear sweep can perform satisfactorily. However, any pulse with a finite duration cannot satisfy Eq. (15) for all resonance frequencies. Most of the initial demonstrations of adiabatic passage were in nuclear magnetic resonance (NMR). In liquids, relaxation times are very long and spectra are very sharp (≈ 0.1–1 Hz lines spread over 10^4 Hz). Therefore, it is possible to exceed the entire spectral bandwidth with reasonable radiofrequency fields used in NMR. On the other hand, it is completely impossible to create laser pulses with Rabi frequencies that exceed the entire optical or infrared spectral bandwidth; in addition, relaxation times are very much shorter and limit the possible pulse duration. Thus, pulses that invert completely over some specific range of frequencies, with minimal perturbations outside that range, have more practical importance. An important example of such a waveform is [48]

$$E(t) = \mathrm{Re}(\mathrm{sech}(\alpha t)^{1+\mu \mathrm{i}} \exp(\mathrm{i}\omega t)) \tag{16}$$

or equivalently

$$\varepsilon(t) = \mathrm{sech}(\alpha t); \quad \Delta(t) = \dot{\phi} = \mu\alpha \tanh(\alpha t)\ . \tag{17}$$

This waveform is shown in Fig. 4a. While it formally stretches to $\pm\infty$, the exponential falloff of the secant hyperbolic envelope means that the truncation effects can be made negligible. The effects of this waveform are analytically solvable; the inversion profile is rectangular and sensitive to the exact amplitude of the pulse (Fig. 4b). Note the dramatic non-linearity of the excitation in this limit: The Fourier transform of the pulse shape (which represents the inversion profile in linear response regime) in Eq. (16) is hardly rectangular. The other well-studied waveform (Fig. 4c) that performs satisfactorily under the adiabatic circumstances (Fig. 4d) is a Gaussian pulse with linear sweep:

$$\varepsilon(t) = \exp(-\alpha t^2) = \exp(-\ln 2(t/\tau_p)^2); \quad \Delta(t) = \dot{\phi} = 2bt\ , \tag{18}$$

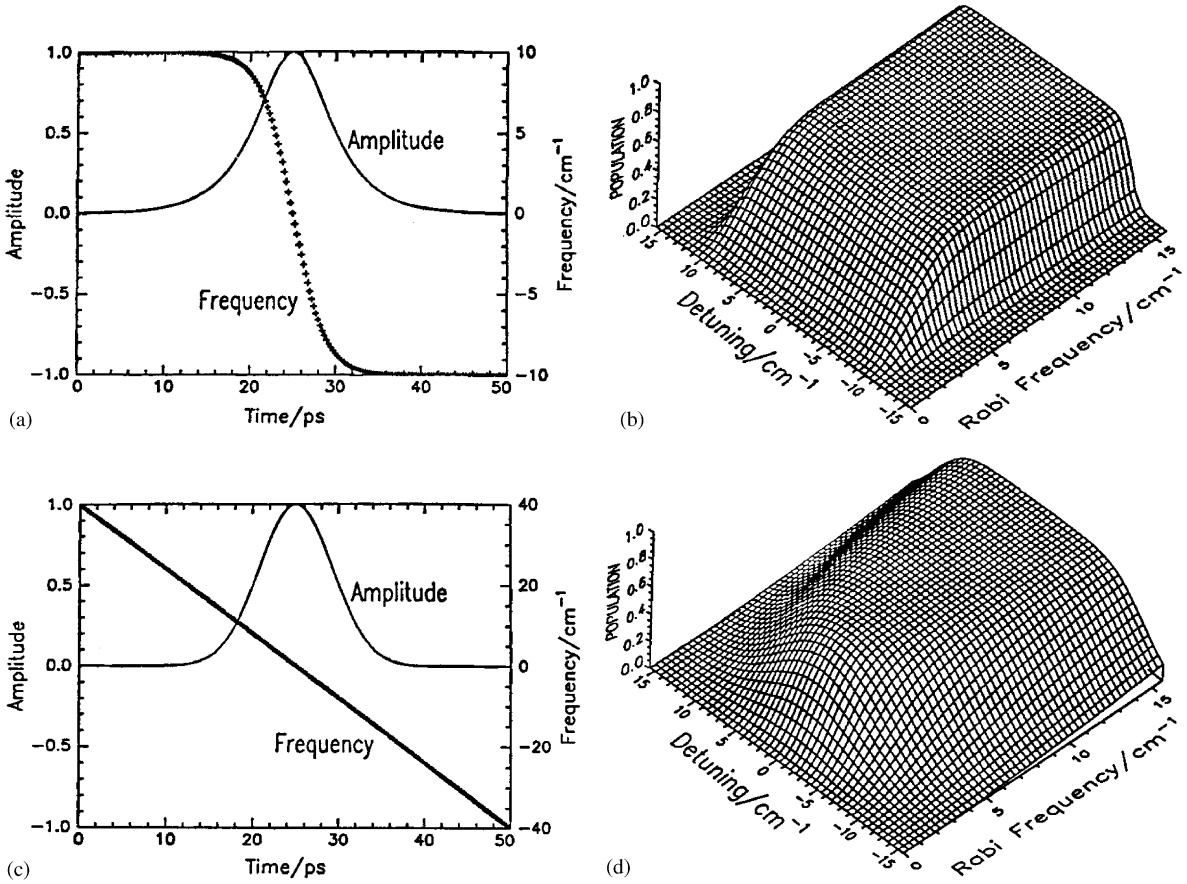

Fig. 4. Analytical pulse shape: (a) Hyperbolic secant amplitude with hyperbolic tangent sweep pulse profile. (b) Corresponding population inversion profile of the excited state in a two-level system, as a function of Ω_1 (Rabi frequency) and Δ (detuning). (c) Gaussian amplitude with linear sweep pulse profile. (d) corresponding population inversion profile in a two level system, as a function of Ω_1 and Δ.

where $\alpha = \ln 2/\tau_p^2 = 0.693/\tau_p^2$ is expressed in terms of τ_p, which is the FWHM of the pulse and b is the sweep rate. While this pulse also produces inversion over a wide range of frequencies, the inversion profile is not rectangular, and does not preserve its shape with increasing Rabi Frequency, unlike the waveform given by Eq. (16). Many other waveforms of comparable or even greater complexity have been investigated theoretically and experimentally. For example, it has been shown that Eqs. (17) and (18) represent only the first member of an infinite family of phase and amplitude modulated pulses, all of which generate rectangular inversion profiles. The additional members of the family are phase-modulated versions of analytic solutions to the Bloch equations in the inverse scattering reformulation. Purely amplitude-modulated pulses with rectangular inversion profiles have been generated as well, mostly by computerized optimization. The waveform in Eq. (17) has been implemented as a laser pulse with a few ns [56], ps [57] and recently to sub-ps [58] resolution with the help of novel arbitrary pulse shaping capabilities. Both of these waveforms in Eqs. (17) and

(18) have been used experimentally in the picosecond regime to perform robust selective excitation [54] in two and three-level systems and we will discuss it in the later sections.

An equivalent picture of ARP uses the eigenvalues and eigenvectors of the combined matter-radiation Hamiltonian, or the so-called dressed states. In this particular case, the laser pulse is applied to the $|1\rangle \rightarrow |2\rangle$ transition such that the laser frequency sweeps through resonance with the transition frequency ω_{21}. For the Hamiltonian of Eq. (3), the eigenvectors are:

$$|\Psi_-(t)\rangle = \cos\Theta(t)|1\rangle - \sin\Theta(t)|2\rangle, \text{ and} \tag{19a}$$

$$|\Psi_+(t)\rangle = \sin\Theta(t)|1\rangle + \cos\Theta(t)|2\rangle \ . \tag{19b}$$

Here,

$$\cos(2\Theta(t)) = \frac{\Delta(t)}{\sqrt{\Delta(t)^2 + |\Omega_1(t)|^2}}, \text{ and} \tag{20a}$$

$$\sin(2\Theta(t)) = \frac{\Omega_1(t)}{\sqrt{\Delta(t)^2 + |\Omega_1(t)|^2}} \ . \tag{20b}$$

The dressed state eigenvalues (eigenfrequencies) are

$$\omega_\pm(t) = \frac{1}{2}[\Delta(t) \pm \sqrt{\Delta(t)^2 + |\Omega_1(t)|^2}] \ . \tag{21}$$

In the dressed state picture, adiabatic passage occurs when changes in the Hamiltonian occur sufficiently slowly so that the system does not change eigenstate as the Hamiltonian evolves, although the eigenstates change composition during the evolution. For a two-level system, there are two important limits, which are relevant to experiments with frequency swept laser pulses. For large positive detuning, and $|\Omega_1(t)| \ll |\Delta(t)|$,

$$|\Psi_+(t)\rangle \rightarrow |2\rangle; \quad |\Psi_-(t)\rangle \rightarrow |1\rangle, \text{ and} \tag{22a}$$

$$\omega_+(t) \rightarrow \Delta(t); \quad \omega_-(t) \rightarrow 0 \ . \tag{22b}$$

And for large negative detuning and $|\Omega_1(t)| \ll |\Delta(t)|$,

$$|\Psi_+(t)\rangle \rightarrow |1\rangle; \quad |\Psi_-(t)\rangle \rightarrow |2\rangle, \text{ and} \tag{22RE1a}$$

$$\omega_+(t) \rightarrow 0; \quad \omega_-(t) \rightarrow |\Delta(t)| \ . \tag{22RE1b}$$

In Fig. 5, we show the energies of the two dressed states evolving with time for a Gaussian pulse with linearly frequency swept pulse under the adiabatic condition. We find that as the system initially begins in dressed state $|\Psi_-(t)\rangle$ (large negative Δ; $|\Psi_-(t)\rangle \rightarrow |1\rangle$), and evolves only along the energy curve associated with $|\Psi_-(t)\rangle$, then adiabatic inversion ($|1\rangle \rightarrow |2\rangle$) will occur after the frequency sweep is completed.

The general condition for ARP for a multilevel system may be expressed as the inequality

$$\left|\langle\Psi_n(t)|\frac{\mathrm{d}}{\mathrm{d}t}\Psi_m(t)\rangle\right| \ll |\omega_n(t) - \omega_m(t)| \ . \tag{23}$$

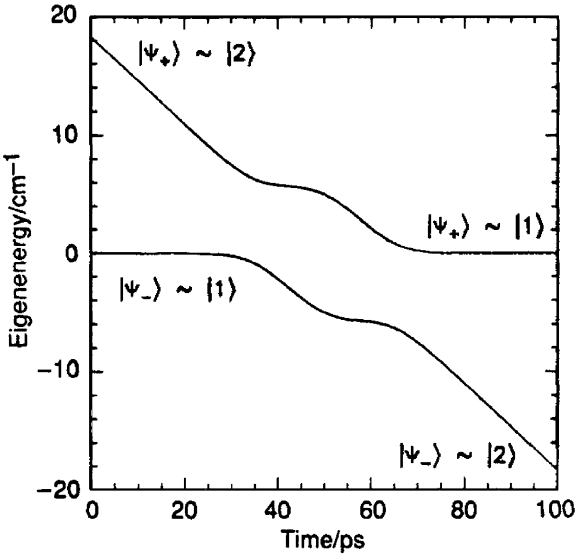

Fig. 5. Time evolution of the dressed energy curves for a two level system excited by a 20 ps Gaussian pulse, $b = 0.18\ \mathrm{cm}^{-1}/\mathrm{ps}$, and $\Omega_1 = 2\pi \times 10\ \mathrm{cm}^{-1}$. When the pulse frequency is well below or above resonance, the dressed eigenstates each correlate with a single "bare" state.

For the special case of the two-level system described by the Hamiltonian of Eq. (3), this inequality reduces to

$$\left| \Delta(t) \frac{\mathrm{d}\Omega_1(t)}{\mathrm{d}t} - \Omega_1(t) \frac{\mathrm{d}\Delta(t)}{\mathrm{d}t} \right| \ll (\Delta^2(t) + \Omega_1^2(t))^{3/2} \tag{24}$$

and is similar to Eq. (14) as described in the Bloch vector picture. Eq. (24) illustrates that ARP requires a sufficiently slow change in both the Rabi frequency and the frequency sweep as has been realized from Bloch vector analysis in Eq. (14). The same concept of sweeping to resonance is termed "adiabatic half-passage".

3.3. Multiphoton situation

In analogy to this single photon interaction as given in Eq. (3), the interaction potential under the effect of an applied laser field in two-photon absorption case (Fig. 2b) can be written as [59]

$$V(t) \propto \mu_{1m}\varepsilon(t)\mathrm{e}^{\mathrm{i}(\omega t+\phi(t))}|1\rangle\langle m|\mu_{m2}\varepsilon(t)\mathrm{e}^{\mathrm{i}(\omega t+\phi(t))}|m\rangle\langle 2| + c.c.\ , \tag{25}$$

where μ_{1m} is the transition dipole moment of ground state to the virtual state (m), while μ_{m2} is the transition dipole moment of the virtual state to the excited state. If we define an effective transition dipole moment μ_{eff}^2 such that it is a product of the individual dipole moments (i.e., $\mu_{\mathrm{eff}}^2 = \mu_{1m}.\mu_{m2}$), we can then rewrite Eq. (25) as

$$V(t) \propto (\mu\varepsilon(t))^2\mathrm{e}^{2\mathrm{i}(\omega t+\phi(t))}|1\rangle\langle 2| + c.c. \tag{26}$$

since for normalized states, $\langle m|m\rangle = 1$. This two-photon scenario can be extended to the N-photon case (Fig. 2c), where for practical purposes, it is important to simplify the problem, since the individual transient dipole moment of the each of the Nth-photon transitions is difficult to follow. We assume that the transient dipole moment of the individual intermediate virtual states in the multiphoton ladder result in an effective transition dipole moment, μ_{eff}^N, which is a product of the individual N virtual state dipole moments, μ_n, (i.e., $\mu_{\text{eff}}^N = \prod_n^N \mu_n$). This approximation is particularly valid where the individual virtual levels are non-resonant, and as such their multiphoton interaction dynamics can be neglected [60,61]. The interaction potential can be written as:

$$V(t) \propto (\mu_{\text{eff}}\varepsilon(t))^N e^{iN(\omega t+\phi(t))}|1\rangle\langle 2| + c.c. \tag{27}$$

and the total laboratory-frame N-photon Hamiltonian becomes

$$H = \begin{pmatrix} \hbar\omega_1 & \frac{1}{2k}(\mu_{\text{eff}}\cdot E)^N \\ \frac{1}{2k}(\mu_{\text{eff}}\cdot E^*)^N & \hbar\omega_2 \end{pmatrix} = \frac{\hbar}{2}\begin{pmatrix} -\omega_R & \frac{(\mu_{\text{eff}}\cdot\varepsilon)^N}{k\hbar}e^{iN(\omega t+\phi)} \\ \frac{(\mu_{\text{eff}}\cdot\varepsilon^*)^N}{k\hbar}e^{-iN(\omega t+\phi)} & \omega_R \end{pmatrix}. \tag{28}$$

The virtual levels for the two-photon (or N-photon) case can exist anywhere within the bandwidth $\Delta\omega$ of the applied laser pulse (Fig. 2) and the individual virtual state dynamics is of no consequence. We can define multiphoton Rabi frequency, as the complex conjugate pairs: $\Omega_1(t) = k(\mu_{\text{eff}}\cdot\varepsilon(t))^N/\hbar$ and $\Omega_1^*(t) = k(\mu_{\text{eff}}\cdot\varepsilon^*(t))^N/\hbar$, where k is a proportionality constant having dimensions of $(\text{energy})^{1-N}$, which in SI units would be $(\text{Joules})^{1-N}$.

In analogy to the single photon case [47,62] discussed in the earlier section, there are two different ways to transform the elements of the above laboratory frame N-photon Hamiltonian into a rotating frame of reference. The usual frame of reference would be to rotate at $N\omega$, which is the phase-modulated frame (PM), and this is derived from the H of Eq. (28) by the transformation:

$$T^{\text{PM}} = \begin{pmatrix} e^{-iN\frac{\omega t}{2}} & 0 \\ 0 & e^{iN\frac{\omega t}{2}} \end{pmatrix} \tag{29}$$

and with the use of Eq. (5) and an additional zero-point energy shift of $\Delta/2$ is given as

$$H^{\text{PM}} = \hbar\begin{pmatrix} \Delta & \frac{\Omega_1}{2}e^{iN\phi} \\ \frac{\Omega_1^*}{2}e^{-iN\phi} & 0 \end{pmatrix}. \tag{30}$$

The time-independent multiphoton detuning is defined as: $\Delta = \omega_R - N\omega$ (Fig. 2). However, in order to investigate the off-resonance behaviour of continuously modulated pulses, as in the single photon case, it is useful to perform an alternate rotating-frame transformation to a frequency modulated (FM) frame with the transformation function:

$$T^{\text{FM}} = \begin{pmatrix} e^{-iN\frac{\omega t+\phi}{2}} & 0 \\ 0 & e^{iN\frac{\omega t+\phi}{2}} \end{pmatrix} \tag{31}$$

to transform the N-photon laboratory Hamiltonian in Eq. (28) to the FM frame with an additional zero-point energy shift of $(\Delta - N\dot{\phi})/2$:

$$H^{\mathrm{FM}} = \hbar \begin{pmatrix} \Delta - N\dot{\phi}(t) & \dfrac{\Omega}{2} \\ \dfrac{\Omega^*}{2} & 0 \end{pmatrix} . \tag{32}$$

As in the single photon case, the time derivative of the phase function $\dot{\phi}(t)$, i.e., frequency modulation, appears as an additional resonance offset over and above the time-independent detuning Δ, while the direction of the field in the orthogonal plane remains fixed. The time evolution of the unrelaxed two-level system can then be evaluated by integrating the Liouville Eq. (9).

3.4. Multilevel systems

The ideal two-level system just discussed works for simple atomic systems, however, in most molecular systems; the inherent rovibrational substructure makes it into a multilevel situation. Nevertheless, the two-level picture discussed before can still be easily generalized to the case of n levels using the concept of density matrices. For an n-level system, the density matrix, $\hat{\rho}$, starts out as the "pure state" [63], which can be represented by the state vector. The initial state vector, Ψ is a sum of "bare states", ψ_n, each multiplied by its corresponding probability amplitude, c_n: $\Psi = \sum_n c_n\psi_n$, and $\hat{\rho} = |\Psi\rangle\langle\Psi|$. Each matrix element of $\hat{\rho}$ is written, $\rho_{nm} = c_n c_m^* = \langle\psi_n|\Psi\rangle\langle\Psi|\psi_m\rangle$, where c_m^* represents the complex-conjugate probability amplitude of c_m. In a mixed state, on the other hand, several different states, $\Psi(\theta)$, each labelled by a parameter, θ, are possible, such that, $\Psi(\theta) = \sum_n c_n(\theta)\psi_n$. If the probability that the system $\Psi(\theta)$ is in state $p(\theta)$, then the mixed state statistical operator is written as: $\hat{\rho} = \int_\theta |\Psi(\theta)\rangle\, p(\theta)\langle\Psi(\theta)|$, with matrix elements, $\rho_{nm} = \int_\theta p(\theta)c_n c_m^*$. When $\Psi(\theta)$ is time-dependent, the more complete expression is, $\Psi(\theta,t) = \sum_n c_n(\theta,t)\psi_n$, and the equation of motion (i.e., the Schrodinger equation) is written as

$$\frac{\mathrm{d}}{\mathrm{d}t}\, c_n(\theta,t) = -\frac{\mathrm{i}}{\hbar}\sum_k H_{nk}(t)c_k(\theta,t) = -\frac{\mathrm{i}}{\hbar}\hat{H}(t)c(t) \tag{33}$$

if the Hamiltonian is independent of the parameter θ. In terms of the density matrix, the equations of motion become:

$$\frac{\delta}{\delta t}\,\rho_{nm}(t) = \int_\theta p(\theta)\left[\frac{\mathrm{d}}{\mathrm{d}t}\, c_{n(\theta,t)}\right] c_m^*(\theta,t) + \int_\theta p(\theta)c_n(\theta,t)\left[\frac{\mathrm{d}}{\mathrm{d}t}\, c_m^*(\theta,t)\right] , \tag{34}$$

$$\frac{\delta}{\delta t}\,\hat{\rho}(t) = -\frac{\mathrm{i}}{\hbar}\sum_k \left(H_{nk}(t)\rho_{km}(t) + \rho_{nk}(t)H_{km}(t)\right) , \tag{35}$$

$$\frac{\delta}{\delta t}\,\hat{\rho}(t) = -\frac{\mathrm{i}}{\hbar}\left[\hat{H}(t), \hat{\rho}(t)\right] . \tag{36}$$

Eq. (36) is equivalent to the two-level Liouville Eq. (9) and is known as the 'von Neumann Equation', which can be integrated to solve for each matrix element of $\hat{\rho}$. So the concept of density matrices can be easily extended to the multilevel systems.

In the simple case of a molecular system having a single vibrational level in the ground and the excited electronic states, a set of n rotational states superimposed on each of the lower and the upper manifolds result in making the two-level system multilevel. This situation results in modifying the adiabatic passage principles applied to even simple diatiomic molecules [49] as is evidenced from experimental results discussed in the later sections. Theoretically, let us consider such a case for a single-photon transition in a closed shell diatomic molecule, where the rotational state selection rule is $\Delta J = \pm 1$, and for a linearly polarized laser, $\Delta M_J = 0$. The general Hamiltonian may be written as

$$H = \begin{pmatrix}
0 & 0 & 0 & 0 & & 0 & \frac{\Omega_1(t)}{2} & 0 & 0 & \\
0 & 2B'' & 0 & 0 & & \frac{\Omega_1(t)}{2} & 0 & 0 & \frac{\Omega_2(t)}{2} & \cdots \\
0 & 0 & 6B'' & 0 & \cdots & 0 & \frac{\Omega_2(t)}{2} & 0 & \frac{\Omega_3(t)}{2} & \\
0 & 0 & 0 & 12B'' & & 0 & 0 & \frac{\Omega_3(t)}{2} & 0 & \\
 & & \vdots & & & & \vdots & & & \\
\cdots & & & & & & & & & \\
0 & \frac{\Omega_1^*(t)}{2} & 0 & 0 & & \Delta_1 & 0 & 0 & 0 & \\
\frac{\Omega_1^*(t)}{2} & 0 & \frac{\Omega_2^*(t)}{2} & 0 & & 0 & \Delta_2 & 0 & 0 & \\
0 & \frac{\Omega_2^*(t)}{2} & 0 & \frac{\Omega_3^*(t)}{2} & \cdots & 0 & 0 & \Delta_3 & 0 & \\
0 & 0 & \frac{\Omega_3^*(t)}{2} & 0 & & 0 & 0 & 0 & \Delta_4 & \\
 & \vdots & & & & & & \vdots & &
\end{pmatrix} \tag{37}$$

where $\Delta_J(t) = [\Delta + 2B'J + \dot{\phi}(t)]$; B'' and B' are the ground state and excited state rotational constants, respectively, and Ω_J is the Rabi frequency for the transition which is given by

$$\Omega_{J\to J-1} = \sqrt{\frac{J^2 - M_J^2}{(2J-1)(2J+1)}}\,\frac{\mu\cdot\varepsilon}{\hbar} \quad \text{(P-branch), and} \tag{38a}$$

$$\Omega_{J\to J+1} = \sqrt{\frac{(J+1)^2 - M_J^2}{(2J+1)(2J+3)}}\,\frac{\mu\cdot\varepsilon}{\hbar} \quad \text{(R-branch)} \tag{38b}$$

for the various M_J values, and for $\Delta M_J = 0$ selection rule. Mathematically, for a given J-value Eq. (38) gives the same Ω_J. It is important to note here that this is not a general statement. In fact, on including the $\Delta M_J = \pm 1$ selection rule, the average matrix element for the R-branch is greater than that for the P-branch [64]. However, for the linearly polarized light cases generally used in the experiments of Ref. [49], one is restricted to the $\Delta M_J = 0$ condition, and the above Hamiltonian is adequate.

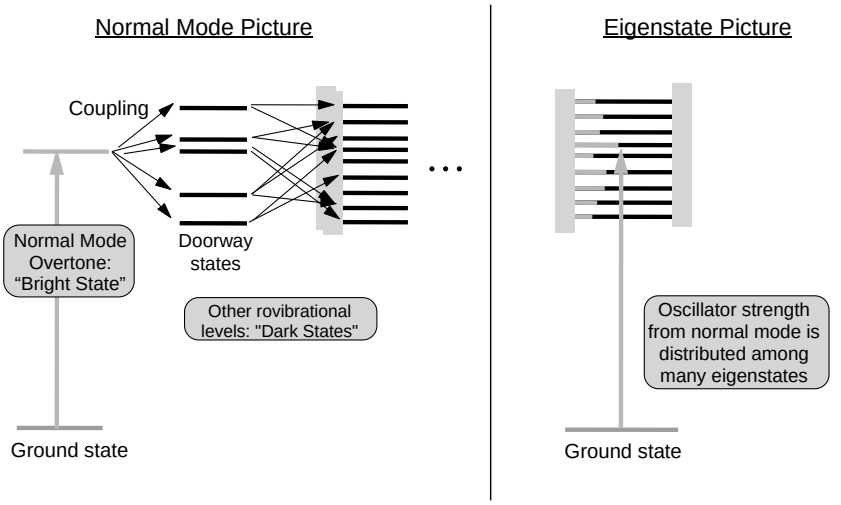

Fig. 6. Schematic of two equivalent pictures of intramolecular vibrational relaxation (IVR). The only way to reverse IVR is to change the eigenstates. Scaling of the number of levels in the dark states is possible although certain restrictions apply as mentioned in text.

3.5. *Multilevel systems involving intramolecular vibrational relaxation*

One of the most common aspects of molecules with vibrational manifolds is the intramolecular relaxation process. Let us next extend the two-level formalism discussed in the previous sections to the multilevel situation involving IVR. In the conventional zeroth order description of intramolecular dynamics, the system can be factored into an excited state that is radiatively coupled to the ground state, and non-radiatively to other bath states that are optically inactive (Fig. 6). These "dark" states have no radiative transition moment from the ground state as determined by optical selection rules. They can belong to very different vibrational modes in the same electronic state as the "bright" state, or can belong to different electronic manifolds. These dark states can be coupled to the bright state through anharmonic or vibronic couplings. Energy flows through these couplings and the apparent bright state population disappears. Equivalently, the oscillator strength is distributed among many eigenstates. The general multilevel Hamiltonian in the FM frame for an N-photon transition ($N \geqslant 1$), expressed in the zero-order basis set, is [65]

$$H = \hbar \begin{array}{c} \begin{matrix} \quad |0\rangle & |1\rangle & |2\rangle & |3\rangle & |4\rangle & \cdots \end{matrix} \\ \begin{pmatrix} 0 & \Omega_1(t) & 0 & 0 & 0 & \cdots \\ \Omega_1^*(t) & \delta_1(t) & V_{12} & V_{13} & V_{14} & \cdots \\ 0 & V_{12} & \delta_2(t) & V_{23} & V_{24} & \cdots \\ 0 & V_{13} & V_{23} & \delta_3(t) & V_{34} & \cdots \\ 0 & V_{14} & V_{24} & V_{34} & \delta_4(t) & \cdots \\ \vdots & \vdots & \vdots & \vdots & \vdots & \vdots \end{pmatrix} \end{array} \tag{39}$$

where, $\Omega_1(t)$ (and its complex conjugate pair, $\Omega_1^*(t)$) is the transition matrix element expressed in Rabi frequency units, between the ground state $|0\rangle$ and the excited state $|1\rangle$. The background levels $|2\rangle, |3\rangle, \ldots$ are coupled to $|1\rangle$ through the matrix elements V_{12}, V_{23}, etc. Both the Rabi frequency $\Omega_1(t)$ and the detuning frequency $[\delta_{1,2,\ldots} = \Delta_{1,2,\ldots} + N\dot{\phi}(t)]$ are time dependent (the time dependence is completely controlled by the experimenter). In general, the applied field would couple some of the dark states together, or would couple $|1\rangle$ to dark states, and thus, the V_{ij} terms would have both an intramolecular, time-independent component and a field-dependent component. As an alternative to Eq. (39), the excited states' submatrix containing the bright state $|1\rangle$ and the bath states $|2\rangle$, $|3\rangle, \ldots$ can be diagonalized to give the eigenstate representation containing a set of Δ_i' as diagonal elements and corresponding Ω_i' as off-diagonal elements. The eigenvalues of such a time-dependent Hamiltonian representation is often referred to as the dressed states of the system. Such a representation corresponds closely to what is observed in conventional absorption spectroscopy. As long as the intensity of the field is very low ($|\Omega_i'| \ll \Delta_i'$) the oscillator strength from the ground state (and hence the intensity of the transition, which is proportional to $|\Omega_i'|^2$ is distributed over the eigenstates, and the spectrum mirrors the distribution of the dipole moment. On the other hand, a pulsed excitation creates a coherent superposition of the eigenstates within the pulse bandwidth. Physically, in fact, the presence of the dark states is the key to the loss of selective excitation to a specified bright state and the root cause of the failure of the "bond-selective" chemistry.

From experimental results on the fluorescence quantum beats in jet-cooled anthracene [66], the respective values (in GHz) of $\Delta_{1,2,\ldots,4}$ are 3.23, 1.7, 7.57 and 3.7; and $V_{12} = -0.28$, $V_{13} = -4.24$, $V_{14} = -1.86$, $V_{23} = 0.29$, $V_{24} = 1.82$, $V_{34} = 0.94$. When these values are incorporated in Eq. (39), one obtains the full zero-order Hamiltonian matrix that can simulate the experimental quantum beats (Fig. 7) upon excitation with a transform-system, considerable dephasing occurs during the second half of the Gaussian pulse. Thus, in a coupled multilevel system, simple unchirped pulses cannot be used to generate sequences of $\pi/2$ and π pulses, as in NMR. The dark states start contributing to the dressed states, well before the pulse reaches its peak, and results in redistributing the population from the bright state ($|1\rangle$) into the dark states (Fig. 7).

The situation becomes completely different if the field is not merely a small perturbation. This is the essential idea behind multiple-pulse NMR, where pulse sequences effectively alter the spin Hamiltonian. One of the simplest experiments uses the spin locking [67] sequence $(\pi/2)_y - \theta_x$ as shown in Fig. 8a. The first pulse creates transverse magnetization (in NMR) or polarization (in optics) exactly in quadrature ($\pi/2$ out of phase) with the irradiating field. If the field is then suddenly phase shifted in quadrature, the vectors are collinear and there is no further time evolution.

A "dressed state" picture for a two level system [68] (Fig. 9) is also instructive. The resonant fluorescence spectrum, without the phase shift, generally reflects the four possible transitions between the dressed states that differ by one photon. Three peaks are observed with a driving laser field that has constant phase: a central peak at the laser frequency, plus two at the laser frequency $\pm(\Delta^2 + 4\Omega^2)^{1/2}$. One fluorescence peak has been experimentally demonstrated to disappear after $\pi/2$ phase shift [69]. The superposition produced by the first $\pi/2$ pulse is an eigenstate of the field-matter Hamiltonian of the phase-shifted field. When the dark states are included in this dressed state picture, they are not split under the strong field interaction (Fig. 9). If the Rabi frequency exceeds couplings to other states, the state that carries the oscillator strength effectively becomes an eigenstate of the field-matter Hamiltonian and the couplings are quenched [70]. In effect, *the multilevel system becomes a two-level system*. This is almost intuitive if phrased in terms of an AC Start effect: the

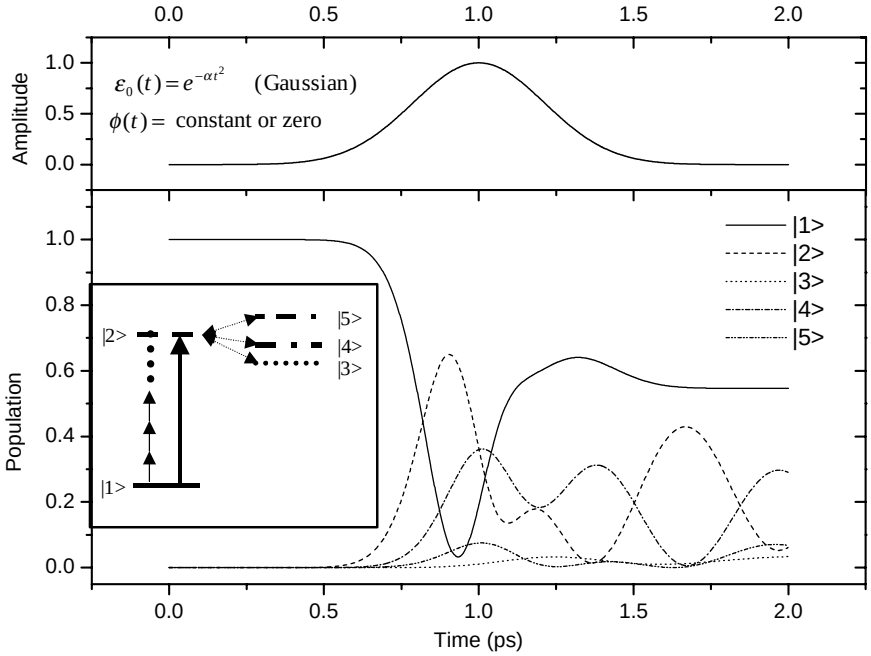

Fig. 7. When a simple Gaussian pulse interacts with a model anthracene system based on data extracted from experimental measurements (see inset) either under the usual single photon mode or under the Nth photon only multiphoton scenario as discussed in text, the population from the bright state gets quickly redistributed into the dark states, well before the pulse reaches its peak in time.

state with the oscillator strength can be shifted out of resonance from the finite number of dark states to which it is coupled (Fig. 9).

A few unsuccessful attempts at photon locking—the optical analogue to spin locking—have been reported [69,71] with laser sequences similar to Fig. 8a. There were several pronounced problems with such experiments. To start with only a small fraction of the inhomogeneously broadened line was fully resonant since these experiments used pulses with many nanoseconds duration. The abrupt transition in the field at the time of the $\pi/2$ phase shift guaranteed Fourier components and thus enabled excitation at "unlocked" off-resonance frequencies. Last but not least, Rabi frequency inhomogeneities made sure that molecules did not see the initial pulse as a $\pi/2$ rotation.

Through model calculations, Goswami et al. [65] have shown the use of tailored frequency sweeps to perform the optical analogue of spin locking (Fig. 8b). Use of frequency swept pulses avoids the technical complication of generating the $\pi/2$ phase shift, with the associated discontinuities in the excitation spectrum. It was shown for coupled multilevel systems that appropriate sweeps permit selective locking over a well-defined range of resonance frequencies with little excitation outside that range. Thus, in some cases, localization of bond energy in a molecule by stopping IVR has been shown to be possible. The specific case of a bright state coupled to a finite number of dark states was demonstrated (Fig. 10a). In the event of an infinite manifold of dark states, one would, at best, expect to see an oscillatory "locking" as one goes through the infinite manifold of coupled states, depending on the nature of these couplings. In practice, it turns out that the fields cannot

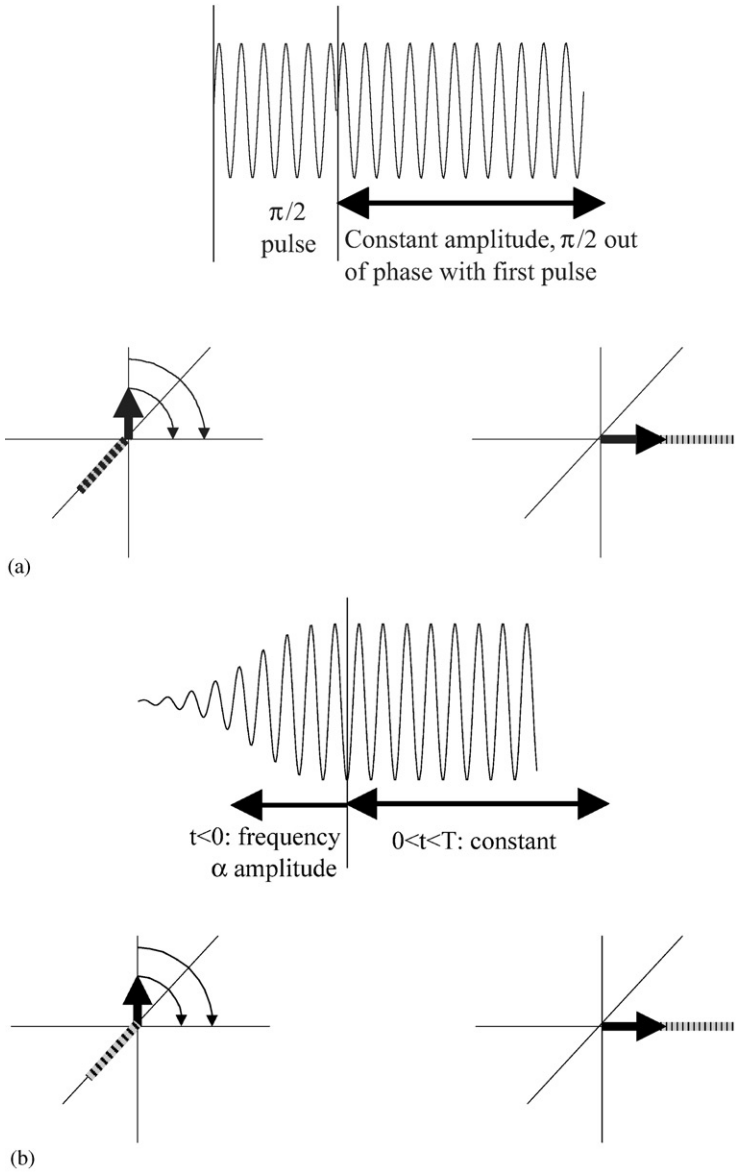

Fig. 8. Schematic of photon or spin locking by two different approaches. (a) A $\pi/2$ area pulse followed by a $\pi/2$ phase shift makes the field and the state vectors parallel. (b) A frequency sweep from far below resonance produces the same state without the sudden phase shift. This makes the swept approach much more practical.

be turned on or off abruptly; the shape of the transition region is crucial. Subsequent simulations also show that a modified version of an adiabatic half-passage experiment, using pulses, whose frequency is proportional to the intensity profile of the pulse [62], will perform photon locking without complications from inhomogeneities or partial excitation of other transitions (Fig. 10b). The frequency sweep turns on the excitation smoothly.

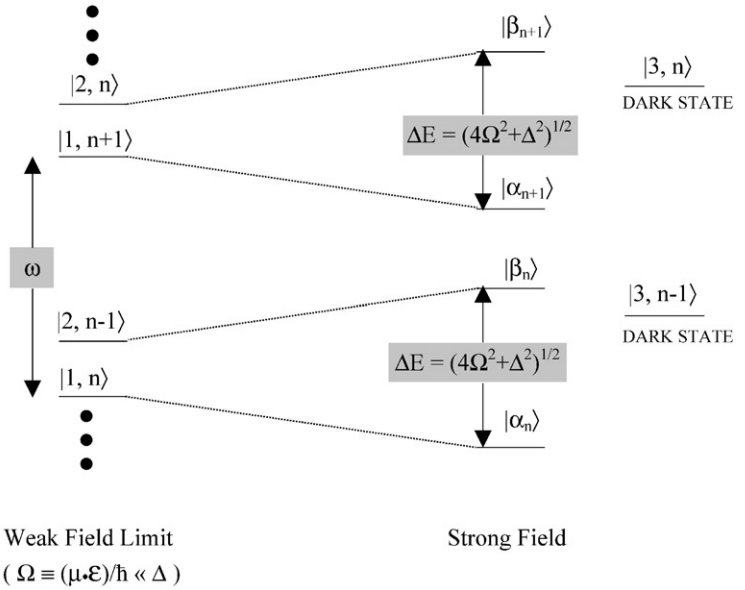

Fig. 9. Dressed state description of the energy levels ($|1\rangle$ is the ground state, $|2\rangle$ is the bright state, ω is the irradiation frequency, Δ is the resonance offset, and Ω is the Rabi frequency). Coincidences between the dressed states and the dark states can be controlled by frequency and amplitude modulation.

Recently, Goswami [51] shows that even simple linearly chirped pulses could restrict IVR in systems, at least as complex as investigated earlier [62,65] with complicated shaped pulses. He proves that higher-order chirps that distort the linear chirps experimentally, in fact, result in better performance in restricting IVR. In case of two-level systems, such shaped-pulses result either in population inversion or self-induced transparency. Similar results hold even in the extreme case of a two- or multiphoton transition occurring with a chirped pulse, where the lower-order photon processes are non-resonant. This makes these results more attractive, since the intensity of the laser fields needed to reach adiabatic limits often leads to multiphoton processes.

A linear sweep in frequency of the laser pulse (i.e., $\dot{\phi}(t)=2b_2t$) can be generated by sweeping from far above resonance to far below resonance (blue to red sweeps), or its opposite. For a sufficiently slow frequency sweep, the irradiated system evolves with the applied sweep and the transitions are "adiabatic". If this adiabatic process is faster than the characteristic relaxation time of the system, such a laser pulse leads to a smooth population inversion, i.e., an adiabatic rapid passage (ARP) [49,54]. If the frequency sweeps from below resonance to exact resonance with increasing power, and then remains constant, adiabatic *half*-passage occurs and photon locking is achieved with no sudden phase shift. However, even under adiabatic *full* passage conditions, Fig. 11 shows that there is enough slowing down of the E field to result in photon locking over the FWHM of the pulse. These results hold even under certain multiphoton conditions where only an Nth ($N \geqslant 2$) photon transition is possible [60]. Theoretically, scaling the number of dark states is possible as long as there is finite number of states and there are no physical limitations on Stark shifting.

The quadratic chirp, i.e., $\dot{\phi}(t)=3b_3t^2$, is the most efficient in decoupling the bright and dark states as long as the Stark shifting of these states prevail at the peak of the pulse. As the pulse is turned

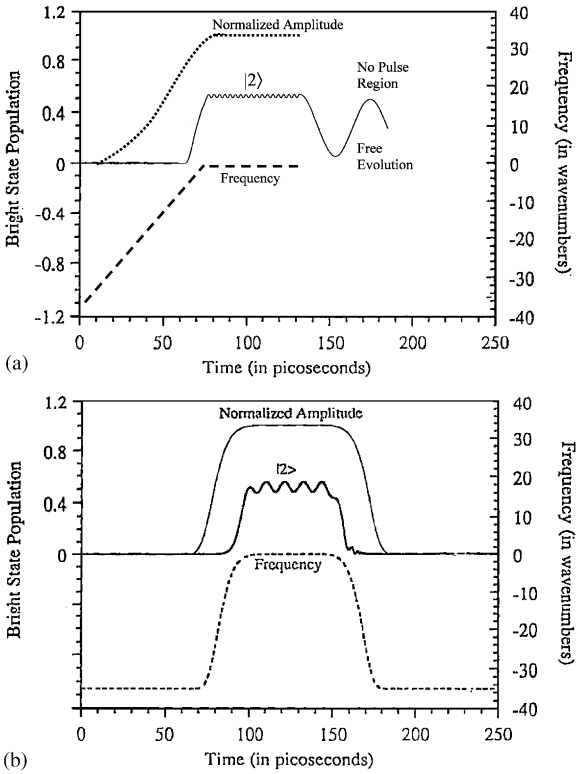

Fig. 10. Calculations for a model five-level Anthracene system as described in Fig. 7. (a) A Gaussian pulse with a frequency sweep linearly approaching resonance and then held constant can "lock" the population between the ground and the resonant excited state while the dark states are unaffected as long as the pulse is on. (b) A flat-top Gaussian pulse $[\varepsilon(t) = \exp(-\alpha t^8)]$ with frequency sweep proportional to the intensity of the pulse can produce the same effect. The pulse shapes in both the cases are shown on the plots for clarity.

off, the system smoothly returns to its original unperturbed condition (Fig. 12). This would be a very practical approach of controlling the coupling of the states with realistic pulse shapes. The cubic term, i.e., $\dot{\phi}(t) = 4b_4t^3$ behaves more like the linear term (Fig. 13). It also decouples the bright and dark states as long as the Stark shifting of these states prevail at the peak of the pulse. However, the oscillatory nature of the "photon-locking" shows that the higher-order terms in the Taylor series involve more rapid changes and fails to achieve perfect adiabatic conditions. As the pulse is turned off, it attempts to invert the bright state population, which quickly dephases, analogous to the linear chirp case. Thus, in an isolated two-level system that does not suffer from the population dephasing, the linear, cubic, and all the higher odd-order terms of the Taylor series (Eq. (10)) yield inversion of population, while the even-order terms produce self-induced transparency.

For a multilevel system, the induced optical AC Stark-shift by the frequency swept pulse moves the off-resonant coupled levels far from the resonant state leading to an effective decoupling. Under the perfectly adiabatic condition, pulses with the even terms in the Taylor series return the system to its unperturbed condition at the end. In fact, all higher-order odd terms behave in one identical fashion and the even terms behave in another identical fashion. It is only during the pulse, that

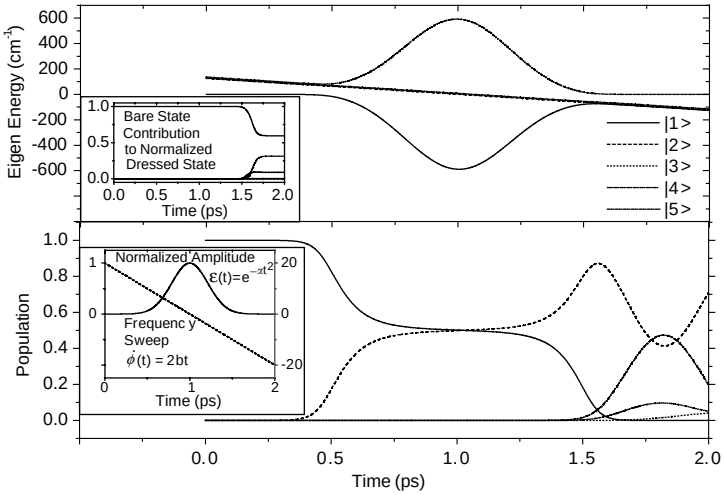

Fig. 11. A linearly swept Gaussian pulse (bottom inset, where $b_2 = 10\ \mathrm{cm}^{-2}$) can generate "photon-locking". The evolution of the dressed state character is unchanged while locking occurs (top inset) but as the pulse is turned off, the eigen-energy curves cross and the bright state population quickly dephases.

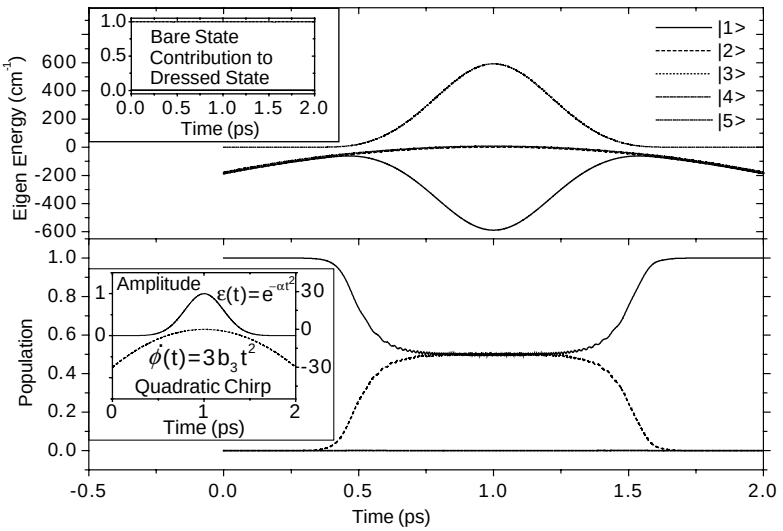

Fig. 12. The quadratic chirped Gaussian pulse (bottom inset, where $b_3 = 10\ \mathrm{cm}^{-2}$) is the most efficient in decoupling the bright and dark states during the pulse. The eigen-energy curves and the corresponding evolution of the dressed state character (top inset) shows that the entire process is highly adiabatic.

the Stark-shifting of the dark states are decoupled and IVR restriction is possible in the multi-level situation. In the present calculations, Goswami used equal values of b_n in Eq. (10), to bring out the effects of the higher-order terms in the series. In practice, since Eq. (10) represents a convergent

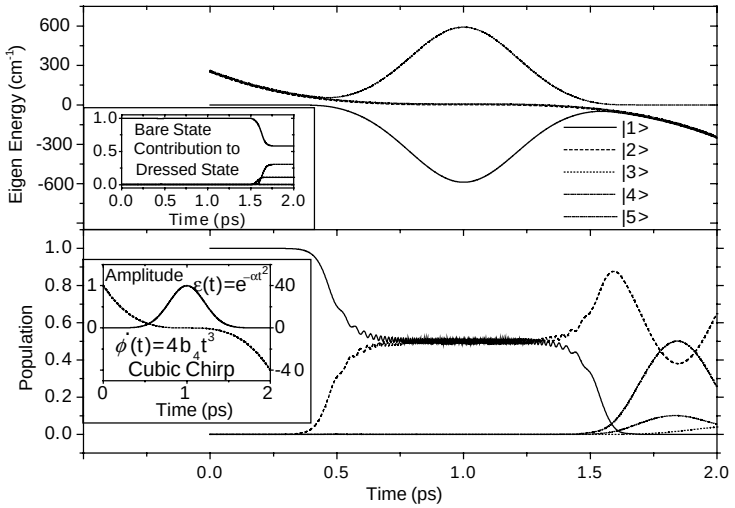

Fig. 13. Effect of a cubic chirped Gaussian pulse (bottom inset, where $b_4 = 10\ \mathrm{cm}^{-2}$) is similar to the linearly swept pulse (Fig. 11), although the evidence of population oscillation indicates that this chirp is not as adiabatic as the linear chirp. The eigen-energy curves cross towards the end of the pulse (top inset) and the bright state population gets redistributed.

series, only lower-order terms are more important, and since all higher-order terms produce the same qualitative results as the lower-order terms, one needs to consider only up to the quadratic term.

The results are generic and illustrate that the intramolecular dephasing can be kept to a minimum for the duration of the "locking" period under adiabatic conditions. Since the effect occurs under an adiabatic condition in all these frequency swept pulses, it is insensitive to the inhomogeneity in Rabi frequency. The simulations have been performed with laser pulses with Gaussian as well as hyperbolic-secant intensity profiles over a range of intensities. They show identical results of "locking" the population in the chosen excited state of a multilevel system, conforming to the adiabatic arguments that there is hardly any effect of the actual envelope profile. Promoting novel chemical reactions during photon locking, or completing several quantum-computing operations can, thus, be accomplished within the pulse before dephasing randomizes the initially prepared state.

Another useful application of the application of adiabatic passage has been in the anharmonic ladder climbing to produce vibrationally hot molecules, which are important in state-selective reactions. Quantum ladders can be used in the coherent control of chemical reactions; for instance, by exciting a specific molecular bond by climbing its vibrational ladder. One problem associated with transferring say a diatomic molecule to its high vibrational state step-by-step has been anharmonicity of its vibrations. This means that spacing between two levels does not stay constant and decreases as molecule climbs up the ladder. Thus, monochromatic laser sources turn out to be inefficient in this process. Corkum and coworkers [72] suggested the chirping the pulse with frequency decreasing as a function of time such as to follow the vibrational spacing. Their calculations showed that one could increase dissociation probability by many orders magnitude in this scheme. The ability to excite selectively chosen high vibrational states in the molecule of interest is very useful for controlling chemical reaction dynamics and in molecular energy transfer processes and the frequency swept pulse approaches would be quite useful. However, the high-power tunable infrared (IR) laser sources that

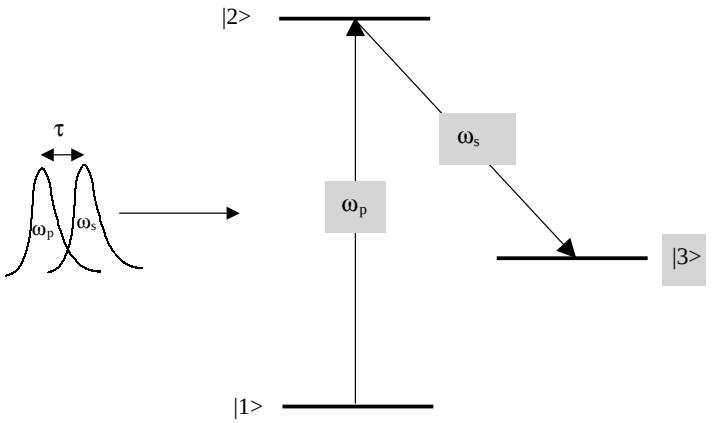

Fig. 14. Typical two-photon transition schematic for SEP and STIRAP. The pump laser (ω_p) connects the ground state and an intermediate level and the Stokes laser (ω_s) connects the intermediate level with the final, desired, energy state. In case of SEP, the pump and the Stokes pulses are applied almost simultaneously or one after the other ($\tau \geqslant 0$), whereas in case of STIRAP, the pulses are applied in the counterintuitive order ($\tau < 0$).

would be necessary for inducing vibrational transitions have not been available, and often, the demands still exceed today's technological state-of-the-art. This technology gap has spurred work with two-photon transitions, such as stimulated emission pumping (SEP) and stimulated Raman adiabatic passage (STIRAP).

3.6. Stimulated Raman adiabatic passage and stimulated emission pumping

A three level system as shown in Fig. 14 can generically represent the two-photon processes of SEP and STIRAP. The two lower levels represent vibrational energy states in the ground electronic potential and the third level represents an energy state in an excited electronic potential. Two laser pulses connect the levels. The pump pulse connects levels one and two, which correspond to one "thermally populated" vibrational level of the ground state and an electronically excited state level, respectively. The Stokes pulse connects levels two and three (a highly vibrationally excited level of the ground state, which shares favourable Frank–Condon factors with state two). In general, these processes are most efficient when each pulse is resonant with its corresponding one photon transition. In SEP [73], the Stokes and pump pulses can be applied simultaneously to "saturate" the transitions, thereby equalizing populations and producing about one-third of the population in the excited state. The Stokes pulse can be applied after the pump pulse if the pulses have insufficient intensity to saturate their respective transitions, and will produce some excited population. If the pulses are applied in the 'counterintuitive' order (the falling edge of the Stokes pulse overlaps the rising edge of the pump pulse, see Fig. 14) [74–77], it is the STIRAP process. In such a case, the Stokes pulse Stark-shifts the ground state vibrational levels so that when the pump pulse is irradiated upon the molecular system, transitions between vibrational states proceed adiabatically. STIRAP requires much higher pulse areas than does SEP, but is capable of eventually inducing complete inversion. The adiabatic character of the transitions also compensates for the Rabi frequency inhomogeneity (for example, from the transverse Gaussian distribution of the laser). Bergmann and co-workers have

used ARP with both CW and pulsed laser sources in STIRAP, the counterintuitive two photon two photon stimulated Raman configuration, to selectively populate excited vibrational states in molecules with nearly 100% efficiency [78]. In the STIRAP approach, ARP is achieved through proper intensity variations of laser field and by proper ordering of the electric field interaction sequence.

The control by phase modulation experiment by Broers et al. [79] is similar to the STIRAP process, which involves two successive adiabatic passages for a three level ladder system 5s–5p–5d of the rubidium atom (Fig. 15). This experiment showed that enhanced population transfer from the lowest 5s level to the highest 5d level occurs by using ultrafast frequency swept laser pulses. The idea was to use frequency sweep twice; first, it makes the pulse resonant with the 5s–5p transition and later with 5p–5d transition. Complete population transfer to upper state can be made in this fashion (Fig. 15). More important is the fact that if the intermediate state experiences severe decay, one would like to keep its occupancy low, which can be achieved by employing counterintuitive frequency sweep very well. The frequency sweep is reversed so that during the pulse, laser frequency is first resonant with the second step of the ladder and later with the first step. This kept the maximum intermediate population very low while the transfer to the upper state remains 100%. This method has some similarity to the STIRAP method where the Stokes and Pump laser are applied in the counterintuitive order. In STIRAP, the Stokes pulse that mixes the final and intermediate state is applied earlier to the Pump pulse that mixes the initial and intermediate state. However, it is important to note that there are limitations on ladder climbing at high intensities [80]. At high intensities, the ladder is distorted due to coupling with other states outside the ladder, which prevents efficient climbing.

In spite of STIRAP's success in creating molecular systems with high vibrational states, it is useful only for certain systems. The reasons being as follows: STIRAP is extremely sensitive to phase jitter in the laser pulses, and is not easily accomplished using nanosecond pulsed-lasers. Nonetheless, the large flip angle requirements (typically $50–100\pi$) make the application of ultrafast lasers very difficult: for example, a 1 ps π pulse requires 10^6 times greater peak power (10^3 times greater pulse energy than does a 1 ns π-pulse). Moreover, since the lasers must be tuned fairly close to the one-photon resonance of the pump and Stokes transitions, the onset of multiphoton processes often stop STIRAP at powers well below the real peak-power of an amplified ultrafast laser system. Consequently, the transition of interest must have a very strong dipole moment if the Rabi frequency is to be large enough for STIRAP to work. The excitation process is mostly very long (many ns) and hence only a small fraction of the thermally excited ground state distribution gets affected. Further features of STIRAP and SEP have been discussed in detail in a review article by Bergmann et al. [16]. There is another technique, useful for selective excitation of high vibrational states, which we discuss next.

3.7. Raman chirped adiabatic passage

Raman chirped adiabatic passage (RCAP) scheme was first proposed by Chelkowski et al. [81,82]. In this scheme (Fig. 16), the pump and Stokes pulses are far from their respective one-photon resonance, while the frequency difference between the pulses is tuned to the transition frequencies between adjacent vibrational levels in the ground electronic potential. Successive adiabatic transitions between these vibrational levels are produced by frequency chirping one or both of the laser pulses so that the difference in frequency between the two lasers follow the change in transition-frequency

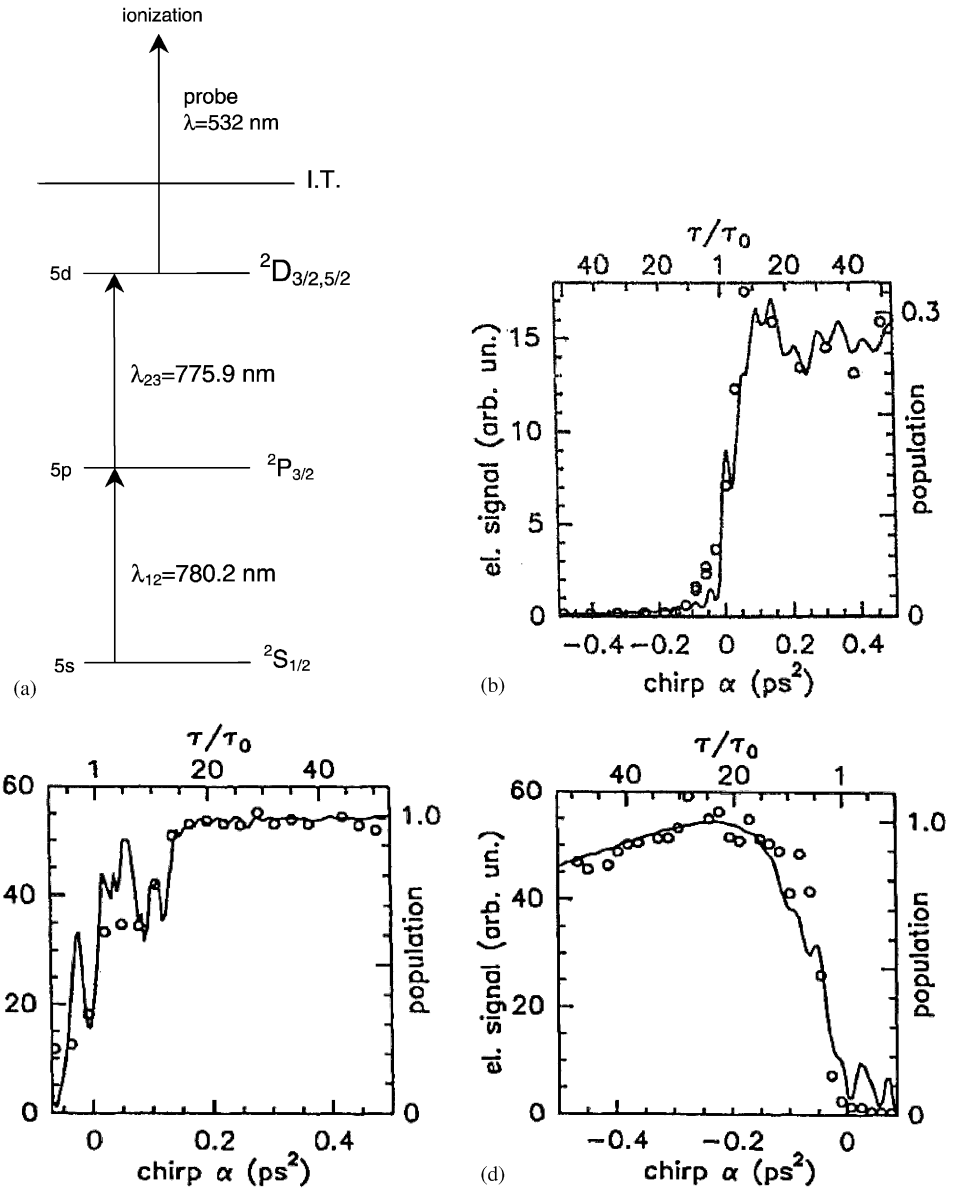

Fig. 15. (a) The three-state ladder energy levels in rubidium (Rb), showing the ionization threshold (IT). (b) Typical result of the measured photoelectron signal [open circles, (○)] and calculated potentials of upper level (solid curve) as a function of frequency sweep at relatively low energy per pulse (25 μJ/cm^2). Central wavelength ($\lambda_c = 778.5$ nm) and bandwidth ($\Delta\lambda = 5.8$ nm) were chosen such that λ_{12} (780.2 nm) and λ_{23} (775.9 nm) are within the pulse spectrum. Upper x-axis indicates the pulse duration (310 fs) relative to a chirp-free pulse. An intuitive red-to-blue sweep (chirp $\alpha > 0$) transfers much more population than the blue-to-red sweep (chirp $\alpha < 0$). (c) Population evolution at much higher laser powers (500 μJ/cm^2), but under similar conditions as in (b), i.e., $\lambda_c = 777.5$ nm and $\Delta\lambda = 5.8$ nm, full population transfer obtained for $\alpha > 0.2$ ps^2 (red-to-blue sweep). (d) However, at $\lambda_c = 780.8$ nm and $\Delta\lambda = 5.8$ nm at high energy (500 μJ/cm^2), full population transfer is obtained around $\alpha < -0.2$ ps^2 (counterintuitive blue-to-red sweep). Calculations show that for the red-to-blue sweep, halfway during the pulse, almost all population resides in the intermediate level. For the pulse with counterintuitive blue-to-red sweep, population of the intermediate state is strongly reduced.

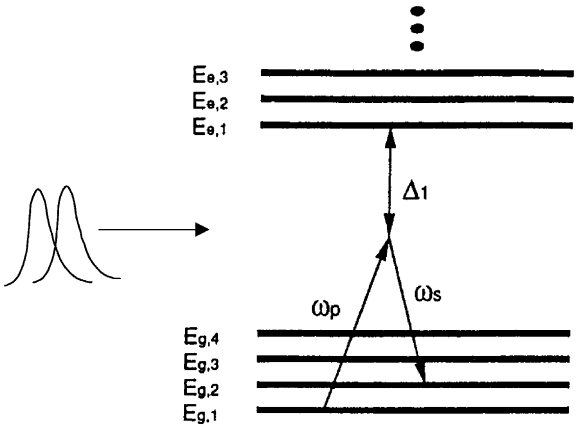

Fig. 16. Schematic of off-resonance Raman. Both Pump and Stokes laser pulses are tuned far from resonance.

between the adjacent vibrational levels. RCAP is and "off-resonance" Raman method. Thus, the one-photon detuning, Δ_1, between the laser pulses and the energy levels in the excited potential is large, whereas the two-photon detuning, $\Delta_{1,2} = E_{g,2} - E_{g,1} - (\omega_p - \omega_s)$, must be $\ll (E_{g,2} - E_{g,1})$, as depicted in Fig. 16. The system of Schrodinger equations describing this three-level system is as follows:

$$\mathrm{i}\frac{\mathrm{d}c_1}{\mathrm{d}t} = -E(t)\sum_{m=3}^{\infty} p_{1,m}\exp(\mathrm{i}\omega_{1,m}t)c_m \ , \tag{40a}$$

$$\mathrm{i}\frac{\mathrm{d}c_2}{\mathrm{d}t} = -E(t)\sum_{m=3}^{\infty} p_{2,m}\exp(\mathrm{i}\omega_{2,m}t)c_m \ , \tag{40b}$$

$$\mathrm{i}\frac{\mathrm{d}c_m}{\mathrm{d}t} = -E(t)\sum_{k=1}^{2} p_{m,k}\exp(\mathrm{i}\omega_{m.k}t)c_k \ , \tag{40c}$$

where c_n, are probability amplitudes, $p_{m,k}$ are transition moments, $\omega_{m,k}$ are the transition frequencies between levels m and k, $m = 3,4,\ldots$ is an index enumerating virtual states in the excited potential, and $E(t) = E_p\cos(\omega_p t) + E_s\cos(\omega_s t)$ is the net electric field comprised of the electric fields from the pump and Stokes laser pulses. All the virtual levels with $m = 3,4,\ldots$ can be "adiabatically eliminated" [33] by taking c_1 and c_2 out the integral and then integrating Eq. (40c) as long as the one photon detunings, $\Delta_m = \omega_{m,k} - \omega_p$, are sufficiently large compared with the Rabi frequencies between levels m and 1 and between levels m and 2 ($\Omega_{m,1}$ and $\Omega_{m,2}$, respectively). After integrating and further manipulating the system of Schrodinger equations (i.e., substituting c_m into Eqs. (40a) and (40b), and dropping all terms with frequency $\geqslant \omega_{1,2}$ with the use of the rotating wave approximation (RWA)) two-state equations for c_1 and c_2 emerge:

$$\mathrm{i}\frac{\mathrm{d}c_k}{\mathrm{d}t} = \sum_{j=1}^{2} q_{k,j}c_j \ , \tag{41}$$

where

$$q_{k,k} = -\sum_{m=3}^{\infty} \frac{p_{m,k}^2}{2}\,\omega_{m,k}\left(\frac{E_p^2}{\omega_{m,k}^2-\omega_p^2}+\frac{E_s^2}{\omega_{m,k}^2-\omega_s^2}\right)\ , \tag{42}$$

$$q_{2,1} = -\frac{\exp(\mathrm{i}\Delta_{1,2}t)}{4}\sum_{m=3}^{\infty}\Omega_{m,1}^p\Omega_{m,2}^s\left(\frac{1}{\omega_{m,1}-\omega_p}+\frac{1}{\omega_{m,1}+\omega_s}\right), \quad \text{and} \quad q_{2,1}=q_{1,2}^*\ . \tag{43}$$

$\Omega_{m,1}^p$ is the Rabi frequency corresponding to the 1 to m transition for the pump pulse and $\Omega_{m,2}^s$ is the Rabi frequency corresponding to the m to 2 transition for the Stokes pulse. Thus, an effective Rabi frequency between levels 1 and 2 may be defined as:

$$\Omega_{\mathrm{eff}}^R = \frac{1}{2}\sum_{m=3}^{\infty}\Omega_{m,1}^p\Omega_{m,2}^s\left(\frac{1}{\omega_{m,1}-\omega_p}+\frac{1}{\omega_{m,1}+\omega_s}\right) \tag{44}$$

and the effective detuning can be written as

$$\Delta_{\mathrm{eff}} = \Delta_{1,2}+q_{2,2}-q_{1,1}\ . \tag{45}$$

If the one-photon detuning is similar that the spacing between two vibrational levels, the equations for the effective Rabi frequency and effective detuning reduce to the three-state formulae:

$$\Omega_{\mathrm{eff}}^R = \frac{\Omega_{3,1}^p\Omega_{3,2}^s}{2\Delta}\ , \tag{46}$$

$$\Delta_{\mathrm{eff}} = \frac{(\Omega_{3,2}^s)^2-(\Omega_{3,1}^p)^2}{4\Delta}\ . \tag{47}$$

In this small detuning and weak-coupling regime, both STIRAP and RCAP yield similar results. However, when the one-photon detuning is large, STIRAP fails to produce the required population transfer—the Stark shifting caused by the STIRAP pump pulse cancels that caused by the Stokes pulse and Rabi oscillations between levels one and two result.

Theoretically, successive transitions "up the vibrational ladder" in oxygen induced by a series of RCAP pulses have been demonstrated [83]. The calculations specifically indicate that even in the presence of rotational levels, high vibrational states of oxygen and chlorine can be excited using a series of non-resonant Raman pulses, where both the pump and the Stokes pulses are chirped with linear frequency sweeps. Though high-powered lasers are necessary in the RCAP process to counteract the generally small transition-moments of the two-photon processes, such lasers are not one-photon resonant and high Rabi frequencies are often achievable before the laser damage issues set in. Thus, the laser pulse parameters (intensity and bandwidth) required in these calculations to invert population into high vibrational states via Raman chirped adiabatic passage are achievable using the technology that is currently available.

3.8. Wavepacket propagation

If we are interested in the final population content of the system under study, the approaches discussed until now are enough. However, it is often important to track the population evolution

as a function of time. In this context, it is important to have a more physical picture for the intermediate time-evolution intervals. With this in mind, let us introduce the concept of wavepackets and their propagation. A wavepacket is a coherent superposition of ground vibrational states of a molecule, such as, $|\Psi\rangle = \sum_n c_n \psi_n$ as defined for the state vector of the density matrix, which upon excitation evolves on the excited state potential energy surface [84]. The approach of wavepacket evolution forms the basis for the wavepacket recurrence study and in the time domain pump–dump coherent control issues discussed later.

Let us consider a time-dependent wavepacket $|\Psi(t)\rangle$ in a system whose field-independent Hamiltonian is H_0. The initial state of the wavepacket $|\Psi(t_0)\rangle$ can be related to some future state at time t with a unitary propagator $U(t,t_0) = \mathrm{e}^{-\mathrm{i}H_0 t/\hbar}$:

$$|\Psi(t)\rangle = U(t,t_0)|\Psi(t_0)\rangle \tag{48}$$

which is essentially the integrated form of the Schrodinger equation for the time independent Hamiltonian (used in Eq. (3)). Given that the H_0 is composed of non-commuting kinetic and potential operators T and $V(q)$, respectively, one can employ a split-operator approximation [85,86] to obtain the time evolution of the wavepacket over a small increment of time $\mathrm{d}t$, valid to second order:

$$|\Psi(t+\mathrm{d}t)\rangle = \mathrm{e}^{-\mathrm{i}V(q)\,\mathrm{d}t/2\hbar} \cdot \mathrm{e}^{-\mathrm{i}T\,\mathrm{d}t/\hbar} \cdot \mathrm{e}^{-\mathrm{i}V(q)\,\mathrm{d}t/2\hbar} \cdot |\Psi(t)\rangle \ . \tag{49}$$

Thus, given only the initial form of the wavepacket and the shape of the molecular potential, one can use Eq. (49) to calculate the state of the wavepacket at any time later. The form of Eq. (49) is computationally convenient. During each iteration of such a calculation, the wavepacket $|\Psi(t)\rangle$ is operated on by the first exponential, which is merely a multiplicative factor in the coordinate space. Then, a fast Fourier transform (FFT) routine [87] may be used to switch into momentum space, where the middle term is a multiplicative factor. Finally, an inverse FFT is used to transform back into the coordinate space and the wavefunction is multiplied by the final term in Eq. (49) to obtain $|\Psi(t+\mathrm{d}t)\rangle$. However, it is the interaction of the external optical field (Eq. (2)) with the evolving wavepacket, which is the important issue. Strictly speaking, in order for the Eq. (2) to be valid for propagation issues, the slowly varying envelope approximation $\dot{\varepsilon}(t) \ll [\omega(t) \cdot \varepsilon(t)]$ must hold. Let us consider a molecular system containing ground and excited electronic potential surfaces V_G and V_E, respectively. The field-inclusive laboratory-frame Hamiltonian H is the same as before: $H = H_0 - \mu \cdot E(t)$, where μ now represents the magnitude of the electronic transition dipole moment between V_G and V_E. The field, $E(t)$ has the perturbative effect of transferring population between the two molecular potentials. In the limit of small $\mathrm{d}t$ we can include the coupling effect into Eq. (48) by writing the following expressions:

$$|\Psi_\mathrm{G}(t+\mathrm{d}t)\rangle \approx U_\mathrm{G}(t,t+\mathrm{d}t)|\Psi_\mathrm{G}(t)\rangle + C_\downarrow(t)|\Psi_\mathrm{E}(t)\rangle \tag{50}$$

and

$$|\Psi_\mathrm{E}(t+\mathrm{d}t)\rangle \approx U_\mathrm{E}(t,t+\mathrm{d}t)|\Psi_\mathrm{E}(t)\rangle + C_\uparrow(t)|\Psi_\mathrm{G}(t)\rangle \ , \tag{51}$$

where $|\Psi_\mathrm{G}(t)\rangle$, $|\Psi_\mathrm{E}(t)\rangle$, respectively refer to the ground and excited state wavepackets; U_G, U_E refer to their propagators; and $C_\downarrow, C_\uparrow$ are "coupling operators" that transfer population between V_G and

V_E. These coupling operators can be written explicitly as

$$C_{\downarrow}(t) = \left[U_G\left(t + dt, t + \frac{dt}{2}\right)\right] \tag{52}$$

$$\times \left[\frac{i\mu_e E^*(t)\,dt}{\hbar}\right]\left[U_E\left(t + \frac{dt}{2}, t\right)\right] \tag{53}$$

and

$$C_{\uparrow}(t) = \left[U_E\left(t + dt, t + \frac{dt}{2}\right)\right] \tag{54}$$

$$\times \left[\frac{i\mu_e E(t)\,dt}{\hbar}\right]\left[U_G\left(t + \frac{dt}{2}, t\right)\right] \tag{55}$$

where $E^*(t)$ denotes the field's complex conjugate. The transient portions of the ground and excited state populations in Eqs. (50) and (51) evolve in their original states until $dt/2$, when they are instantaneously "pumped" into their respective destination states. Once these transitions have occurred, the transferred portions evolve for the remainder of the interval as per the evolution operators for their destination states. These methods are supposed to be generally applicable to the strong laser field conditions also.

The form of optimized fields to reach desired target-state $|\Psi_\Gamma\rangle$, at any time τ would depend on V_G and V_E, and can be obtained by performing time-reversed wavepacket propagation [88]. In this time-reversed calculation, we begin by setting the following initial conditions: $|\Psi_\Gamma\rangle$ is placed in V_E, while V_G is populated by some chosen $|\Psi_G\rangle$ (normally a populated eigenstate of V_G). The normalization constraint ($|\Psi_G|^2 + |\Psi_\Gamma|^2 = 1$) must be maintained, and τ is set to be the initial time. Thus, the complete initial conditions in this time-reversed calculation match the *final* conditions desired. To obtain raw information about the optical field necessary for creating these "initial" conditions, we merely propagate the system in time from $t = \tau$ to $t = 0$ (i.e., backward propagation), and calculate the overlap integral between the ground and excited wavepackets $\Phi(t) = \langle\Psi_E(t)|\Psi_G(t)\rangle$, at every instant in time.

Explicitly, the system can evolve backward in time by means of the time-reversed propagator: $U^{-1}(t, t - dt) = e^{iH\,dt/\hbar}$. This allows us to modify Eq. (48) to obtain

$$|\Psi_G(t - dt)\rangle = U_G^{-1}(t, t - dt)|\Psi_G(t)\rangle\ , \tag{56}$$

$$|\Psi_E(t - dt)\rangle = U_E^{-1}(t, t - dt)|\Psi_E(t)\rangle\ , \tag{57}$$

where

$$|\Psi_E(t)\rangle = U_E^{-1}(t, \tau)|\Psi_\Gamma(\tau)\rangle\ . \tag{58}$$

In principle, the optimal pumping field $F_\phi(t)$ in the rotating frame (and forward time) is related to $\Phi(t)$ by

$$E_\phi(t) = [\Phi^{-1}(t)]^*\ , \tag{59}$$

where $\Phi^{-1}(t)$ is the temporal inverse of $\Phi(t)$. It must be noted, however, that such fields when calculated in reality can be improved upon by other methods; it is often the case that the calculated

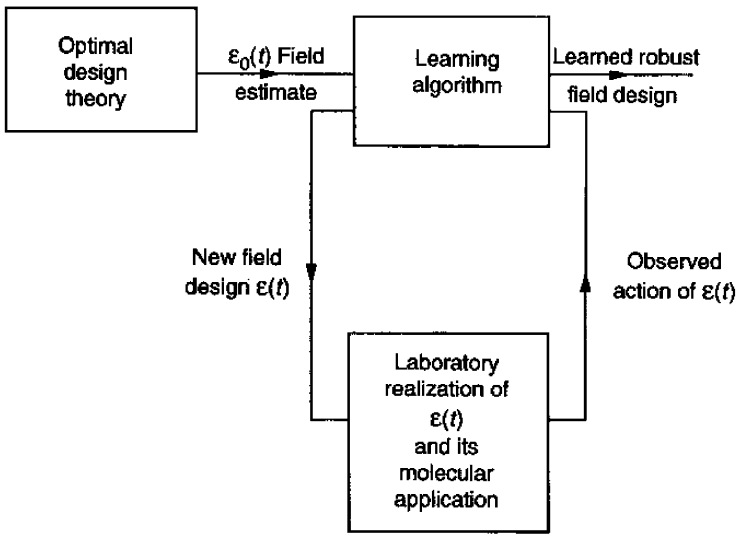

Fig. 17. Schematic of an adaptive-learning algorithm approach with iteratively shaped pulses for controlling molecules. The algorithm is initiated by an optimal control estimate $\varepsilon_0(t)$ of the control field, followed by its laboratory refinements in a computer-controlled sequence of experiments coupled to a learning algorithm.

pulses contains unwanted secondary "pulses" and other defects, which can be manually "filtered out" in order to manually improve the optimized waveform. This optimization approach has been popularly used in coherent control community as the optimal control scheme.

3.9. Optimal control theory

Optimal control theory is the method that enables one to design a laser field $E(t)$, which drives a system from an initial state $\Psi_0(t)$ at time $t=0$ to a final target state $\Psi_f(t)$ at a fixed time $t=T$. The problem can be formulated in terms of a functional that also takes into account experimental constraints. Varying this functional leads to a set of coupled differential equations for the desired laser field $E(t)$. Iteration results in an optimal field as a self-consistent solution to the system. The process essentially involves the idea of manipulating the frequency, envelope and phase of the pulse in order to create a shaped wavepacket whose evolution favours the dissociation to specific channels or creation of specific products. The optimized laser pulse shape was obtained for the specified initial and final states as two-point boundary value problem under the condition of fixed laser energy. This breakthrough concept is 'optimal control' or 'feedback control' and was theoretically proposed by Rabitz and co-workers [89] (Fig. 17), and was extensively used in various control experiments. Conceptually, one leaves the pulse designing for the fantasy of a learning loop that comprises a computer, a pulse shaper, the molecules and feedback spectroscopy. The computer offers a particular pulse shape that is shined on the molecule and subsequently a probe light is sent that analyses the effect of the shaped pulse. An evolutionary algorithm iteratively refines the shape until an 'optimal shape' produces the desired effect. Such global optimization computations can become very difficult as complexity of the molecule increases and perturbation methods are used for practical computations.

Fujimura and coworkers [90] have developed local optimization scheme, in which Schrodinger equation describing the time evolution of the system is divided into short time slices. The optimization is then carried out for each time slice with the approximation that the system remains invariant at such short time slices for evolution with the linear Schrodinger equation. This approach has been shown to be valid in both strong and weak field regimes. This approach of coherent control theory has been applied to dissociation of hydrogen fluoride, isomerization of hydrogen cyanide and pump–dump pulse control of reaction. Several previous authors [10,13,91] have extensively reviewed the concept of optimal control theory, and the reader is referred to them for further reading.

3.10. Driving wavepacket recurrences

A general feature of coherent control strategies is the spatial localization of nuclear or electronic wavepackets. For example, atomic ionization from a short, intense laser pulse can be suppressed by keeping the wavepacket away from the core of the atom. Charge oscillations in multiple quantum well structures can be generated by electronic wavepackets. In fact, the "Holy Grail" of chemical coherent control—laser selective bond breaking—can be viewed as a problem of localizing nuclear wavepackets on a dissociation coordinate. For example, an ultrafast pulse produces a wavepacket, which propagates on an excited electronic potential surface. When the wavepacket reaches the region of the potential that is Franck–Condon overlapped with the desired dissociative potential energy surface, a correctly delayed and phased dump pulse transfers this wavepacket onto the dissociative potential energy surface.

However, a major limitation to these techniques is the wavepacket dispersion, which occurs on anharmonic potential energy surfaces. Because the eigenenergies of an anharmonic oscillator are non-linearly spaced, an initially localized wavepacket will spatially dispersive as it propagates in an anharmonic potential. Techniques have been developed which can localize the wavepacket at an arbitrary position within the anharmonic potential energy surface actually focusses the wavepacket as it propagates. However, the time window over which the wavepacket is localized is still limited by the anharmonicity of the potential in the linear response regime. Furthermore, since spatial localization requires the excitation of multiple eigenstates with large quantum numbers, there is generally a trade-off between the initial localization of the wavepacket and the time period over which the localization will be maintained.

Wilson and coworkers have investigated theoretically [92] and experimentally [93] the waveform necessary to create a specific target state from the knowledge of potential energy surfaces of the molecule [94] by using the idea of optimal control techniques for wavepacket propagation. An interesting corollary to this work has also been theoretically demonstrated by Goodson et al. [95], which serves to extract the information of unknown excited potential surfaces in diatomic and in polyatomic molecules. In the weak-response limit, they calculate the laser pulses necessary to induce vibrational wavepacket recurrences in the excited state potential for Morse oscillators and a real system (the $X^1\Sigma^+$ and $A^3\Pi(1)$ states of IBr). The schematic of such approach is shown in Fig. 18 in case of a model Morse potential and in Fig. 19 for a real molecule IBr. It involves a modulated pump pulse to transfer the population from ground to set of target states on an excited surface, creating a vibrational wavepacket that evolves in time. With suitable modulation, the pump pulse induces a vibrational recurrence in Frank–Condon region. Then a dump pulse at the time of recurrence will depopulate the excited state. The optimization criterion is to create a desired recurrence in the

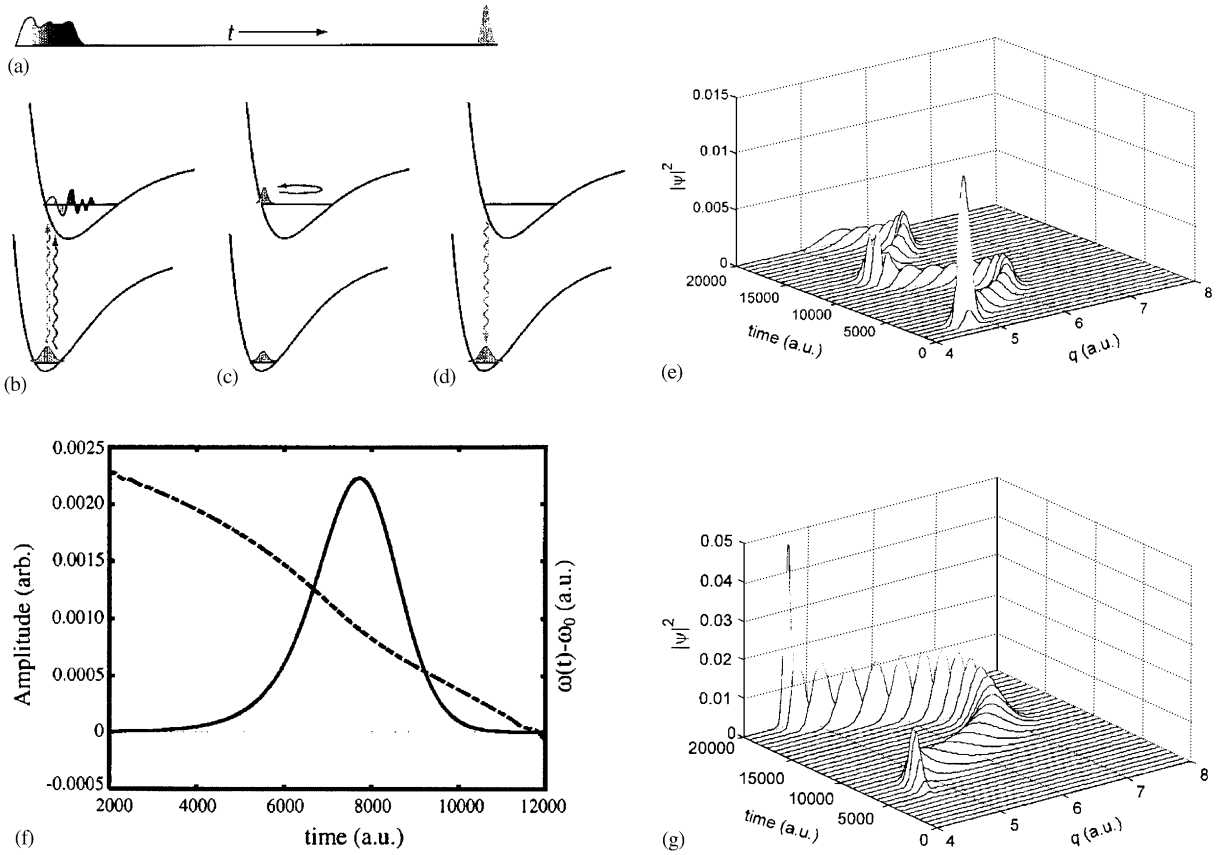

Fig. 18. Schematic of driving the wavepacket recurrences for a Morse Potential system: (a) A modulated pump pulse transfers the population from ground to a set of target states on an excited surface. (b) A vibrational wavepacket is created that evolves in time. (c) Suitably modulated pump pulse induces a vibrational recurrence in Frank–Condon region. (d) The recurred wavepacket can be dumped with an appropriately timed dump pulse. (e) Wavepacket propagation in the excited state potential induced by an unmodulated 1200 a.u. (30 fs) pulse. (f) Amplitude and frequency modulation for the pulse optimized for the wavepacket recurrence in a Morse system. (g) Wavepacket propagation in the excited state potential driven by the above optimized laser pulse. Note the strong recurrence at time $t = 20,000$ a.u.

sense that maximum depopulation takes place on the application of dump pulse. The performance of the optimized pulses was studied via simulated wavepacket propagation as developed in Eqs. (50), (51), (56) and (57). It is desired that $|\Psi_I(\tau)\rangle$ be shaped such that the ultrashort dump pulse effectively returns as much as of the excited state population as are physically possible. In the limit of a delta function (infinitely short) dump pulse, it follows that $|\Psi_I(\tau)\rangle$ must tend towards a scaled replica of $|\Psi_G\rangle$, with an appropriate displacement that centres it directly over the location of $|\Psi_G\rangle$ in the ground state potential.

In this limit, $|\Psi_G\rangle$ is replicated upon the excited state potential when an infinitely short pump pulse is applied; the action of the dump pulse can be intuitively treated as the time reversal of this behaviour. The modulation of the pulse can be done using various pulse-shaping techniques [14,38,30] and optimization can be achieved using learning control algorithms [45,96], which enable

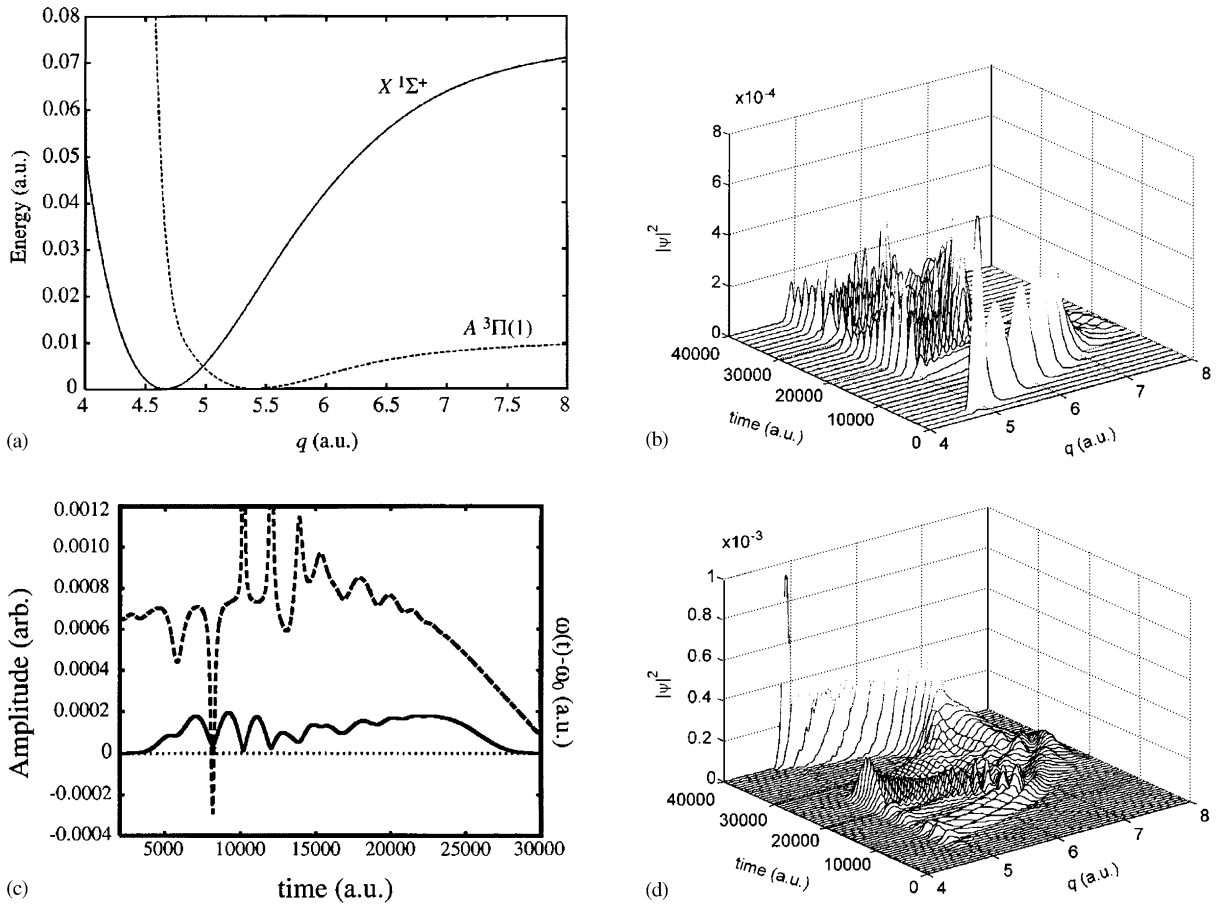

Fig. 19. Driving the wavepacket recurrences for a real molecule: (a) Ground and excited electronic state potential of the IBr molecule. (b) Wavepacket propagation in the excited state potential induced by an unmodulated 1200 a.u. (30 fs) pulse. (c) Amplitude and frequency modulation for the pulse optimized for the wavepacket recurrence for the IBr model. The modulation is more complicated than that described earlier for the Morse system. In spite of the complex frequency modulation, the overall negative chirp is still evident, especially in the latter portion of the pulse. (d) Wavepacket propagation in the excited state potential driven by the above optimized laser pulse. Note the strong recurrence at time $t = 40,000$ a.u.

testing of thousands of differentially modulated pump pulses per second. Such optimal light fields may be computationally generated given only the form of the electronic potential surfaces, knowledge of the particular ground state supplying population, and simple molecular constants. Thus, it should be possible to use the modulation of light fields experimentally optimized to achieve recurrences in order to obtain substantial information regarding previously uncharacterized potential surfaces in both diatomic and polyatomic molecules. This new characterization technique claims to improve upon the RKR method for a variety of situations (including mapping the potential wells of polyatomics, curve-crossing situations, and regions of wells that lie far beyond the Franck–Condon region), and be quite general in terms of its application to different magnitudes of applied field intensity on the system

under study. This would enable a more realistic assessment of the field free state ("unperturbed" state), besides providing an appropriate potential surface for most given field intensities where actual experiments are being conducted. A similar theoretical calculation and analytical solution has been presented by Walmsley et al. [97] for model multilevel system at high intensities.

3.11. Wavepacket pump–dump scheme

This technique proposed by Tannor and Rice [98] is based on wavepacket dynamics. First, a sequence of pump pulses is used to create a wavepacket of excited molecular states, where it evolves by translation and dephasing. Then another pulse sequence after some delay will dump the amplitude from the wavepacket of excited molecular states to the some reaction channel. This sequence of time-delayed pulses can follow two quantum paths to final products. The interference phase between two paths is related to the time delay between the pulses. Thus, for a given delay between the pump and the dump, the reaction channel will be selected based on the location of wavepacket on the potential energy surface for that delay. Greater selectivity results if both the phase structure of the pulses and the time delay between them are controlled.

In order to optimize the efficiency of this control scheme different experimental approaches have been utilized. One approach involves the control of ground state and/or excited state population by controlling the intensity of ultrashort laser pulse, which couples the electronic states. Control of population in an excited state can also be obtained by manipulating the relative phase between two pulses delayed in time.

Girard and co-workers [99] discuss the theory and experiment of temporal coherent control of Cs_2 photodissociation in detail. They create superposition of two vibrational wavepackets in bound electronic state of Cesium dimers using two identical femtosecond pulses. Quantum interference between them is controlled by time delay between the pulses and thus controlling the ionization probability. They also detect the oscillations between the wavepackets after the photoionization of the system. They show that they observe both, the interferences between quantum paths when pulses are well separated in time and the optical interferences between two pulses having temporal overlap and they can clearly distinguish between them.

As discussed above, the approach of using quantum coherence properties of light and matter to introduce quantum interference terms in the system dynamics has been quite successful for unimolecular processes. The control of bimolecular collision processes is, however, much more challenging. In a recent paper, Abrashkevich et al. [100] have demonstrated coherent control over bimolecular reactions. They show that by control over quantum reactive scattering can be obtained by scattering from initially prepared superposition of degenerate diatomic states. Their results of three-dimensional calculations for the reaction $D + H_2 \rightarrow H + HD$, indicate that reactive vs. non-reactive cross-sections can be extensively controlled by varying the phases and amplitudes in the initially prepared superposition state. As discussed above, the approach of using quantum coherence properties of light and matter to introduce quantum interference terms in the system dynamics has been quite successful for unimolecular processes. The control of bimolecular collisional processes is, however, much more challenging. Fleming and coworkers have shown that the development of a technique to control both the temporal separation of the pulses and the relative phases of the pulses at the optical carrier frequency has important implications on this type of pump–dump method.

Gerber and coworkers [102,103] and Zewail and coworkers [104] have done experimental work in the area of wavepacket pump–dump scheme. In order to optimize the efficiency of this control scheme different experimental approaches have been utilized. One approach (Gerber and coworkers) involves the control of ground state and/or excited state population by controlling the intensity of ultrashort laser pulse, which couples the electronic states. Zewail and coworkers, on the other hand show that by varying the time between the two pump pulses and probing the excited state population with a third pulse they could control population of the B-state of I_2. This control of population in the excited state was obtained through the adjustment of the time delay between the pump pulses, which, in effect, is manipulating the relative averaged phase between two pulses delayed in time. Similarly, Dantus and coworkers [105] have demonstrated the use of non-linear three pulse four-wave mixing based control of population transfer between ground and excited states, utilizing the intrinsic vibrational motion, in timing a pulse sequence that controls the excitation.

3.12. Control using interfering pathway

Mainly Brumer and Shapiro proposed this picture of control of chemical reactions [27,106]. They were one of the first to realize the importance of coherence and ways to use it in control of chemical reactions. The idea is based on often-quoted picture of Young's two slit experiments. Instead of interference between light waves, here we have a molecular analogue with quantum mechanical interference between the reaction pathways. In this scheme, at least two laser fields are used to create two coherent pathways between initial state and degenerate set of final states. The resulting Superposition State has information about final branching ratio of products in terms of the coefficients of its two different components (i.e. two different paths). Now these coefficients and hence the branching ratio is determined by the relative phases and amplitudes of the two laser fields. That means by varying the relative phases and amplitudes we can control the interference between the wavefunctions of the system produced by the different lasers and hence controls the outcome. The technical implementation of this method requires controlling the phase difference and amplitudes between the two CW-laser sources driving the different excitation routes. Gordon and co-workers have done important work in this area, which has been recently reviewed by them [10].

One of the important examples of frequency domain control in a chemical reaction has been shown by Zhu et al. [107] in selective photo-dissociation of molecules. In their experiment, HI molecules are excited above their ionization thresholds by two competing paths. One path involved absorption of three UV photons (ω_1 each) and other involved one-photon transition ($\omega_3 = 3\omega_1$). On controlling the phase between the lasers, the ion signals (HI^+ and I^+) were shown to be modulated due to interference between two channels. A definite phase lag was also observed between the two ion signals, with HI^+ signal lagging behind I^+ signal by $150° \pm 15°$. Various authors have also discussed the origin of this phase-lag theoretically [108,109]. Lee indicates the origin of phase lag due to effects of molecular phase and shows that his conclusions match the observations in the experiment discussed above.

Wang et al. [110] have demonstrated control over branching ratio of photoionization of atomic barium into two different continuum channels. Control is obtained over product state (which is ionic core state and photoelectron) distribution using interference between two two-photon excitation processes. Each interaction couples initial state of the absorbing system to the same final states in the continuum but they are resonantly enhanced by different intermediate states. The interference does

not depend on relative phases of the two lasers driving the process, but rather on phase relationship between two pathways. The strong interference in their experiments manifests as asymmetric line shapes of the photoionization spectra. It is interesting to note that authors observed destructive interference in the case when both the lasers were tuned to the resonance of the respective transitions.

Meshulach et al. [60] gives another example of quantum interference between two-photon transition probabilities. They demonstrated the coherent control of two photon transitions in cesium by tailoring the spectral phases of pulses. They use pulse shaper with programmable liquid-crystal spatial light modulator (SLM) to apply periodic spectral phase distributions. In certain symmetric spectral phase modulations about two-photon transition centre frequency, they are able to show the cancellation of transition probability due destructive interferences, the so-called dark pulses. They show better than one part in 200 control over the final transition probability by using spectral phase modulation.

3.13. Control of electron transfer reactions

Some theoretical studies [111] have been performed for the case of applied alternating current (ac) electric fields and CW laser fields on electron transfer reactions. These studies suggest that the progress of the non-adiabatic electron transfer reactions can be significantly perturbed and perhaps even controlled by varying the intensity or frequency of the applied field. In particular, coherent oscillations can be induced in the electronic state populations of an electron transfer reaction in a polar solvent by subjecting the system to a sequence of monochromatic laser pulses on the picosecond time scale. These oscillations are produced by pumping the system between different steady state distributions attained in the presence and absence of a strong continuous-wave electric field. Changing the pulse duration and the electric field strength may alter the amplitude and rise time of these time-dependent oscillations. The experimental realization of the proposed scheme will require strong electric fields ($\approx 10^7$ V/cm) and the effect will be most pronounced for activationless reactions. Such strong CW fields for polar liquids would lead to the possible complication of solvent dielectric breakdown [112]. Use of short pulses could alleviate this problem, since energy dissipation into the solvent is more efficient with short pulses. However, if the pulses get shorter than the electron transfer event itself, the CW electric field model adopted in these theoretical calculations breaks down, and new calculations based on dressed state picture are needed. Nevertheless, the CW laser calculations do indicate the experimental feasibility of modulating and controlling the ET reactions with the help of pulsed lasers.

4. Various aspects of experimental pulse shaping

Given the principles of pulse shaping, we now discuss the various experimental demonstrations of different pulse shaping techniques and some of their applications, which are essentially based on the principles discussed in the earlier section.

4.1. Frequency chirping

One of the easiest available pulse modulation schemes is frequency chirping. “Chirping” essentially refers to the process of arranging the frequency components in a laser pulse with certain phase

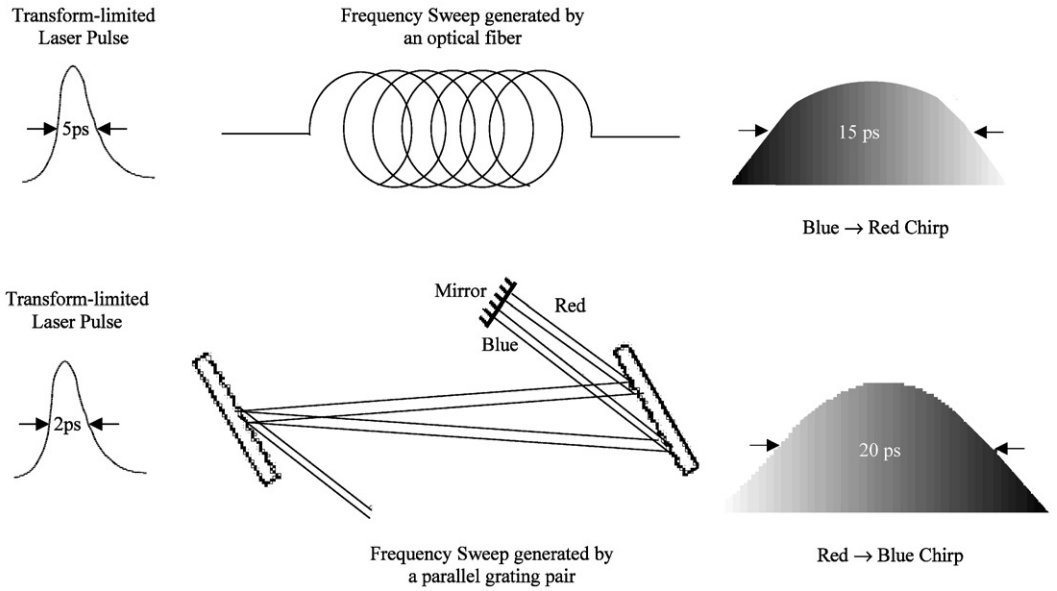

Fig. 20. Generation of linear chirp using either dispersion through fibre or by using a pair of parallel gratings. The sign of chirp is opposite in between the two cases and pulse length increases for both of then when they are chirped.

ordering. Linear "ordering" can be easily achieved by dispersing the ultrafast pulses through a pair of grating or through pulse propagation in optical fibre (Fig. 20). Due to the uncertainty principle, this "ordering" of frequency components results in the lengthening of an otherwise bandwidth-limited ultrafast pulse. Typically, linear frequency chirping is the most often used shaped pulses, although higher-order chirp generation and some of their recent experimental uses have also been predicted [51].

The first experimental demonstration of "control" using chirped pulses was by Warren and coworkers [49,54] in the early 1990s. Excitation by transform-limited pulses is not robust, since the degree of inversion is sensitive to the pulse area. Fig. 21a shows the plots of the upper-state population evolution as a function of applied Rabi frequency and detuning from the resonance frequency. The pulse used in this calculation is either a 2 ps transform-limited pulse, or a 20 ps frequency swept pulse of equivalent bandwidth for an isolated two level model as discussed above. The familiar Rabi oscillations occur when a transform-limited pulse excites the two-level system. In contrast, in the case of excitation by a frequency swept pulse, no Rabi oscillations occur. Instead, the degree of excitation rises to complete inversion when the Rabi frequency becomes strong enough to satisfy the adiabatic condition. Beyond this threshold, the inversion is robust, i.e., it remains insensitive to further increases in the applied Rabi frequency. This was experimentally demonstrated on quasi-two-level systems (pentacene/*p*-terphenyl crystal and Na vapour), quasi-three-level systems (Na vapour), and on more complex multilevel systems (I_2 vapour) [49,54]. Fig. 21b shows the experimental results corresponding to excitation of 0–0 line in pentacene/*p*-terphenyl mixed crystal system. It can be seen that in low field regime ($I_{\text{unchirped}} \leqslant 0.7 \times 10^8$ W/cm^2) fluorescence yield is the same for both

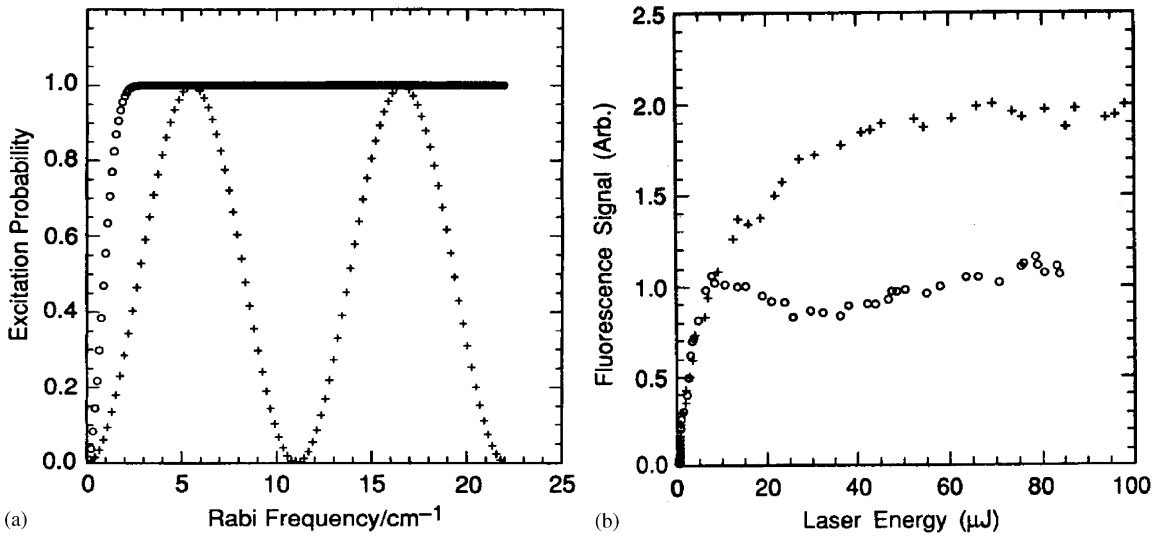

Fig. 21. Effect of linearly chirped laser pulses as compared to the transformed-limited pulses from theory and experiments. (a) Comparison of the probability of excitation as a function of applied Rabi frequency on a model two-level, for 2 ps transform-limited (Gaussian) pulses, indicated by crosses (+), and bandwidth equivalent 20 ps frequency-swept (Gaussian) pulses, indicated by circles (◯). (b) Fluorescence excitation curves for the pentacene/*p*-terphenyl mixed crystal system excited by 3 ps near transform-limited laser pulses, indicated by circles (◯), and by bandwidth equivalent 20 ps laser pulses chirped by the diffraction grating method, indicated by crosses (+). Each point is the average of 10 laser-shots.

unchirped and chirped cases. This is due to the fact that at low field the degree of excitation at frequency ω is proportional only to the pulse energy at frequency ω, hence any frequency modulation that does not alter pulse spectrum will have no effect. At high fields, the unchirped pulse shows Rabi oscillations with weak maxima and minima located at 8 and 30 μJ, respectively. The reasons for the weak maxima and minima in the Rabi oscillations are due to the well-known experimental issues like the laser inhomogeneity in real systems, in the contrast to the theoretical model results of Fig. 21a. The chirped case is very different from unchirped, and there are no Rabi oscillations but clearly the fluorescence excitation is nearly twice than that in unchirped case. In this regime, the condition for ARP is satisfied.

Fluorescence excitation spectra in a three-level system of Na-vapour were also obtained by pumping with chirped Gaussian pulses. It was shown that in the adiabatic limit there is selective excitation to one of the two Na 3p levels ($^2P_{3/2}$ and $^2P_{1/2}$) depending on the pulse-sweep direction, although the bandwidth of the pulse overlaps the two levels. However, when multilevel effects become significant, e.g. in a molecular system like I_2, which has complicated electronic transition structure due to the presence of rotational substructure, the success of simple frequency technique depends upon proper matching of the absorption spectrum of the material to the spectrum of the laser pulse and the fact remains that the high-J transitions are easier to invert than the low-J transitions. When rotational structure is important, even under the limit when the laser bandwidth becomes much broader than the spacing between rotational transitions, the infinite "rotational ladder" can prevent the expected effective collapse of a multilevel system to a two-level system. These results are shown in Fig. 22.

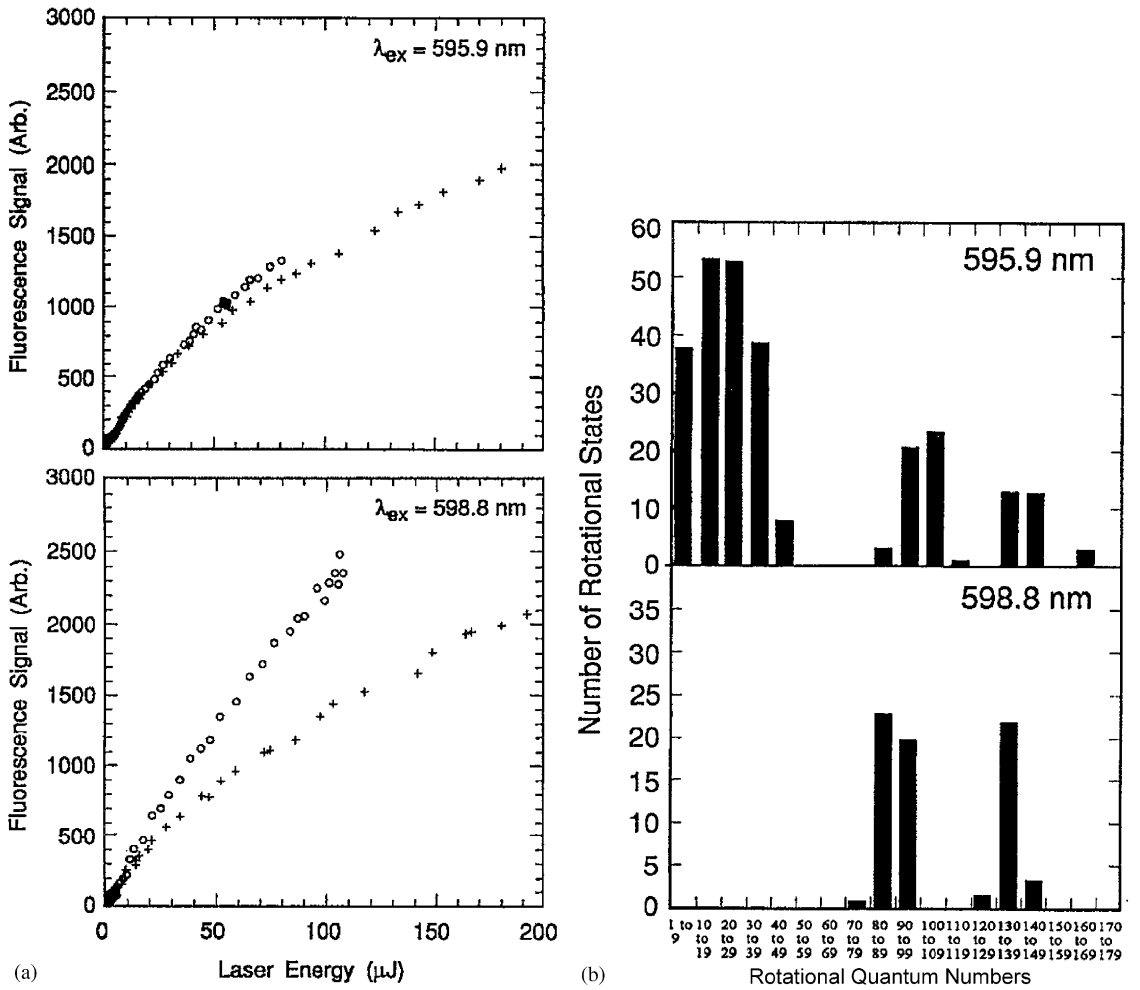

Fig. 22. Effect of rotational substructure on population inversion. (a) Fluorescence excitation curves for I_2 with 2 ps unchirped excitation [crosses (+)], and bandwidth equivalent 20 ps chirped pulse excitation [circles (◯)]. Two distinct cases are shown, which correspond to two different distributions of ro-vibronic transitions as shown by the histogram plots in (b): Case (I) $\lambda_{ex} = 595.9$ nm and case (II) $\lambda_{ex} = 598.8$ nm. Density matrix calculations with 100 model levels simulate the experimental results quite nicely as shown in (c).

4.2. Ultrafast phase-locked pulse sequences

G.R. Fleming and coworkers [101] developed an attractive method for setting and maintaining control of the relative phases of a sequence of femtosecond optical pulses. This particular application of the phase-controlled pulses in studying the transient fluorescence interferogram from I_2 is form of interference spectroscopy. Such an experiment offers a definite optical phase angle between the pulses while the interpulse delay is varied, which results in three different scenarios: in phase, in quadrature and out-of-phase pulse pairs (Fig. 23). The first pulse of a two-pulse sequence transfers

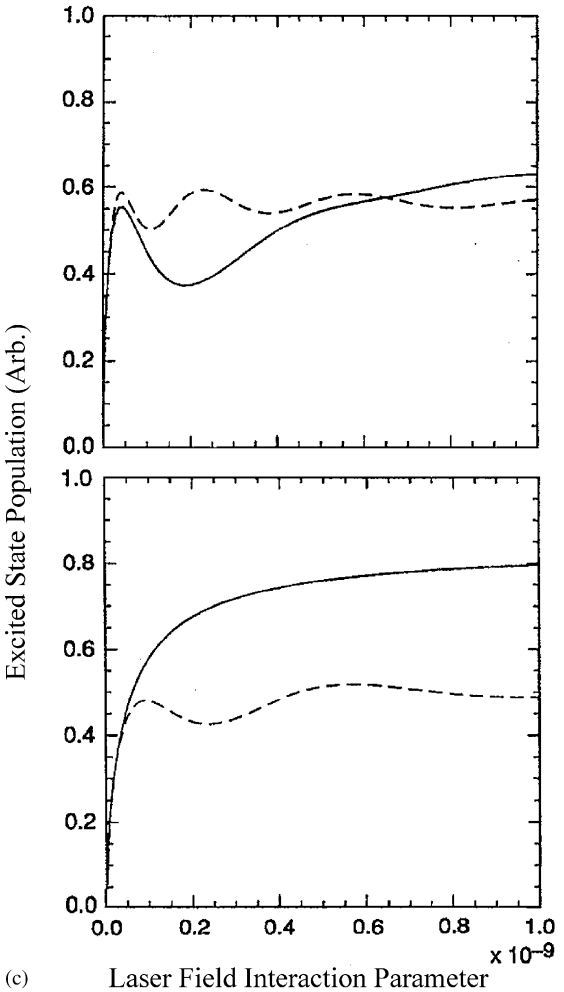

Fig. 22. *continued.*

probability amplitude from the electronic ground state vibrational wave function; that replica evolves as a wavepacket on the excited state potential energy surface during the interval between pulses. The second pulse of the sequence, whose phase is locked to that of the first one, also creates a wavepacket in the excited electronic state, which is in superposition t the initial propagated wavepacket. The average excited state population is determined after the second pulse by measuring the total fluorescence from a collection of identically driven molecules. This is related to but not identical with the Tannor–Rice scheme [98] for enhancing the formation of a selected product in a reaction, which was discussed in the control theory section. This version of phase-locked spectroscopy is designed to control the total population on the excited state surface by superposing amplitudes rather than control the population of a product formed in one region of the ground state as in the Tannor–Rice scheme. However, the emphasis on the role of the time delay between pulses to control transition probability is the same in both the cases.

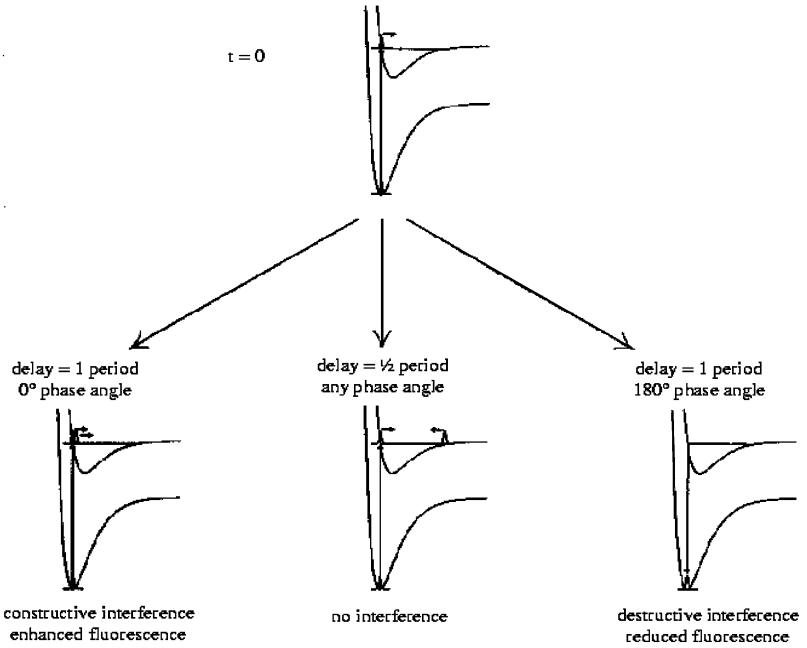

Fig. 23. Schematic illustration of wavepacket interferometry applied to molecular systems. First pulse prepares an excited-state amplitude; the subsequent pulse can cause constructive or destructive interference for relative phase angles of 0° or 180°. There is interference for delay times that are not integral multiples of the vibrational period of the excited state. This figure refers to a homogeneous system. In actual systems, the observed behaviour will result from a superposition of responses from the inhomogeneous ensemble.

4.3. Molecular pulse shaping

We discuss another interesting pulse shaping technique for molecules that uses the equal-arm interferometer setup. Consider iodine, for example, the spectrum of room temperature bulb has 5–10 transitions per wavenumber. Thus, even a 1 ps pulse with an approximate bandwidth of 13 cm^{-1}, excites about 100 different closely spaced transitions. Existing pulse shaping techniques neither can have such frequency resolution nor could generate such complex waveforms to generate efficient inversion. However, the molecule itself can generate such a complex waveform, since the optical free induction decay after a short pulse excitation would have the right frequency characteristics. Goswami et al. [113] applied this interferometric pulse shaping technique, by saving the free induction decay while deleting the original intense pulse with a Michaelson interferometer (Fig. 24). When the two arms of the interferometer are exactly equal, it produces constructive interference in one direction and destructive in the other independent of the wavelength. When the sample is inserted in one of the arms, it attenuates the resonant frequency components, and introduces phase shifts depending on the optical density of the cell. This results in the destruction of perfect cancellation in destructive interference direction, leaving only the molecular free induction decay. Misadjusting the interferometer by half wavelength separates the beams, thus separating the destructive interference direction from the input beam. The analysis with the 10 ps resolution streak camera verified that

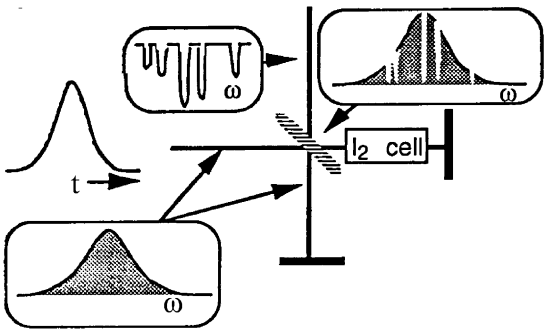

Fig. 24. Principle of Molecular Pulse Shaping in I_2 (for example). A Michelson interferometer with an iodine cell shapes a picosecond pulse to create a waveform which, when amplified, is extremely efficient for iodine inversion.

an elongated pulse was produced which, when amplified with an Excimer pumped dye amplifier resulted in efficient iodine inversion.

4.4. Liquid crystal modulated pulse shaping

The basic pulse shaping apparatus consists of a pulse shaping mask that is arranged inside a configuration known as a "zero dispersion pulse compressor", which consists of a pair of diffraction gratings and lenses (Fig. 1). The individual frequency components contained within the incident ultrashort pulse (that is usually bandwidth limited but not always) are angularly dispersed by the first diffraction grating, and then focussed to small diffraction limited spots at the back focal plane of the first lens, where the frequency components are spatially separated along one dimension. Essentially the first lens performs a Fourier transform, which converts the angular dispersion from the grating to a spatial separation at the back focal plane. Spatially patterned amplitude and phase masks (or a SLM) are placed in this plane in order to manipulate the spatially dispersed optical Fourier components. After a second lens and grating recombine all the frequencies into a single collimated beam, a shaped output pulse is obtained, with the output pulse shape given by the Fourier transform of the patterned transferred by the masks onto the spectrum.

In order for this technique to work as desired, one requires that in the absence of a pulse-shaping mask, the output pulse should be identical to the input pulse. Therefore, the grating and lens configuration must be truly free of dispersion. This can be guaranteed if the lenses are set up as a unit magnification telescope, with the gratings located at the outside focal planes of the telescope. In this case the first lens performs a spatial Fourier transform between the plane of the first grating and the masking plane, and the second lens performs a second Fourier transform from the masking plane to the plane of the second grating. The total effect of these two consecutive Fourier transforms is that the input pulse is unchanged in travelling through the system if no pulse-shaping mask is present. This dispersion-free condition also depends on several approximations, e.g., that the lenses are thin and free of aberrations, that chromatic dispersion in passing through the lenses or other elements which may be inserted into the pulse shaper is small, and that the gratings have a flat spectral response. Distortion-free propagation through the "zero dispersion compressor" has been observed in many experiments with pulses down to roughly 50 fs. For much shorter pulses, especially in the

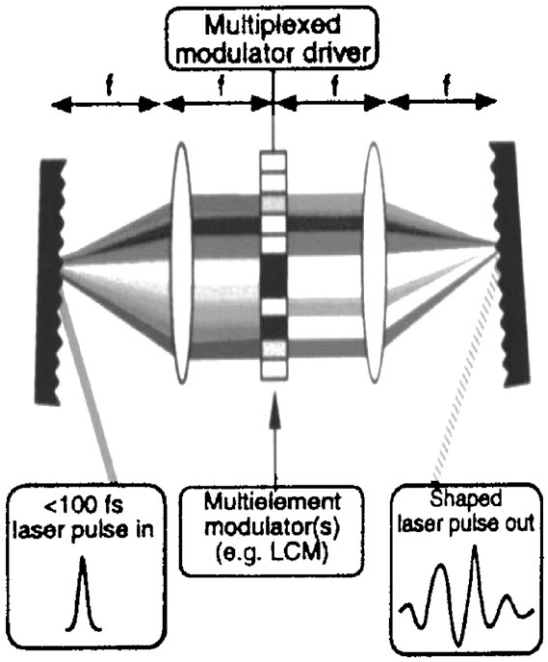

Fig. 25. Multielement liquid crystal modulators (LCM) in the Fourier plane of a 4-focal plane of a grating lens pair. Programmable change in the applied voltage to the LCM elements of the LCM array leads to programmable pulse shaping.

10–20 fs range, more care must be taken to satisfy these approximations. For example, both the chromatic aberration of the lenses in the pulse shaper and the dispersion experienced in passing through the lenses can become important effects. However, by using spherical mirrors instead of lenses, these problems can be avoided and dispersion-free operation has been obtained (Fig. 1b).

Use of liquid crystal modulator (LCM) arrays as spatial modulator generates a position-dependent transmission function or position-dependent phase shift on applying voltages and results in programmable pulse shaping (Fig. 25). The waveform update rate for the LCM arrays is limited by reorientation time of the liquid crystal molecules, typically on the order of 50 ms. The LCM arrays involve discrete pixels, and the index of refraction of each pixel can be changed for each pixel. The typical number of pixels is 128, and the best devices used till date have resulted up to 640-pixel resolution [114]. One ramification of the discrete pixels is the inter-pixel gaps that cause undesirable distortions and satellite peaks, which restrict the amount and nature of the phase shift that can be imposed and make the technique unsuitable for applications where sophisticated and complex frequency modulation is required [115]. The overall limitations for real LCM devices include slow update rate ($\leqslant 100$ Hz), complex modular alignment, pixel gaps, pixel calibration, and on–off isolation in individual pixels. These problems have been greatly reduced in recent years with the use of micro-lens arrays and advances in LCM technology. The simultaneous phase and amplitude modulation requires two LCM arrays [116], since a single LCM array can impose either phase or amplitude modulation. Furthermore, a 1024×768 programmable phase modulator is now available from Hamamatsu Corporation, which could become very effective in the near-future. A major

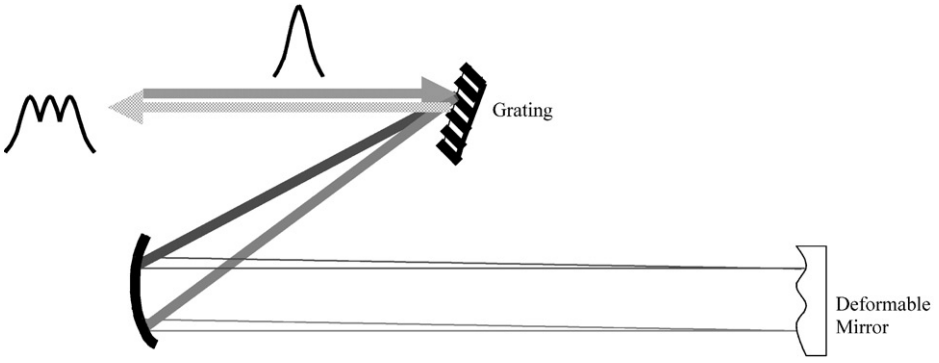

Fig. 26. Deformable mirror placed in the Fourier plane fold of a 4-focal plane of a grating lens pair generated shaped pulses.

advantage of the LCM pulse shaper lies in its significant light throughput. The LCM has minimum insertion loss, and also has the capability to hold the mask for high repetition rate lasers, such as the unamplified laser oscillators, thus avoiding the need for a pulse picker. The LCM pulse shaping scheme has been discussed in detail in several recent reviews [10,38].

4.5. Holographic patterned and deformable mirror pulse shaping

The spatial pulse shaper in Fig. 1 can also be a holographic pattern, written in some material that exhibits photorefractive effect. Holographic patterns are not subject to the limitations discrete pixelization and have been generated with approximately 100 effective pixel resolutions [43]. However, generation of the shaped hologram has not been achieved in real time to date, reducing the flexibility for quantum molecular control applications and data transmission rates in optical communications. The best results on generating programmable holographic grating by Ding et al. [117] are limited to the response of the photorefractive materials that are in the microseconds. Spatial pulse shaping scheme using deformable mirror [42] has also been used (Fig. 26). Currently, the number of pixel available from deformable mirror scheme is limited and experiments where only rudimentary shapes were sufficient to demonstrate the effectiveness of pulse shaping has been used.

4.6. Acousto-optic modulated pulse shaping

The acousto-optic modulator (AOM) pulse shaping technology in the spatial mode [41] uses a large aperture TeO_2 (visible) or InP (infrared) AOM crystal oriented at Bragg angle [118] at the central Fourier plan of a zero-dispersion line, which consists of a pair of gratings and a pair of lens in a 4-F configuration as shown in Fig. 27. A shaped RF signal driving the AOM's transducer creates an acoustic wave that propagates through the crystal. The AOM has a large clear aperture size of $50 \times 2.3\ \text{mm}^2$. The full-width at the half-maximum of the spectrum is ≈ 30 nm on the AOM, with the exact number depending on the focal length of the lens in the 4-F geometry, and the spectral width of the incident laser. The RF propagates at the speed of sound in the crystal, which is 4.2 mm/μs for the TeO_2 AOM. Light travels at a much faster speed of $\approx 2 \times 10^5$ mm/μs

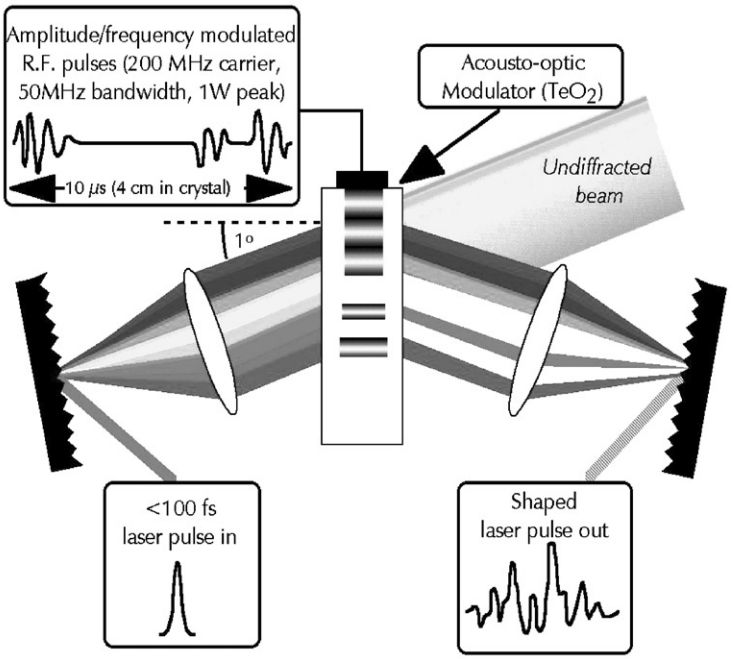

Fig. 27. Use of AOM at Bragg angle instead of LCM in the Fourier plane of a 4-focal plane of a grating lens pair offers background free high repetition (up to ~ 1 MHz as compared to only a few Hz in case of LCM) programmability.

in these AOM crystals. Thus, the acoustic wave looks like a fixed modulated diffraction grating at that moment [30]. The amplitude and phase of the acoustic wave determine the diffraction efficiency and phase shift at each position along at that point. the (spatially dispersed) laser beam The AOM is located in the central Fourier plane where the laser beam is dispersed in wavelength along the spatial axis x. It imposes both amplitude and phase modulation onto the spectrum of the input laser pulses in the way described above. The beam is diffracted ≈ 46 mrad by the AOM through the photoelastic effect [118]. The modulated spectrum of laser pulses is then collected by the second lens and is recombined by the second grating. Thus, one is able to impose essentially arbitrary modulations on the spectrum of laser pulses and, according to Fourier transform theory, achieve arbitrary pulse shaping of the laser pulses in time. The amplitude and frequency modulation of the RF signal completely controls the output laser pulse shape. A continuous RF wave does not alter the frequency spectrum of laser pulses, apart from a linear phase shift, which conserves the shape of input pulses. If the input pulse is extremely short (20–30 fs) one has to compensate for dispersion in the material and slightly different path lengths and diffraction angles for the different optical frequency components. The corrections are straightforward and not an important issue for the pulse lengths $\geqslant 80$ fs. However, it is important to use reflective curved mirrors instead of lenses as in Fig. 1b (with the AOM in place of the mask) for the ultrashort pulses (< 50 fs).

There have also been recent developments in pulse shaping technology with the help of acousto-optic programmable dispersive filter (AOPDF) [119], which is based on a collinear acousto-optic interaction that maximizes the interaction length. Currently available as commercial product [120] for

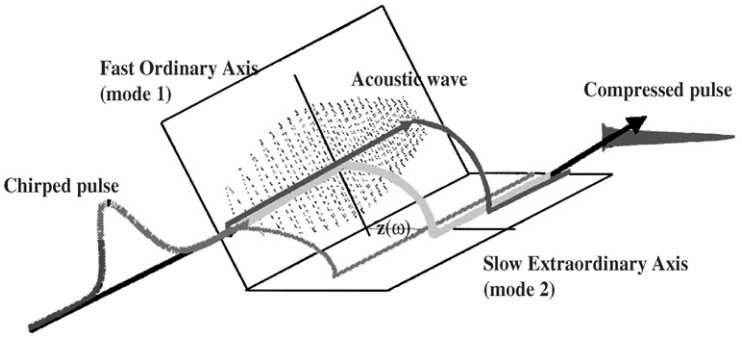

Fig. 28. Schematic of AOPDF pulse shaping for generating compressed pulses.

large dispersion compensation of femtosecond pulses, the AOPDF does not have to be positioned in the Fourier plane of a dispersive line which makes it a compact device. Fig. 28 shows a schematic of AOPDF concept where the amplitude of the output pulse, or diffraction efficiency, is controlled by the acoustic power at position $z(\omega)$. Since the technique involves a long material interaction length (e.g., 2.5 cm TeO_2 for 3 ps group-delay range), either a chirped pulse input or a compressor after the AOPDF is necessary for dispersion compensation. A maximum resolution of 450 points is expected in the 3-ps group-delay range with a maximum efficiency of 30%. Further work on this promising approach is in progress [121]. Hereafter, will focus on the more established spatial AOM pulse shaping issues.

4.6.1. *Principles of spatial acousto-optic modulated pulse shaping*

Let us assume the input laser pulse has a Gaussian spatial profile with the beam waist of a. In the frequency domain such a laser pulse is given by

$$E_{\text{in}}(t) = \frac{1}{2\pi}\int_{-\infty}^{\infty} E_{\text{in}}(\omega)\exp[\mathrm{i}(\omega-\omega_0)t]\,\mathrm{d}\omega\ . \tag{60}$$

According to Danailov and Christov [122], the output laser pulse after the second lens and grating pair in frequency domain is going to be:

$$E_{\text{out}}(\omega) = \int_{-\infty}^{\infty} E_{\text{in}}(\omega)\exp\left\{-\frac{\left[x-\frac{\alpha}{2\pi}(\omega-\omega_0)\right]^2}{2\gamma^2\left(\frac{f\lambda_0}{2\pi a}\right)^2} + \mathrm{i}\,\frac{x-\frac{\alpha}{2\pi}(\omega-\omega_0)}{\gamma\frac{f\lambda_0}{2\pi a}}x_{\text{out}}\right\}M(x)\,\mathrm{d}x\ , \tag{61}$$

where as before, x is the spatial axis along which the laser beam is dispersed in wavelength. The AOM is located in the central Fourier plane (x, y). The dependence of amplitude on the variable y is that given by propagation in free space. x_{out} is the x-axis respect to the output beam propagation. The dependence of the electric field on x_{out} gives the field distribution normal to the field propagation. λ_0 is the central wavelength of the laser pulse, ω is the laser frequency, ω_0 is the central laser frequency, f is the focal length of the lenses in the 4-F configuration, and γ is the geometrical

factor that accounts for the beam size change when the direction of beam propagation changes, which is defined by

$$\gamma = \frac{\cos\theta_{\text{in}}}{\cos\theta_{\text{out}}} \tag{62}$$

where θ_{in} is the input angle to the first grating and θ_{out} is the output angle of the centre wavelength out of the first grating. Since 4-F configuration is symmetric respecting to the central Fourier plane, the input angle and output angle are reversed at the second grating so that all the frequency components can be recombined properly. Note that the denominator of the quadratic term in the exponential function, viz., $\gamma(f\lambda_0/\pi a)$, is actually the effective Gaussian beam waist after the first lens/grating pair for single frequency component which occurs at the central Fourier plane. Also, in Eq. (61), α is the dispersion parameter that is defined in terms of the grating period Λ, velocity of light c, central laser wavelength λ_0, and the focal length of the lens f, as

$$\alpha \equiv 2\pi\frac{\partial x}{\partial\omega} = -\frac{\lambda_0^2}{c}\frac{f}{\Lambda\cos(\theta_{\text{out}})}\ . \tag{63}$$

It is usually expressed in the units of mm/THz. Finally, $M(x)$ is the modulation pattern created by the acoustic wave along the central Fourier plane. The spatial coordinate x is related to the RF time t_{RF} by the velocity of the acoustic wave in the crystal, V_{ac} through the relation:

$$x = V_{\text{ac}}t_{\text{RF}}\ . \tag{64}$$

When the modulation function $M(x)$ is a slowly varying function in comparison to the exponential term in Eq. (61), which requires that the smallest feature of $M(x)$ is larger than the effective Gaussian beam waist at the central Fourier plane, i.e., $\gamma(f\lambda_0/\pi a)$, Eq. (61) can be simplified to

$$E_{\text{out}}(\omega) = E_{\text{in}}(\omega)M(x)\big|_{x=\frac{\alpha}{2\pi}(\omega-\omega_0)} = E_{\text{in}}(\omega)M(\omega)\ . \tag{65}$$

Eq. (65) is similar to Eq. (1) on which the spatial pulse shaping technology is based. Eq. (65) also establishes a relationship between the spatial coordinate x and the laser frequency ω:

$$x = \frac{\alpha}{2\pi}(\omega-\omega_0)\ . \tag{66}$$

Use of Eq. (64) with (66) also enables to establish a relationship between the laser frequency ω and the RF time t_{RF} as

$$(\omega-\omega_0) = \frac{2\pi V_{\text{ac}}}{\alpha}t_{\text{RF}}\ . \tag{67}$$

The temporal shape of the output laser beam can be obtained by Fourier transforming Eq. (65), which is

$$E_{\text{out}}(t) = \frac{1}{2\pi}\int_{-\infty}^{\infty} E_{\text{in}}(\omega)M(\omega)\exp[\mathrm{i}(\omega-\omega_0)t]\,\mathrm{d}\omega\ . \tag{68}$$

In the actual experimental set-ups used in the Warren group [41,125–127], the input beam waist a was estimated to be 2.27 mm assuming Gaussian input beam. For the communication relevant laser pulse whose central wavelength is 1.55 μm, 1100 groves/mm dense grating was used, which

gives the grating period Λ as 0.91 μm. The focal length of the lens pair was 125 mm. The velocity of the acoustic wave in the InP AOM material V_{ac} is 5.1 mm/μs. The dispersion parameter α is about 1.887 mm/THz by fitting the experimental data with theory; the output angle of the centre wavelength θ_{out} is calculated using Eq. (63) to be 54.3°. According to grating equation

$$\lambda = \Lambda(\sin\theta_{in} + \sin\theta_{out}) \ . \tag{69}$$

θ_{in} is estimated to be 63.2°; so the geometric factor γ is 0.77; and the effective Gaussian beam waist at central Fourier plane is $\sim$ 21 μm. The smallest feature size that was put into the modulation is larger than 100 μm and therefore satisfied the requirement of approximation used in Eq. (65). For the 800 nm central wavelength, 1800 groves/mm dense grating was used, which gives the grating period Λ as 0.91 μm.

Experimentally, as mentioned before, an acoustic optic modulator usually consists of a crystal (e.g., InP or TeO_2) with an attached piezoelectric transducer (Fig. 27). The transducer converts RF signals into a travelling acoustic wave, which interacts with light field in the crystal through the photoelastic effect. Since the speed of light in crystal is much larger than the speed of sound, when a laser pulse is passing through the crystal the travelling acoustic wave moves in very small amount of distance and essentially the light pulse only sees a fixed acoustic modulation pattern in the crystal. The complex amplitude of this fixed acoustic modulation pattern in the crystal along the x-axis is essentially the modulation function $M(\omega)$ (with a difference of a constant factor that is related to the photoelastic coefficient of the material), in which the laser frequency ω is now scaled to the spatial coordinate x in the central Fourier plane through the dispersion of the first grating and the collimating for different frequency components by the first lens [123] as in Eq. (66), which again through Eq. (64) connects to the RF time. Hence the modulation function $M(\omega)$, ideally, is directly proportional to the complex amplitude of the RF signal, $M_{RF}(t_{RF})$, which is imposed on a carrier RF wave of central frequency at 150 MHz in these experiments. As shown in Fig. 29, one channel of modulation signal corresponds to the real part of the desired waveform and is mixed onto the in-phase version of the carrier wave. The second channel of modulation signal corresponds to the imaginary part of the desired waveform and is mixed onto the $\pi/2$ phase-shifted carrier wave. The real and imaginary parts are then recombined with a 0° splitter/combiner. The real and imaginary parts of the temporal RF waveform then correspond to the desired real and imaginary parts of the laser spectrum. Any imperfectness of this quadrature circuit can be balanced by precompensating the relative amplitudes and phases between two channels of the waveform generator.

Since this pulse-shaping technique uses a travelling wave AOM, the acoustic waveform has to be properly centred in the crystal for single laser pulse per acoustic transit time as also indicated by other authors [124]. The effective laser repetition rate must be reduced to the AOM repetition rate with a pulse picker. In Yang et al.'s 1.55 μm pulse shaping set-up, an AO pulse picker with about 5 ns rise time was used [125]. Synchronization of RF pulses and laser pulses is achieved by triggering the waveform generator with the Er-doped fibre mode lock laser, which has a repetition rate of 37 MHz. Note that the source for the carrier wave in the mixing schemes in Fig. 29 does not need to be phase locked to the laser, since phase jitter in carrier wave will only impose an unobservable overall phase shift of the shaped pulse [30]. The arbitrary waveform generator, however, was running with external clock and was synchronized to the fifth harmonic of the repetition rate of mode-lock laser. Therefore, each single channel data point was synchronized with laser pulses that lasted 5.4 ns.

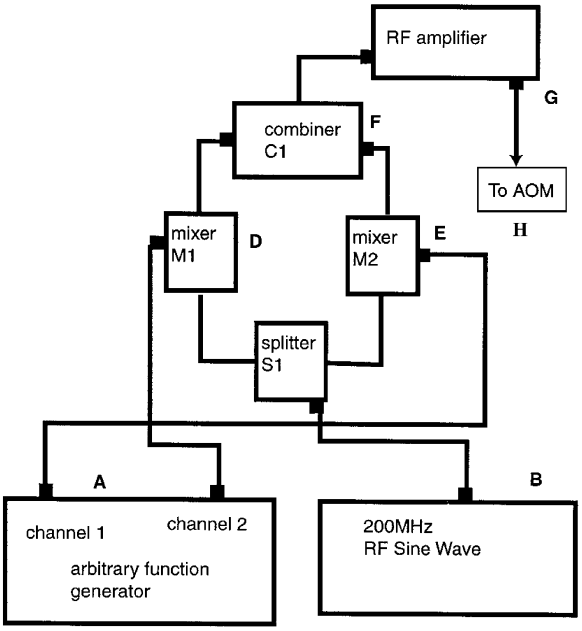

Fig. 29. RF circuitry for the AOM pulse shaper. The arbitrary function generator produces a shaped pulse in two channels, real and imaginary (A). The 200 MHz sin wave (B) is split into real and imaginary components (C). This is then mixed with the arbitrary function (D, E). The RF wave is then sent to the combiner (F), amplified (G) and then goes to the AOM through a directional coupler (H).

Briefly, the AOM imposes a modulation $M(\omega)$ onto the wavelength components of the input laser pulse ideally. Nonidealities associated with the finite beam size also have been discussed in detail in Ref. [123]. This simplification introduces insignificant effects as long as the effective focal spot size of each frequency component on the central Fourier plan is smaller compared with the smallest feature size that the acoustic modulation put into the AOM [123]. This requirement, however, imposes a practical limit of resolution for spectral encoder that one should consider into the design issues.

A fundamental difference between AOM and LCM pulse shaping is that the AOM will diffract the input light, with the diffraction determined by the input RF wave to the crystal. The LCM, in contrast, will transmit the light, not diffract it. The fact that the AOM diffracts the light will mean that very high contrast ratios can be obtained in AOM pulse shaping, which will be determined by the contrast ratio of the RF wave. The RF electronics used can be specified to have a contrast ratio of 40 dB. The AOM approach does not have the discretization problem and has significantly faster update rates as compared to the LCM array. The update rate is solely limited by the time it takes the acoustic waveform to travel the crystal and thus depends on the crystal size. The advantage of minimal discreteness in the imposed shape in case of the AOM approach also enables more modulation features (pixels) to be incorporated in the shaped pulse. The number of possible features (N_f) in the AOM is given by: $N_f = L \times (A/V_{ac})$, where L is the crystal length which for Warren's group is 4 cm, V_{ac} as before is the velocity of sound in the crystal, and A is centre modulator frequency, which for the TeO_2 AOM is 200 MHz. The minimum feature size is defined as V_{ac}/A

which is ≈ 21 μm, and so the number of features $N_f = 1900$, in contrast to a maximum of 640 in case of the LCM. Furthermore, in contrast to the LCM scheme, the AOM shapes the pulses by deflecting the shaped wavelengths in a different path from the transmitted or undiffracted part of the beam. Thus, the isolation in the diffracted beam of an AOM is significantly better than the isolation of a LCM array used in amplitude modulation configuration. The calibration of AOM is simple and phase and amplitude of RF pulse are directly transferred to the laser beam.

However, AOM technique also has its disadvantages. The travelling acoustic wave results in time-dependent spatial grating thus the pulses separated by few microseconds will see different gratings. To the first order, this implies that shape of the output pulse will stay the same but the centre frequency will change. This may be desirable in some applications [126], however in general; the AOM technique is best suited for applications in which selected or amplified pulses (ranging to a tenth of MHz repetition) are required while the LCM techniques are preferred for high frequency laser oscillator applications.

4.6.2. Design issues in spatial AOM pulse shaping for optical communication

In this section we will address the practical design issues of an AOM pulse shaper or spectral encoder for communication wavelengths. Let us define the parameters of the optical source and AO modulator first. For optical source, the related parameters here are the central wavelength λ_0 and the optical bandwidth of $\Delta\lambda$ FWHM. For AOM, the related parameters are the centre RF driving frequency ω_{RF0}, RF bandwidth $\Delta\omega_{\mathrm{RF}}$, length of the AOM L, and the speed of the acoustic-wave in the material, V_{ac}. The component parameters to be determined are grating period Λ, focal length of the lenses f, the input beam size a, and the sizes of the optics. The related set-up parameters are the input angle of the first grating θ_{in}, the output angle of the first grating for the centre laser wavelength θ_{out}, the angular dispersion parameter β (will be defined later), and the spatial dispersion parameter α. The first requirement to minimize the non-ideality of the AOM pulse shaper is $\theta_{\mathrm{out}} = 0$. This is to comply the implied assumption in Ref. [122] for deriving the Eq. (61), which is the basis of this spatial pulse shaping technique. This requirement together with the consideration of diffraction efficiency and the dispersion power of the gratings, gives out the design rule No. 1 on the grating period, which is

$$\Lambda > \lambda_0 \ . \tag{70}$$

This also suggests the input angle θ_{in} to be $\sin^{-1}(\lambda_0/\Lambda)$ and the angular dispersion parameter β, which is defined as

$$\beta = \frac{\lambda_0}{2\pi c}\,\frac{1}{\Lambda\cos\theta_{\mathrm{out}}} \tag{71}$$

to be $\lambda_0^2/2\pi c\Lambda$.

The second requirement to minimize the distortion of AOM pulse shaper is letting most part of the laser spectrum passing the AOM pulse shaper, which is limited by the length of the AOM crystal. Experimentally, it has been shown that it is a good balance to let the edges of the AOM crystal aperture the Gaussian laser spectrum at approximately the 5% intensity points, which compromises the size of the device and the unwanted distortion in the laser pulse shape. These requirements in addition to the angular dispersion and the optical bandwidth of the laser pulse gives out the focal

length of the lenses as:

$$f = 0.48\,\frac{\Lambda}{\Delta\lambda}\,L\ . \tag{72}$$

This also results in a spatial dispersion parameter, α, which is defined as

$$\alpha = f\beta\ . \tag{73}$$

The value of α is $0.48L/\Delta\omega$ where $\Delta\omega$ is the bandwidth of the laser pulse in frequency domain and is related to the $\Delta\lambda$ by

$$\Delta\omega = -\frac{\Delta\lambda}{\lambda_0}\,\omega_0\ . \tag{74}$$

The third requirement is to minimize the non-ideality of the AOM pulse shaper, which implies that the effective beam size of the single frequency component should be smaller than the smallest modulation feature size. The smallest modulation feature size, on the other hand is determined by the modulation bandwidth and the velocity of the acoustic wave in the material by the relation:

$$S = \frac{2\pi}{\Delta\omega_{\mathrm{RF}}}\,V_{\mathrm{ac}}\ . \tag{75}$$

The AOM length L over this smallest modulation feature size will give the number of individually adjustable effective pixels. This requirement implies that the effective beam waist of single frequency component as given by Eq. (63) be less than S, resulting in a third design rule for the input beam size:

$$\gamma\,\frac{f\lambda_0}{\pi a} < S \ \Rightarrow\ a > \gamma\,\frac{f\lambda_0}{\pi S}\ , \tag{76}$$

where a is the input beam waist, which is approximately equal to the beam size for collimated beams.

For a typical optical communication system operating at the centre wavelength of 1.55 μm and having a bandwidth of 40 nm, the first design rule Eq. (70) gives out the grating period should be about and larger than 1.55 μm. Gratings with grove density of 600 groves/mm requiring a input angle θ_{in} about 68.5° is a quite reasonable and convenient choice for both layout and efficiency reasons. For a typical AOM working at 1.55 μm wavelength range, the length of the crystal is about 20 mm long, the RF bandwidth is 100 MHz, and the velocity of the acoustic wave in the material is 5.1 mm/μs. According to Eq. (75), this gives out the smallest modulation feature size to be about 50 μm and total maximum number of effective pixel to be 400. According to Eqs. (72) and (76), the optimized focal length and input beam size comes out to be 400 mm and 1.5 mm, respectively.

4.6.3. Generation of high intensity shaped pulses

Most often, the shaped pulses only have nanojoule level energies and for most practical applications in coherent control, higher pulse energies are necessary. Amplification of shaped pulses is a non-trivial issue since pulse distortion and characterization are critical elements for consideration. In the following section, we discuss such issues for the AOM pulse-shaping scheme, the only pulse-shaping scheme where high-fidelity amplification has been demonstrated to hundreds of microjoule level (200 μJ/pulse) [127].

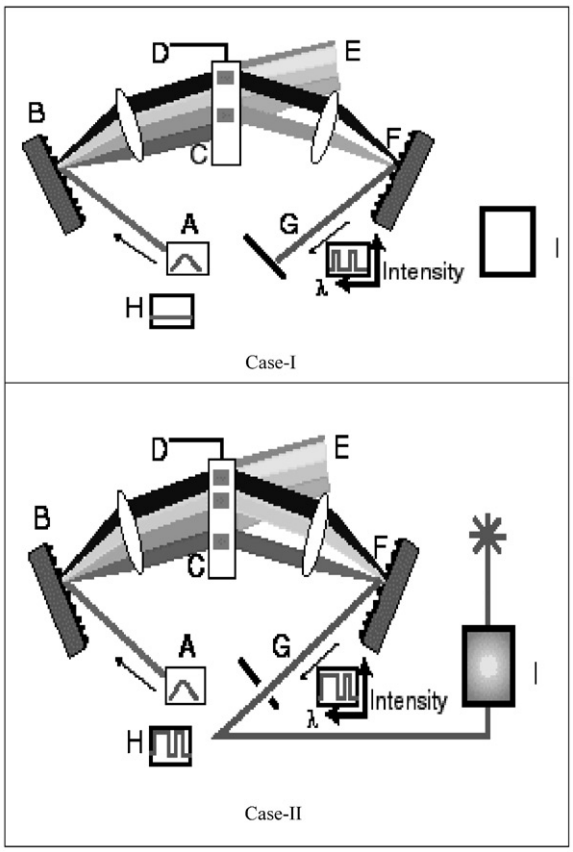

Fig. 30. Amplification scheme of AOM pulse shaping approach. Several legends used in the figure are as follows: **A:** femtosecond Gaussian pulse (plotted as a function of time in the box below A); **B:** grating that spectrally spreads the pulse; **C:** acousto-optic modulator is in the center of the system; **D:** the RF-wave propagates through the AOM, creates a spatial mask inside the crystal and shapes the optical pulse; **E:** the undiffracted beam passes out of the system; **F:** grating that recombines the spectrum; **G:** pulse picker picks the **s**haped output pulse. In this schematic, the input optical pulse is modeled as consisting of four different wavelengths, blue, yellow, orange, and red, which would represent a 4-bit system. In principle, the AOM is capable of shaping 1000 bits. The white parts of the diffracted spectrum are left undiffracted by the AOM. The output **(G** and the box below the **G**) shows the shaped output pulse as a function of wavelength. As the RF wave propagates, different shapes are created. The pulse picker **G** picks the pulse at the correct time out of the pulse train (Case II) otherwise it blocks them (e.g., Case I). Here the pulse picker is shown separately selecting a particular pulse **H**, but in the experiment, the pulse picker is located inside the regenerative amplifier **I**.

Let us begin with a few practical aspects of amplified femtosecond AOM pulse-shaping scheme developed by Warren and co-workers who pioneered this technique and applied it in various experiments. As shown in Fig. 30, the pulse shaper is inserted before regenerative amplifier in a commercially available amplified Ti : sapphire laser system. It would also have been possible to place the pulse shaping in the regenerative amplifier, or after the regenerative amplifier. The option of putting the pulse shaper in the regenerative amplifier would have required a complete redesign

of the amplifier, which would be less user-friendly. There are clear advantages in putting the pulse shaper before the regenerative amplifier, rather than after. Assume that the regen-amplifier has an output power of P_0. The pulse shaping system has a low efficiency of about $\varsigma = 5$–10%. The regenerative amplifier is a saturated amplifier, which means that even if the power into the amplifier is low, the output power will still be P_0, or whatever the output power turns out to be. However, in this arrangement, caution is required not to seed a narrow band pulse into the stretcher and amplifier because the stretcher will not be able to expand the pulse long enough so as not to damage the amplifier. If the pulse shaper is put after the amplifier, the system output power will be reduced to $P_0 \bullet \varsigma$. This particular pulse shaper operates at 800 nm and consists of a grating (1800 lines/mm) that disperses the femtosecond pulse, which is then collimated with a 30-cm lens to form a linear spectral image at the centre of the $4F$ system (point C in the Fig. 30). The shaped radio-frequency pulses generated by an arbitrary waveform generator (LeCroy) with a resolution of 400 MHz were used to create the desired modulation pattern on the AOM (TeO_2 crystal). As mentioned earlier, since the transit time of the acoustic wave is very slow as compared to velocity of light in the TeO_2 crystal, hence, light pulse sees acoustic wave as stationary pattern. Thus, acoustic wave acts as a transmission diffraction grating. Putting the pulse shaper before regenerative amplifier also makes it compatible with the commercial laser set-up without any modifications. The pulse shaper is characterized before and after amplification by replacing AOM with a transmission grating with dark lines equally spaced at 50 μm that does not change with time (Ronchi grating [128]). This allows the calibration of the zero-dispersion line without using the amplifier or a pulse picker. It was observed that AOM gives pulse shaping resolution and contrast ratio as good as Ronchi grating. As the acoustic features travel across the AOM, each pulse sees a different grating function. Thus, it is necessary to select only one pulse at the correct timing, which sees grating function corresponding to the desired pulse shape. This is achieved by Pockels-cell cavity dumper, which injects only right pulse in regenerative amplifier.

4.7. Characterization of the ultrafast shaped pulses

Quite an important aspect of ultrafast pulse shaping lies in appropriate characterization of the generated shaped pulses as the reliability of their generation often relies on how accurately they can be measured. To the readers not familiar with ultrafast laser science, it may not be obvious as to why so much effort was expended on measurement techniques. For CW lasers, it is sufficient to use a monochromator as a spectrometer. In fact, the easiest approach to determine the wavelength profile of a shaped pulse is still a powerful technique, especially for determining the number of features imposed on an amplitude only modulated pulse as shown in Fig. 31b. For transform-limited (time-bandwidth product defined by Heisenberg uncertainty) pulsed lasers with known envelope profiles, such as the commercial lasers that produce pulses anywhere from nanoseconds to subpicosecond duration, it is sufficient to use either an oscilloscope or an autocorrelator. For the arbitrarily shaped ultrafast femtosecond pulses, however, it is necessary to at least use techniques, such as, cross-correlation (Fig. 34) or techniques that are more sophisticated, such as, frequency resolved optical gating (FROG) [129], spectrally and temporally resolved upconversion technique (STRUT) [130], temporal analysis by dispersing a pair of light electric field (TADPOLE) [131], spectral phase interferometry for direct electric field reconstruction (SPIDER) [132], etc. SPIDER, TADPOLE, STRUT and FROG techniques give both amplitude and phase information

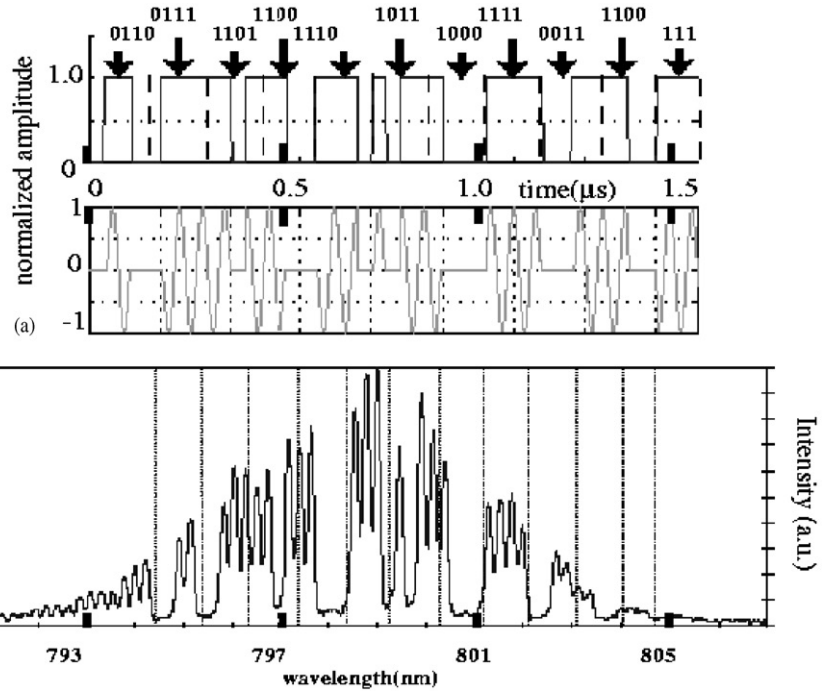

Fig. 31. High Resolution Amplified Pulse Shaping. (a) The RF signal used to modulate the spectrum. The topmost plot shows the bit stream. The numbers show the imposed bit pattern, a 43-bit sequence. The lower figure shows that the actual RF signal was the product of this bit stream with a sinusoidal wave. (b) The spectrum resulting from the modulated RF signal of A. This being an amplitude only modulated pulse, a monochromator is sufficient to record the spectrum and characterize the shaped pulse. The dotted lines represent that the bit pattern has been successfully retained in the pulse shaping and amplification process.

unlike the spectrometer, the autocorrelator or even the crosscorrelator, which only gives the field intensity profile as a function of either wavelength or time, respectively, but not both.

The cross-correlation is quite similar to the autocorrelation, except a reference pulse is used. In cross-correlation detection, the shaped pulses are cross-correlated with unshaped replica from the laser, which is sent through a mechanical variable delay line. Typically, a 10 cm focal length lens focuses the beams to cross in a thin BBO crystal to generate the cross-correlation signal, which is then measured on an amplified photodiode. The cross-correlation is useful to measure shaped pulses for two reasons. First, the reference pulse is unshaped, so that the output signal is simpler than if an autocorrelation was performed. Second, the cross-correlation allows us to measure very weak pulses, because the reference pulse could be intense. Like the spectrometer, cross-correlation does not give phase information.

Mathematically, to completely describe the ultrafast pulse in the Fourier domain, we need to find the function

$$E(\omega) = A(\omega)\exp(\mathrm{i}\phi(\omega)) \ . \tag{77}$$

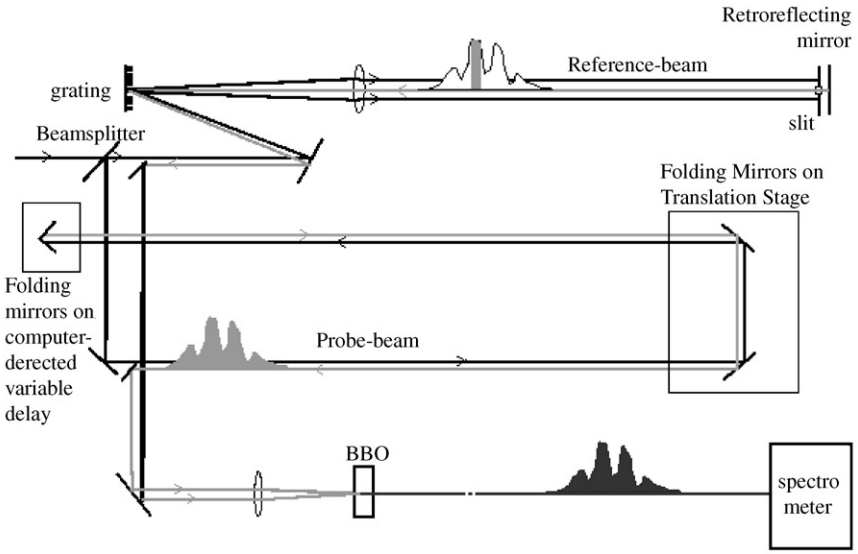

Fig. 32. Experimental schematic of the spectrally and temporally resolved upconversion technique (STRUT).

The phase function $\phi(\omega)$ gives us the phase of one frequency in the pulse with respect to another. For a monochromatic pulse, since there would only be one frequency, this phase function would not be necessary and the envelop function $A(\omega)$ would fully correspond to the electric field $E(\omega)$. Thus, to describe an ultrafast pulse, more information is required then to describe a monochromatic pulse. In simple terms, STRUT or FROG can be viewed as time domain correlator that is also resolved in wavelength. While FROG and several other similar iterative techniques are very powerful, the STRUT algorithm is fast and does not require iteration. Besides this, in spite of using only the second-order non-linear process (second harmonic generation), STRUT can give the sign of chirp while second order FROG cannot. Furthermore, although the STRUT only uses intensity-dependent detection devices (a diode array), it can still recover all the amplitude and phase information. TADPOLE is a combination of FROG with spectral interferometry to yield extremely sensitive and general method for temporal characterization of nearly arbitrary weak pulses (pulses as weak as 42 zeptojoules, or 42×10^{-21} J average power) even when reference pulses are non-transform-limited [131]. SPIDER uses spectral shearing interferometry to retrieve the spectral phase of the incident pulse by measuring interference between two time-delayed pulses that are identical expect for their central frequencies [132]. For generating spectrally sheared pulse pair in the laboratory, non-linear processes are required and both upconversion and downconversion techniques have been used. Both TADPOLE and SPIDER techniques are improvements over the FROG technique and have significant benefits (linear, fast algorithms, etc.) and are widely used. We will, however, in the subsequent sections focus on the STRUT technique that has been implemented largely for the spatial AOM modulated shaped pulse characterization.

A schematic of STRUT is shown in Fig. 32. The input pulse is split up into two beams: the probe beam and the reference beam. The reference beam is spread spectrally and filtered by a rectangular slit and is correlated with the probe beam. Fig. 33 shows the capability of STRUT in using the

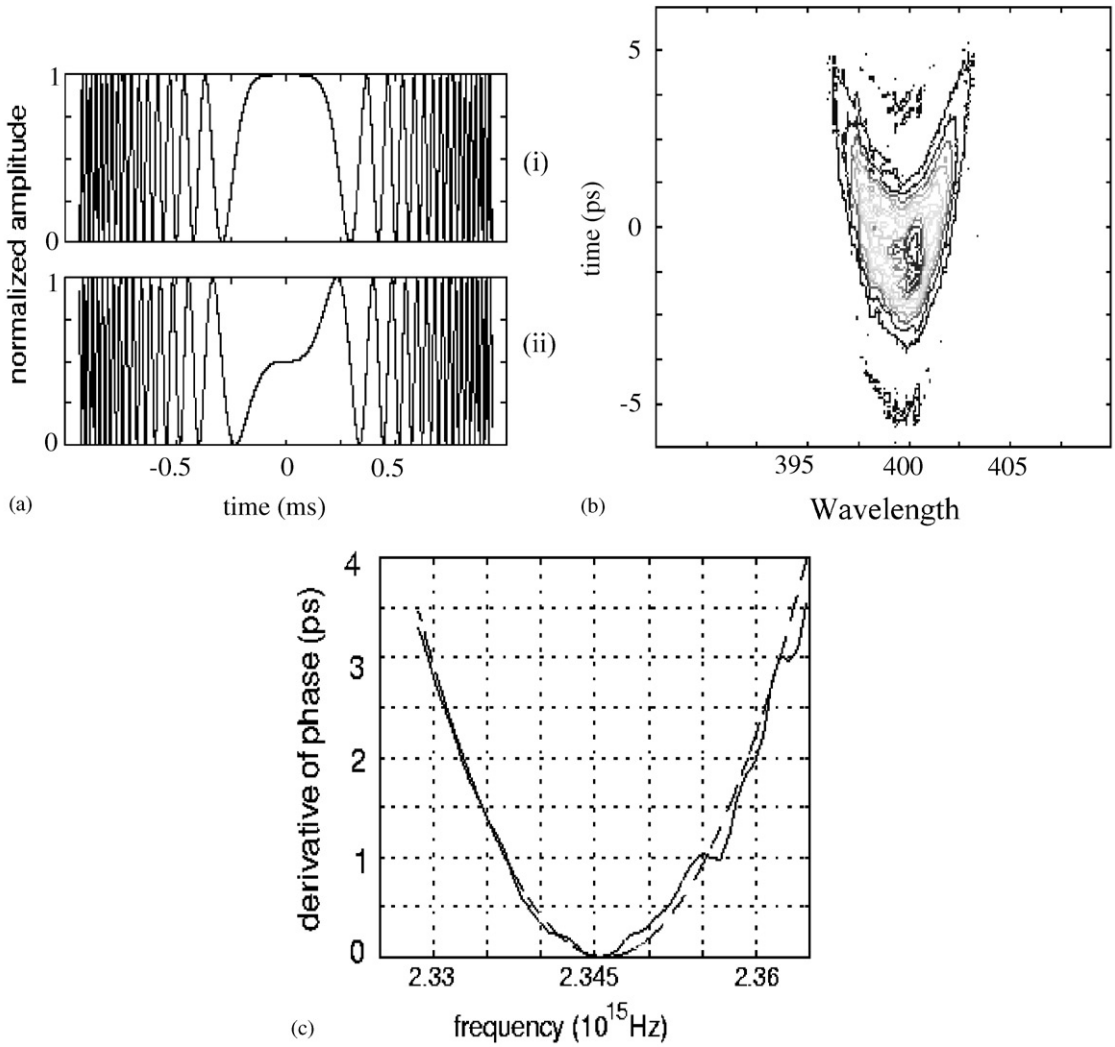

Fig. 33. (a) RF pulses that have been used to generate a shaped pulse with cubic phase factor. Both the real (i) and imaginary (ii) components are shown. (b) STRUT image of a pulse with cubic phase factor. (c) The phase derivative of the pulse as recovered from the STRUT image (solid curve) as compared to the theoretical expectation (dashed curve).

spectrally sliced rectangular probe pulse ($A(\omega) = 1$) generated in its reference arm to characterize an amplified AOM pulse shape with cubic phase, such that,

$$E(\omega) = \exp(\mathrm{i}\rho\omega^3) \ , \tag{78}$$

where, as in Eq. (77), $E(\omega)$ is the electric field, ω is the optical frequency, and ρ is a chirp parameter. The function that relates the optical frequency of the laser to the transverse spatial position at point C in Fig. 30 is given by

$$x(\omega_{\mathrm{L}}) = \rho(\omega - \omega_0) \ . \tag{79}$$

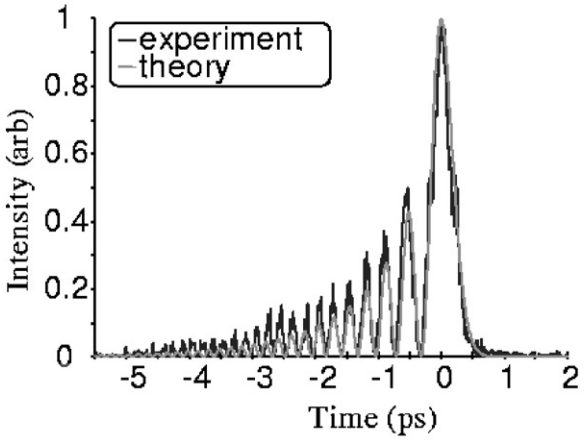

Fig. 34. Cross-correlation measurement of a pulse with cubic phase with an unshaped pulse. While theory and experimental curves fit very well once the parameters are known, it is not possible to predict the phase measurements from this measurement alone, as discussed in the text.

This is essentially equivalent to Eq. (66), where $\rho(\equiv \alpha/2\pi)$ is a parameter depending on the specific system parameters, such as the focal length of the lenses, and as before ω_0 is the centre laser frequency. The RF wave propagates through the AOM, so that if t_{RF} is the RF time-base and V_{ac} is the speed of sound in the crystal, which is related by Eq. (64). Equating Eqs. (79) and (64) allows each optical frequency ω to be mapped into a unique RF time t_{RF}, and one can write a function $f(t_{RF}) = \alpha\omega$ to express this mapping. Fig. 33a shows the input RF pulse into the AOM, given by $f(t_{RF}) = \exp[i(\beta t_{RF})^3]$, with $\beta = 3$ and t_{RF} in μs. The top curve is the real part of the RF pulse, $x = \cos[(\beta t_{RF})^3]$, while the bottom curve is the imaginary part, $y = \sin[(\beta t_{RF})^3]$. In this case, only the phase is being modulated and not the pulse amplitude. Such a RF pulse would give an optical pulse:

$$E_{out}(\omega) = \exp[i \cdot \alpha^3\beta^3(\omega - \omega_0)^3] \cdot E_{in}(\omega) \tag{80}$$

Fig. 33b shows the experimental STRUT image resulting from this RF pulse. Fig. 33c shows a comparison between the derivative of the phase $d\phi/d\omega$ that is recovered from the STRUT image and the theoretically predicted phase derivative from Eq. (80). The two curves agree quite well considering the fact that non-idealities, such as, propagation attenuation of the RF pulse, are not taken into account in this analysis. In fact, for such well-behaved analytical shapes such as the cubic phase, the cross-correlation measurements can also lead to a good fit between theory and experimental plots once the phase information becomes available as shown in Fig. 34.

Fig. 35 shows the STRUT image of a complex pulse shape given by Eqs. (16) and (17). This pulse essentially represents a sech electric field envelope with a tanh frequency sweep (if μ is positive, the frequency proceeds from blue to red). In particular, the parameters used in the pulse shape shown in Fig. 35 are: $\alpha = 1.75 \times 10^{12}$ Hz is a time width parameter, t is the pulse time in seconds, and $\mu = 8$ is a frequency sweep parameter. The interaction between intense (50 MW peak power), shaped ultrafast laser pulses and optically dense samples of Rb vapour has been studied. Study of excited state Rb is also interesting, since it is a key reagent in the preparation of the spin-polarized noble

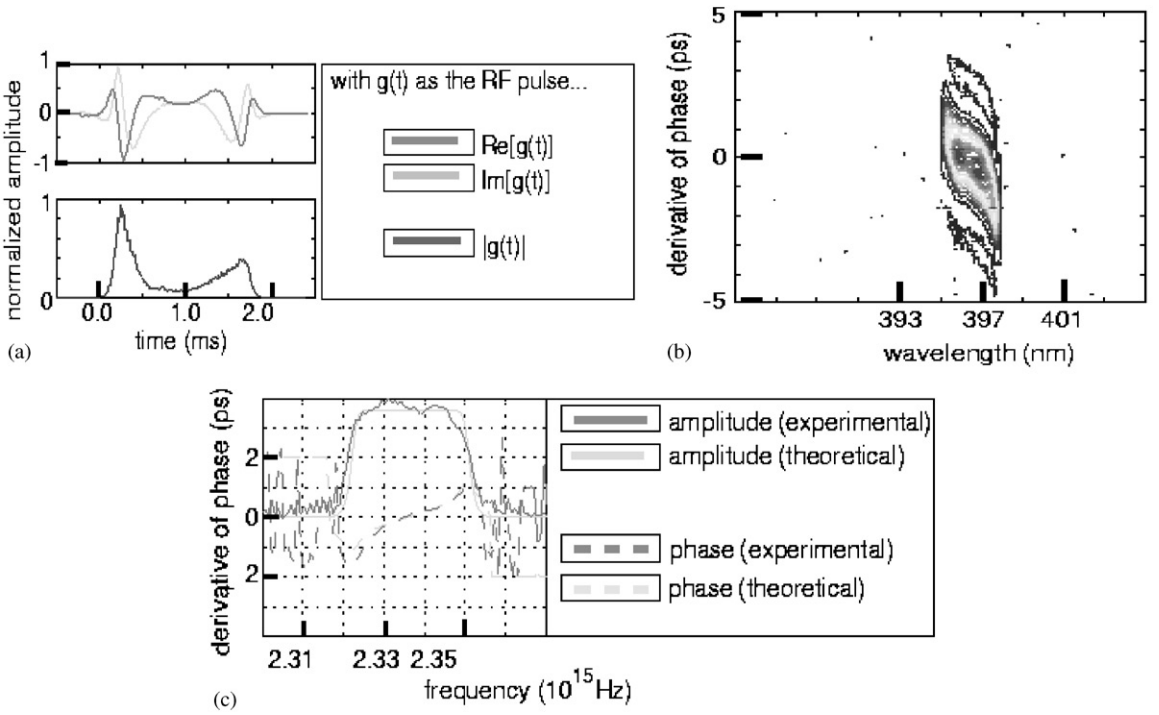

Fig. 35. Results for hyperbolic secant amplitude with hyperbolic tangent frequency sweep pulse, i.e., $[\mathrm{sech}(\alpha t)]^{(1+5i)}$. (a) Upper: the real and imaginary parts of the RF signal used for the complex secant hyperbolic sweep. Lower: the magnitude of the RF signal. (b) STRUT dataset for this pulse. (c) The results of the analysis of the above STRUT data to recover Intensity and Phase are shown.

gases that are used in MRI lung studies [133]. The STRUT was used to measure the laser pulses both before and after propagating through Rb vapour (Fig. 35). Experimentally, it was observed that the Gaussian pulse induced inversion, and that the two different frequency-sweep directions of the hyperbolic secant pulse would cause different responses in the atomic system [134]. This contradicted the theoretical expectations [135] based on Maxwell–Bloch pulse-propagation equations, which predicted that the secant hyperbolic pulse would propagate through an optically thick medium without changing its shape or inversion profile. A re-examination of the theory showed that it was valid for the case where the optical spectral bandwidth was narrower than the atomic linewidth. In the Rb experiment, however, the optical spectrum was much wider than the atomic linewidth. Computer simulation results showed that, with this important adjustment to the theory, experimental and theoretical results do agree [136] (Fig. 36). Such experimental results indicate that the atomic state can be prepared by choosing different pulse shapes.

Pulse shaping has also been accomplished by using stretcher technology to stretch the pulse in time. Then, an electro-optic modulator (with GHz speed) can be used to modulate the pulse, and the pulse is then recompressed. This particular work in Ref. [137] only demonstrated the pulse amplitude modulation; however, it could be extended to both the amplitude and phase domains. This pulse shaping technique is more difficult to achieve experimentally than the LCM and the AOM

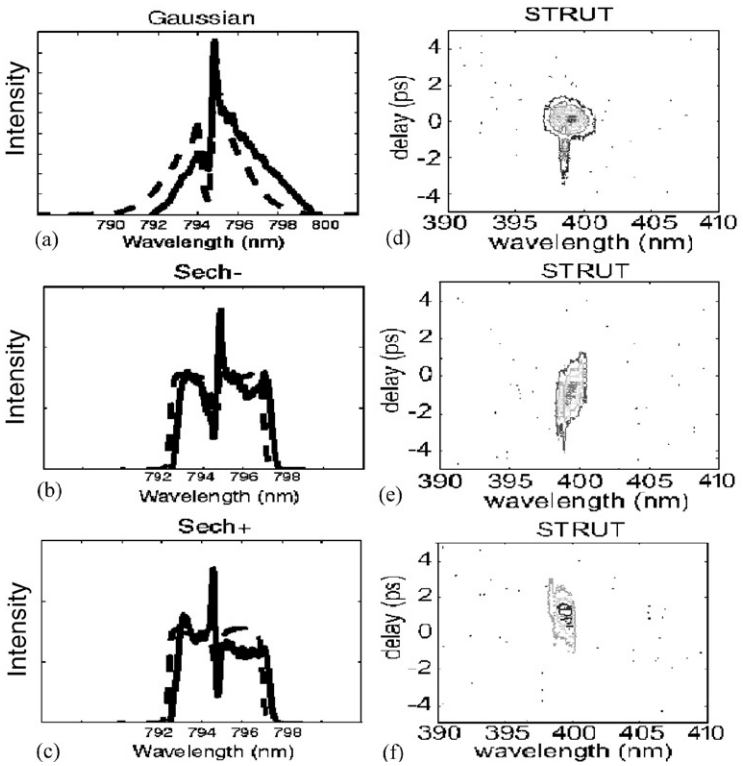

Fig. 36. Study of the propagation of shaped pulses through optically thick rubidium (Rb) vapour. Experimental spectral shapes [solid curves in (a), (b), (c)] and STRUT traces [(d), (e), (f)] for the optical pulses whose bandwidth exceeds the atomic linewidth of Rb-sample after passing through the sample. Sech− represents the $[\mathrm{sech}(\alpha t)]^{(1-5i)}$ pulse, while Sech+ represents the $[\mathrm{sech}(\alpha t)]^{(1+5i)}$ pulse. Experimental reshaping of the shaped pulses can be explained with computer simulations [dashed curves in (a), (b), (c)] that use Maxwell–Bloch propagation equation.

techniques. It requires modulators that work at speeds of 20 GHz, and arbitrary function generators that can also achieve this speed. In contrast, the arbitrary function generators that we discussed above for the AOM pulse shaping work at 200 MHz.

4.8. Ultrafast timed sequences of femtosecond pulses

As an example of the application the LCM pulse shaping approaches, Nelson, Weiner and coworkers [138] showed enhanced optical control over elementary molecular motion with timed sequences of femtosecond pulses produced by pulse-shaping technique. These experiments exploit the sudden (impulse) driving force that a sufficiently short pulse (i.e., short compared to the vibrational oscillation period) exerts on a Raman-active vibrational mode through a mechanism called impulsive stimulated Raman scattering (ISRS). The experiment is arranged in a transient grating geometry, shown schematically in the inset of Fig. 37a. Passing a single femtosecond pulse through an optical pulse shaper consisting of two gratings, two lenses, and a spatially varying mask (same schematic as in Figs. 1 and 25, spatially varying mask replacing the LCM), terahertz-rate trains of femtosecond

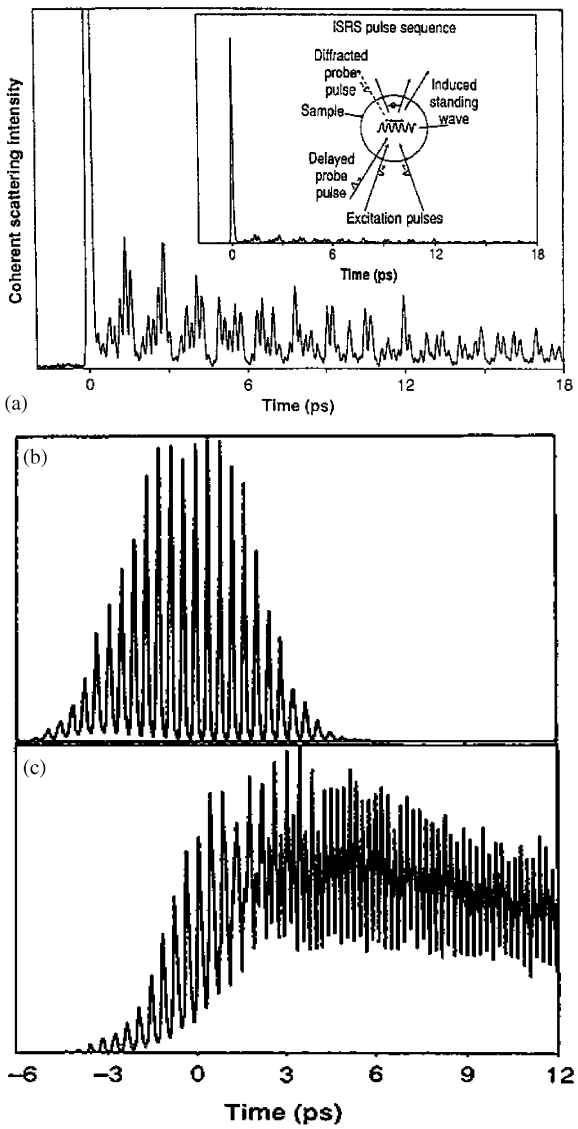

Fig. 37. (a) ISRS data from the α-perylene organic molecular crystal. The femtosecond excitation pulses drive several phonon modes whose combined response yields a characteristic beating pattern. The pattern somewhat changes over time since the modes have different dephasing rates. The "spike" at $t = 0$ is a purely electronic response of the crystal to the excitation pulses. Since the three pulses are inside the sample, which provides a measure of the excitation pulse duration an internal calibration for the ISRS response. The inset shows the relative signal intensities of the electronic spike and the vibrational response. (b) Cross-correlation measurement of a sequence of femtosecond pulses with a repetition rate of 2.39 THz (419 fs between pulses) produced through LCM pulse modulation techniques. Such pulses can repetitively drive a selected vibrational mode to increase the vibrational amplitude. (c) ISRS data from the α-perylene organic molecular crystal driven by sequence of (p polarized) pulses spaced at 419 fs to match the vibrational period of the 80 cm^{-1} mode. The diffracted signal from the mode grows stronger with each successive pulse, eventually reaching intensity levels comparable to the strongest electronic response. Selective amplification of the 80 cm^{-1} mode has been demonstrated.

pulses were generated (Fig. 37b). The impulsive force initiates coherent vibrational oscillations that were monitored by variably delayed probe pulses. Nelson, Weiner and coworkers used appropriately timed pulse sequences to drive repetitively selected vibrations of a crystal lattice (α-perylene molecular crystal) to build large amplitudes while discriminating against other modes. The extent of control over the nuclear motion that could be demonstrated was small, approximately 10^{-4} Å for molecular displacements in translational optic phonon modes of the crystalline solids. This was limited by the sample damage problems that occur at high peak intensities. Nevertheless, the ISRS signal in Fig. 37c clearly demonstrates mode-selective vibrational amplification. Fig. 37b is the pulse profile. In Fig. 37c the initial part of the ISRS signal is dominated by the crystal's electronic responses to each of the pulse sequence of Fig. 37b. However, after several pulses, the ISRS signal due to the amplified 80 cm^{-1} mode becomes apparent. By the end of the input pulse train ($t = 3$ ps) the ISRS signal is almost as intense as the strongest scattering peak.

4.9. Pulse shaping applications in optical fibres

Even with the current state of art technology for various electronic devices being pushed to limits, various schemes based on all optical have been pursued aggressively for the inherent advantages it offers. Optical fibres with their unique properties have been able to realize various applications. The waveguide nature and near negligible attenuation of the signal of desired wavelength makes it the backbone for the optical communications. Its long interaction length offered for the light has made it possible to observe various non-linear optical effects very easily. Also, it has been an extremely useful candidate as a device in all-optical switching and so on. Pulse shaping holds the promise for further extending this limit besides opening up various other new possibilities right from increasing the speed of the data transfer rate in optical communications to exploring various new non-linear optical effects, to enhance the performance of the ultrafast switching and others.

4.10. Optical communications

Most of the present day research effort in optical communication is directed towards achieving an extremely high data transmission rate of terabit/s. With the present day available technology, it has reached data transmission of gigabits/s. Ultrafast pulse shaping holds the promise to achieve the data transmission capacity of a terabit/s. The very high transmission capacity of a terabit can perhaps be appreciated from the fact that about million movies can be transmitted simultaneously. This can be achieved by taking advantage of the various light modulation techniques available like time-division multiplexing (TDM), wavelength division multiplexing (WDM), and code-division multiple accessing (CDMA).

Communication through optical fibres allows one to use the extremely large bandwidth of about 20 THz sustainable in the fibre for transmitting data. With the currently available encoding and decoding schemes, one has not been able to exploit this bandwidth fully. Ultrafast pulse shaping technology can help form ultrashort bit of data streams to be transmitted as short burst of light, thereby allowing an increase in the data transfer rate. This is essentially TDM [139]. This does not demand any ultrafast electronic devices to be operated at this fast speed, nor does it demands much changes in the present day infrastructure available for optical communication.

Another technique commonly used is the WDM, where the broad spectral content of the ultrafast pulses are wavelength encoded with an optical pulse shaper. Normally, to encode the data at various wavelengths, one would require multiple light sources at different wavelength. Moreover it also requires that all these different sources to be stabilized, which is very difficult. Mode-locked laser can be used as a self-stabilizing source for multiple optical wavelengths. A modulator array placed within optical pulse shaper can be used to place independent data on the individual wavelength channels. This avoids the use of stabilized multiple laser sources at different wavelengths, since the entire wavelengths are derived from a single mode-locked laser. The idea of applying pulse shaping to dense wavelength-division multiplexing was first proposed by Weiner et al. [140] and was later experimentally confirmed by Nuss et al. [141].

Finally, in the technique of CDMA [142], which essentially utilizes a combination of TDM and WDM techniques; an ultrafast pulse shaper helps to encode and decode signals. Encoding of ultrafast pulses can be achieved by utilizing pseudorandom phase patterns to scramble (encode) the spectral phases. This can be achieved by, say, using a fixed pseudorandom phase mask [143]. To reconstitute the original femtosecond pulse, a second, phase conjugate mask is used to unscramble (decode) the spectral phases, thus restoring the initial pulse. If the encoding mask matches the decoding phase conjugate mask, like a key to a lock, then any phase changes introduced by the first mask are undone by the second and the original ultrafast pulse emerges unaffected. And since use is made of both packing the information in time domain as well as in the frequency domain, larger rate of data transmission is achieved.

We also note that pulse shaping can be utilized to achieve the dispersion compensation necessary for ultrashort pulse CDMA. One can compensate for a constant (wavelength independent) dispersion simply by adjusting the grating separation in the pulse encoding or pulse shaping masks in order to compensate for cubic or even higher order dispersion. Also for high-speed communications over a long distance, data is being transmitted in form of "solitons" packets, which travel through the optical fibre without changing the shape as well as they do not seem to interfere, as they pass through each other. In the subsection that follows, we will see how pulse shaping has helped to produce various kinds of "solitons" exploiting the non-linear optical technique helping to undertake various experiments as well as for different applications.

4.11. Pulse shaping in ultrafast non-linear fibre optics

Pulse shaping of ultrafast optical pulses has helped considerably to study various non-linear optical processes like formation of "dark" optical solitons, shaping the pulse to avoid the break-up of the high intensity pulses in the all-optical switching to remove the undesirable frequency components from the pulse, for producing higher order solitons and so on.

"Bright solitons" are being used for high-speed long distance communications [144], ever since Hasegawa and Tapper [145] proposed that the non-linear refractive index in glass fibres could compensate for group velocity dispersion and result in optical solitons that could propagate in the fibre. A bright temporal soliton is the result of cancellations between the chromatic dispersion of the material and its self-phase modulation. This is obtained when the material dispersion is anomalous and when the medium has a positive non-linear index (or alternatively, with normal dispersion and negative non-linear index). These solitons are resistant to dispersive effects in the time domain, frequency domain, or in space.

For normal dispersion ($\lambda < 1.3$ μm), bright pulses cannot propagate as solitons, and the interaction of the non-linear index with dispersion leads to spectral and temporal broadening of the propagating pulses. However, 'dark-pulse solitons', which consists of a rapid dip in the intensity of a broad pulse or CW background, are predicted to exist for normal dispersion [146]. Pulse shaping has played an instrumental role in producing suitable dark input pulses for experiments verifying soliton propagation of dark pulses in fibres. The fundamental dark soliton, also called a black soliton, is an odd function of time, with an abrupt phase shift at $t = 0$. The intensity of the black soliton is completely extinguished at $t = 0$. The phase function of dark solitons was a major obstacle for many years, hindering experimental investigations; only through the use of pulse shaping techniques has it become possible to create individual dark pulses with the required phase variation. Weiner et al. [147,148] synthesized even- as well as odd-symmetry femtosecond dark pulses, which led to a convincing demonstration of fundamental dark soliton propagation. Dark soliton propagation is remarkably robust against perturbations arising from a finite duration background pulse (this is because true dark solitons include a continuous-wave background of infinite duration) [147,149]. Besides this pulse shaping has also enabled the production of "higher order" bright optical solitons in the anomalous dispersion regime where the original spectrum and pulse shape has been restored after every integral number of solitons 'periods'.

4.12. Ultrafast all-optical switching

All-optical switches can have much higher operating speeds as compared to the electronic or optoelectronic devices. As the technology for all optical communication is being pursued aggressively, these all-optical switches become all the more essential being an integral part of such technology.

Pulse shaping can also play a role in studies of all-optical switching devices, which potentially can operate at speeds much higher than those obtainable with current devices. A number of all-optical fibre switching geometries have been reported using glass optical fibres [150] and switching times as short as 100 fs have been demonstrated [151]. Nevertheless, one universal problem arises with nearly every all-optical switching device. Because the switching is controlled by the instantaneous optical intensity, switching can occur within a pulse, so that the high and low intensity portions of the same pulse are directed to different output ports [151–154]. Such pulse break-up can degrade switching performance in a variety of all-optical switching geometries. Through the use of pulse shaping, problems associated with pulse break-up in all-optical switching can be largely avoided.

4.13. Spectral windowing

In fibre and grating pulse compressor, under some conditions the external frequency components generated by self-phase-modulation in the optical fibre are not linearly chirped and therefore cannot be efficiently compressed. By placing a band-pass spectral filter, or spectral window, into the grating pulse compressor, one can eliminate these non-compressible frequency components which otherwise would contribute to an undesirable pedestal on the compressed pulse. Normally, the self-phase-modulation spectrum is symmetrical, and therefore the band-pass filter is symmetrically placed in the pulse shaper. This simple application of pulse shaping to fibre and grating pulse compressor is referred to as spectral windowing [155].

4.14. Chirped pulse amplification applications

Quest for table top coherent light sources in the shorter wavelength of extreme ultraviolet or soft X-ray regions of the spectrum have led to the use of two very promising techniques: lasing in ionized plasma [156] and high harmonic generation from intense femtosecond laser pulses [157]. High harmonic generation essentially involves the non-linear interactions induced by the strong light in the medium. This allows one to extend the production of coherent light sources at shorter wavelengths. In gases higher harmonic generation up to several hundred have been generated from the incident laser pulses, but the efficiency is low and the energy is spread out over many harmonic orders. However by shaping the ultrafast pulse it is possible to increase the efficiency by an order of magnitude. The generated harmonic can be channelled into a single harmonic order, thereby directing a majority of the emitted energy into it. The output of the harmonic can be further increased if we have intense chirped pulses. As mentioned earlier chirped pulse amplification [158,159] is not straightforward. In brief, the pulse to be amplified is first stretched (chirped) in a dispersive delay line in order to reduce the peak intensity. This avoids optical damage and unwanted non-linear optical effects during the amplification process. After amplification the chirped pulse is recompressed to the bandwidth limit. To date, chirped pulse amplification has yielded the highest level of energy output per pulse, e.g. pulses with durations of 30 fs at energies above 100 mJ [160]. This corresponds to peak powers in the multi-terawatt range.

4.15. Photon polarization effects on control

Fujimura and co-workers [161] have treated polarization effects theoretically, showing photon polarization effects in quantum control of isomerization of hydrogen cyanide and in intermolecular interaction induced quantum beats in femtosecond time resolved light scattering from molecules. Such theoretical work has been done with the help of the wavepacket propagation and optimal control theory. Such work has shown; for example, in case of hydrogen cyanide photoisomerization that the application of two linearly polarized light pulses shortens the reaction time as compared to a single linearly polarized laser pulse.

A recent demonstration of laser polarization induced selectivity involves the control of a non-linear process, such as supercontinuum generation (SG) with the polarization-state of the laser [162]. Fig. 38 shows that the threshold for SG and the total amount of supercontinuum generated depends on ellipticity of incident laser for isotropic samples. Irrespective of the nature of the samples chosen, SG efficiency decreases as the incident laser polarization changes from linear to circular. The ratio of the overall SG between the linear and circular polarization (i.e., measure of suppression) undergoes an intensity-dependent decrease from large initial values to asymptotic limits, irrespective of samples.

Molecular alignment in intense picosecond and femtosecond laser fields has been shown to be dependent on polarization. Also in multiphoton ionization of N_2, the kinetic energy and ion yield have been found to depend on ellipticity of the incident laser [163]. Manakov et al. [164] observe that in weak static electric field induced interferences between one and two photon ionization amplitude, phase and polarization are important control parameters. Total ionization yield in two-colour ionization process using fundamental and second harmonic radiation shows circular dichroism and is completely controllable by phase. Huck et al. [165] have demonstrated the dynamic control and amplification of molecular chirality by using circularly polarized light. Using circularly polarized light

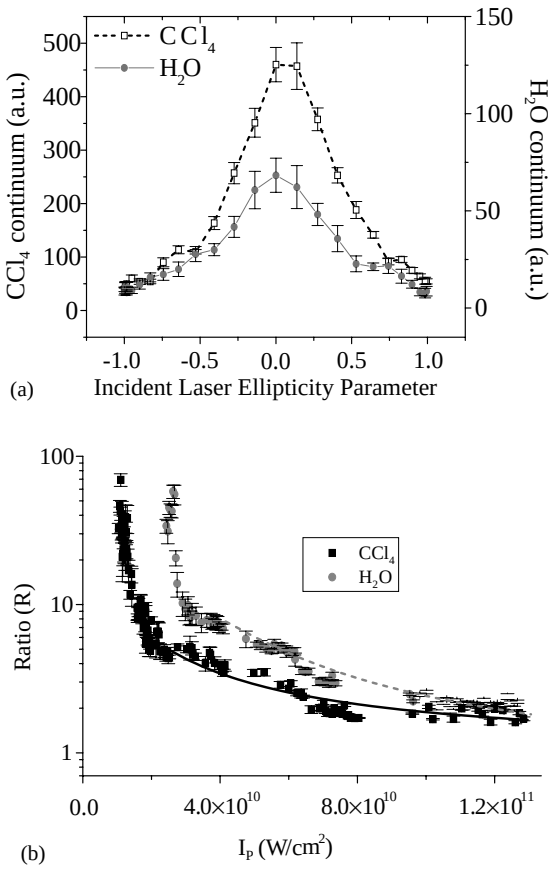

Fig. 38. (a) Ellipticity dependence of continuum generation (CG) in CCl_4 and H_2O as a function of the incident laser polarization. (b) Plot of the ratio $R=(I_{CG})_{Linear}/(I_{CG})_{Circular}$ between linear and circular polarization as a function of incident laser intensity I_P. The actual error-bars for the data are also shown on the plot. The solid and dotted curves are fits to the actual data assuming an intensity-dependent gain model. (Decrease of gain with intensity can be justified by simultaneous occurrence of processes like inverse Raman scattering.)

they were able to show the inter-conversion of enantiomers of helical molecules, and this represent two distinct states of a racemic photoresponsive material.

Recently, an experimental and theoretical investigation of the quantum control of ground-state rotational coherence in a linear molecule was presented [166]. A sequence of two temporally separated laser pulses creates a rotational superposition state in CO_2 whose evolution is monitored through a polarization technique. Hertz et al. studied the influence of the phase difference between the two pulses and showed that the overlapping of the two wavepackets, produced by each pulse, gives rise to quantum interference that affects the orientation anisotropy of the sample. Because of the large number of coherently excited levels, the interference produces well-separated temporal structures, whose magnitude can be controlled through the relative delay of the two pulses.

Another concept of control of polarization of the optical field using quantum coherence in an atomic system has also been demonstrated by Wielandy et al. [167]. They show that by applying the

optical field with frequency tuned near resonance of one transition, an initially isotropic vapour can be made to behave as linearly or circularly birefringence material for fields tuned near an adjoining transition.

An experimental realization of adaptive polarization control has been recently forwarded by Brixner et al. [168]. A 256-pixel, two-layer LCM spatial pulse shaper was used to modulate the degree of polarization ellipticity as well as the orientation of the elliptical principal axis within a single laser pulse. The temporal variation of intensity, momentary frequency, and light polarization has been achieved through the computer-controlled femtosecond pulse shaping apparatus.

4.16. Crafting atomic wavepackets

The most recent and significant advance in the field coherent control has been the demonstration of ability to shape and control the atomic electron wavepackets. Most of work in this area has been by Bucksbaum and coworkers [169], Wilson and coworkers [170] and Stroud and coworkers [171]. Wavepacket formation takes place when an ultrashort laser pulse coherently excites matter. Wavepacket is a non-stationary superposition state, composed of number of eigenstates that are determined by the frequency bandwidth of the exciting laser. The simplest of experimentally realizable wavepackets is one electron Rydberg wavepacket. Initial demonstrations were of wavepacket creation by simple Gaussian transform-limited pulses. Parker and Stroud [172] used single laser pulse tuned to excite several closely spaced Rydberg states simultaneously. The result of such excitation is that wavepacket now is localization of electron in the radial coordinate to a shell of probability that oscillates in and out from the mean excitation level. Since the atomic potential is anharmonic, the electron wavepacket spreads out after making several orbits and begins to interfere with it. This interference eventually leads to complete reformation of the wavepacket known as “full revival”. At the fractions of full revival time, the wavepacket splits into several miniature replicas of the original wavepacket spread evenly around the Kepler orbit. Noel et al. [171] also developed a control scheme that mimics the fractional revivals seen in the free evolution of the wavepacket by directly exciting them with a train of transform-limited pulses rather than a single pulse. In this case, both probability and phase distribution are important and were experimentally controllable. This technique of controlling wavepacket shape is particularly useful when there are relatively few superposition states in the wavepacket. In addition to simple atomic systems, this technique can also be extended to molecules, semiconductor super-lattices and excitons.

Since the population and relative phases of eigenstates in the wavepacket are completely determined while the laser pulse is interacting, the excitation process determines the future behaviour of the system, even at asymptotic times. Hence, different excitation pulses have been tried experimentally. Electronic wavepacket control using non-transform-limited pulses has been demonstrated experimentally in both atoms and semiconductors [173,174]. Wilson and coworkers [170] have demonstrated they can generate transient nanostructures in position and/or momentum from the wave function of an electron using tailored ultrashort laser pulses. For simple targets with well-separated substructures, the excitation pulse can often be viewed as consisting of independent (non-phase-locked) pulses. Targets that are more complex require amplitude and phase modulation and can be created using various pulse-shaping technologies. As an example, they demonstrate the synthesis and detection of a five-peaked structure. They show this structure acts as a time-dependent grating and can be detected via ultrafast XUV diffraction. Successful completion of such experiments

may lead to the ability to use lasers to control the electronic fabric of matter, and have applications in the production of nanoscale devices, communication, or chemical synthesis.

Another recent demonstration of control of shape of wavefunction is by Bucksbaum and coworkers [169]. They use computer controlled feedback based laser pulse shaping approach to manipulate the shape of atomic cesium's radial electronic wavefunction. They show that using a variation of quantum holography, to reconstruct the measured wavefunction, the quantum state can be reshaped to match the target within two iterations of the feedback loop. The shape of wavefunction is measured using state selective field ionization technique, which allows them to independently measure the amplitude of each state comprising the wavepacket. Further, the correlations in the fluctuations of pair of states serve to indicate the relative phase difference between two states in the object wavepacket and their corresponding states in the reference wavepacket. Then this measured amplitude and phase information can used to reconstruct the wavepacket as coherent superposition of eigenstates.

Chen et al. [175] report the observation of non-decaying wavepacket in a two electron atom. They show that they can manipulate wavepackets in the Rydberg states of atomic calcium via electron–electron correlations between core electron and the Rydberg electron, which is mediated by a strong excitation of the core transition. When Rabi oscillations of core transition are synchronized with the classical oscillation frequency of the Rydberg wavepacket, the wavepacket is shaped into a form that inhibits decay or autoionization.

Femtosecond laser pulse amplitude/phase masking techniques have been employed to control the formation and detection of rotational wavepackets in the electronic state of lithium dimer [176]. The wavepackets were prepared by coherent excitation of rovibronic states of Li_2 from a single intermediate state, and probed by time-resolved photoionization. In the detection step, the wavepacket is projected onto the state of Li_2. New resonance structure in the ionic state continuum was obtained by measuring the wavepacket signal modulation amplitude as a function of the frequencies removed from the spectrally dispersed probe pulse by insertion of a wire mask in a single-grating pulse shaper. A split glass phase mask inserted into the pulse shaper is used to produce step function changes in the spectral phase of the pulse. The phase relation among the wavepacket states is varied by changing the relative phases of spectral components in the pump pulse and is monitored by measuring the changes in the phase of the rotational wavepacket recurrences using an unmodified probe pulse. By altering the relative phases among the wavepacket components, the spatial distribution of the initial wavepacket probability density is varied, resulting in phase-dependent "alignment" of the probability density in angular space. Phase changes in the signal recurrences have been also observed when a phase-modified pulse is used in the wavepacket detection step after wavepacket preparation with an unmodified pulse. The formation and detection of the wavepackets have been discussed in terms of quantum interference between different excitation routes. It was shown that the relative phase factors encoded in a *single* optical pulse "pump or probe" are transferred into the interference term of the measured signal through the molecule–photon interaction.

Theoretical work has also been done on coherently exciting atoms or molecules into auto-ionizing states emit electrons in a series of pulses [177]. It was found that the phase does not change rapidly across an electron pulse if the laser has little chirp. By choosing the delay between the two laser-pulses, it is possible to have the electron wavepackets interfere. This interference can be exploited to partially control when the electron will be emitted and to partially control the time dependence of the channel into which it will be ejected. A comparison of the interference of different

ejected wavepackets gives information about the probability and phase to be initially excited into different channels.

4.17. Ultimate aspects of pulse shaping: feedback based quantum control

Most of the control experiments in past have been on small molecules, usually in gas phase or in molecular beams. Extension of quantum control to large molecules in condensed phase, which is directly relevant for most of chemistry and biology, faces major obstacles: the great complexity of such system and our lack of sufficiently detailed and precise knowledge about them. The traditional time-domain approach to quantum control has been to explicitly calculate the quantum dynamics and optimize the light field using knowledge of the potential energy surfaces of the molecule [178,179]. However, in case of large molecules the fields are often quite complicated and even impossible to create in the laboratory given the present state of laser technology. These considerations have led to the proposal to use experimental feedback rather than quantum calculations to find the optimal laser field [91]. In this approach computer controls a pulse-shaping device (e.g. AOM pulse shaper discussed earlier in this review) and analyses the output of the experiment. This experimental feedback is then used to modify laser pulses for achieving optimal field required for a particular process. Bardeen et al. [45] used this technique and demonstrated the control of molecular electronic population transfer. Femtosecond pulses tailored by a computer-controlled acousto-optic pulse shaper were used excite fluorescence from laser dye molecules in solution. Fluorescence and laser power was monitored, and the computer uses the experimental data and a genetic algorithm [180] to optimize the population transfer from the ground state to first excited state of dye molecule IR-125 in methanol solution. In their experiment, the most efficient transfer is the one that maximizes the yield of the excited state population with respect to the given laser power. Similarly, the most effective transfer is the one that maximizes the total amount of excited state population regardless of the laser power. The results they obtained are shown in Fig. 39.

The demonstration [181] of control of "chemical reactions" using feedback-optimized phase-shaped femtosecond laser pulses is an important example of this technique. In this experiment, Gerber and coworkers tried to optimize the branching ratios of different photodissociation reaction channels. The use of computer-controlled femtosecond pulse shaper with an evolutionary algorithm and feedback from product yields (Fig. 40a) lead to optimization without having to deal with electronic population transfer within the parent molecule. This work uses a LCM modulator, and places the pulse shaping system after the amplification system. The beam is then focussed into a high vacuum chamber, where it excites a molecular beam composed of iron pentacarbonyl [$Fe(CO)_5$] molecules, leading to different multiphoton ionization and fragmentation process. A detector was set up to record the percentage of ionized molecules and use the branching ratio of two different exit channels as a feed back signal in the optimization scheme. Using a feedback system and a learning algorithm, the system is set up to maximize the ionization value. It is shown that, with this technique, the ionization can be improved by a factor of 10 within 30 generations of the evolutionary algorithm and minimization is almost immediate. Their results are as shown in Fig. 40b. The optimal pulse is not known in advance. Since the variation shape of the possible pulse shapes is huge, scanning the entire parameter space is impossible and as such the optimized pulse shape could not have been predicted by theory.

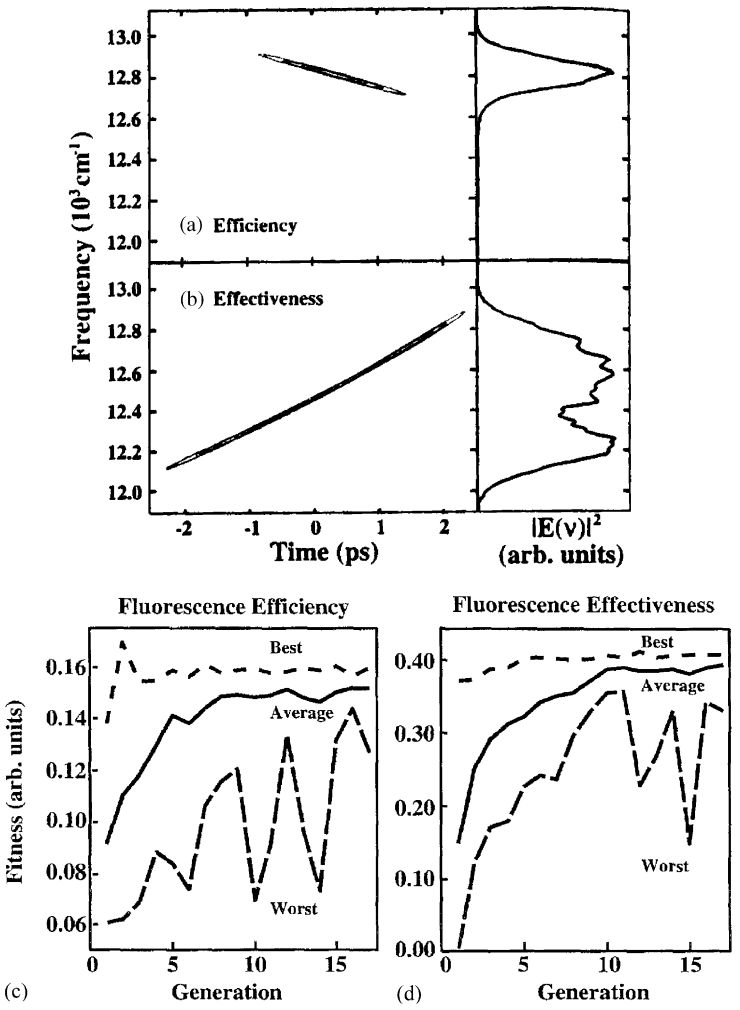

Fig. 39. (a) A sample optimal pulse for the fluorescence efficiency as determined experimentally by the feedback program. The left side is a plot of the experimentally determined Wigner transform, which shows the intensity of the electric field in time and frequency space. The right side shows the spectral projection $|E(v)|^2$ (where $v = c/\lambda$), with the leakage spectrum extending to lower frequencies. Since the efficiency does not depend strongly on the linear chirp, other sample optimal pulses can have chirps of the opposite signs. (b) As in panel (a), but showing an optimal pulse for the fluorescence effectiveness. (c) The convergence of the generic algorithm as measured by the best (small dash), average (solid), and worst (large dash) fitness defined by the fluorescence efficiency (ratio of fluorescence to laser power). (d) As in panel (c), but the fitness is now defined as the fluorescence effectiveness, proportional to fluorescence power alone.

In case of more complex molecule, such as $CpFe(CO)_2Cl$ (here, Cp denotes the cyclopentadienyl ion) from Ref. [181], there are two product channels leading to $CpFeCOCl^+$ or $FeCl^+$ depending upon bond cleavage. In this case, however, the maximization of $CpFeCOCl^+/FeCl^+$ does not correspond to the bandwidth limited pulse. In fact, in both the cases they get a complex pulse structure

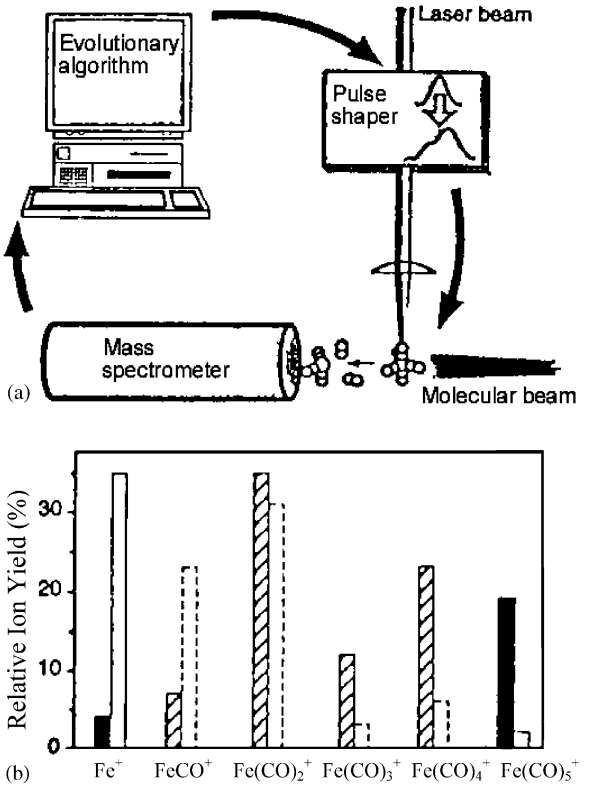

Fig. 40. (a) Schematic experimental set-up. Femtosecond laser pulses are modified in a computer-controlled pulse shaper. Ionic fragments from molecular photo-dissociation are recorded with a time of flight mass spectrometer. This signal is used directly as feedback in the controlling evolutionary computer algorithm to optimize the branching ratios of photochemical reactions. (b) Relative $Fe(CO)_5$ photo-dissociation product yields. The yields are derived from the relative peak heights of the mass spectra. The ratio of $Fe(CO)_5^+/Fe^+$ is maximized (solid blocks) as well as minimized (open blocks) by the optimization algorithm, yielding significantly different abundances of Fe^+ and $Fe(CO)_5^+$ in the two cases. The peak heights of all other masses [$Fe(CO)^+$ up to $Fe(CO)_4^+$] have not been included in the optimization procedure.

and an increased pulse-duration (lower intensity) as compared to bandwidth-limited case, thus again confirming that it is spectral optical phase and not the pulse intensity that is responsible for the optimization results. Considering that the organometallics are widely used as photo-catalysts in many organic reactions and in microelectronics, this experiment represents the first practical example of coherent control of chemical reactions. This is perhaps an important step towards the synthesis of chemical substances with higher efficiencies while reducing unwanted by-products simultaneously.

In these demonstrations discussed until now involving feedback loops for both AOM and LCM pulse-shapers, complex algorithms like the evolutionary algorithm [182] and the simulated annealing algorithm [183] have been used and over 1000 iterations were performed in one experiment for optimization. In using such complex schemes, both the AOM-based and LCM-based pulse shapers have been used as discussed here. Both the LCM and AOM based arbitrary spatial pulse shapers have their own advantages and disadvantages. The on-off isolation between the pixels for the LCM pulse

shaper is at best 20 dB while that of AOM is 40 dB and the refresh rate of at least a millisecond for liquid crystal arrays in the LCM technique is orders of magnitude slower than the AOM-based spatial shaper [41]. Thus, a large number of iterations can take a time that is too long to avoid complications caused by the drifting effects inherent to most laser systems, among other problems. On the other hand, there is significantly higher throughput for LCM devices that could avoid the complexity of additional amplifier and the capability to hold the mask once the optimal solution is found. LCM devices now allow polarization shaping [168] that could provide an additional "control-knob" for further advancing the feedback loop control experiments. More recently, deformable mirror [42] scheme has also been used for optimizing efficient high-harmonic generation [157]. Currently, the number of pixel available from deformable mirror scheme is limited and only rudimentary shapes were sufficient to demonstrate the effectiveness of the closing the loop in the reported experiments. One hopes that other promising pulse shaping techniques, such as that of AOPDF [119], would soon be adapted to such closed-feedback loops for more optimal performances.

More recent experiments under the strong field regime on closing the loop for control of gas-phase photochemical reactivity have been successfully achieved in organic molecules [184] and alkali clusters [185]. Such experiments with close-loop learning control have been successful in spite of starting off blindly and have worked for laboratory control of many quantum processes and to optimize a desired process, which include adaptive pulse compression [186,187], control of pulse phase [188], manipulation of pure rotational [189] and vibrational dynamics [190] in diatomics, one and two photon transition in atoms [60,191], creation of specific wavefunctions in Rydberg atoms [169], and generation of high harmonics in argon gas [157]. Control in liquid phase has also been demonstrated with such adaptive pulse shaping techniques through the demonstration of chemically selective molecular excitation [192], maximization of stimulated Raman signal from methanol in solution [193], and the optimization of coherent antistokes Raman emission [194].

Very recently, Motzkus and coworkers [195] have for the first time demonstrated optimal control of biological function using the feedback control approach. They applied certain optimally shaped colours of light to *Rhodpseudomonas acidophila* light harvesting molecule (LH2) instead of disordered, noise-like sunlight, and LH2 responds with different patterns of energy flow. This experiment is also the first successful control of the energy flow in a molecule. Interestingly enough, Motzkus and coworkers had a hard time to find a pulse shape that would enhance the natural transfer, while it was easy to make transfer even worse. Thus, when they used the algorithm to find a pulse with more losses than natural, the "convergence curve" was exponentially achieved. Optimized pulse shapes deposit energy in the light-harvesting complex in such a way that more of the harvest is dissipated instead of transferred to the acceptor states as compared to the unshaped (transform limited) pulses and the harvest is no longer divided 50:50 but rather 68:32. Given the complexity of the biological system, it was not possible to have any previous knowledge of how an optimal pulse might look like in this optimization and they used FROG techniques to look at the shaped pulses generated in the feedback loop. The optimized pulses induce more internal conversion and a little energy transfer, which upon a π-phase shift has comparable flow into the two channels, and this behaviour of an oscillating feature of 30% modulation continues with increasing π-phases. Thus, 30% of the energy flow is shifted around coherently, which implies that the light-harvesting complex is excited into a quantum mechanical matter wave with designed interferences. Thus, Motzkus and coworkers [195] demonstrate control over concerted motion of a biological complex. The interferences decide about the fate of this very special harvest—collected or lost.

5. Emerging technologies

The unique pulse shaping technology discussed here for coherent control applications is also useful for more technologically relevant issues, such as, optical-communications, remote-sensing, enhancing signal acquisition and in medical diagnostics (e.g., measuring variations in oxygen concentration in living tissue). The ramifications for optical communications are quite immediate. As the information highway demands increase, the necessity for faster communication keep rising exponentially and there is a perpetual need to increase the speed and throughput of the transmitted information. Among the available choices for communication: wireless, twisted-pair, coax cable, etc., the optical fibres have minimal loss and maximal available bandwidth, which makes it the best possible option. Such communication systems work best at 1550 nm where distortion through the fibre is minimal. Presently the best possible throughput available from the commercial systems is gigabit/s, and these use fibre-optic technology. In optical fibres, the information transfer process essentially involves encoding the data by light modulation techniques. Two different modes of light modulation are commonly used: One is the wavelength domain modulation and the other is the time domain modulation [technically: wavelength division multiplexing (WDM) and time division multiplexing (TDM)]. Each of these schemes has asymptotically approached a maximal data transmission limit of gigabit/s; however, recent studies show that AOM-based ultrafast pulse-shaper could possibly pack even more information. If the broad spectral content of the ultrafast pulses were wavelength coded with an optical pulse shaper while the pulses remain confined to a short time, several such time-bursts could be transmitted within a second to achieve over a trillion bits of data per second (terabit/s) transmission. Terabit/s transmission is thousand times faster than the best commercially available fibre optic system. The very high transmission capacity of a terabit can perhaps be well appreciated from the fact that a terabit contains enough bandwidth to transmit about a million movies simultaneously. Unfortunately, LCMs-based pulse shapers have slow update rates (maximum 100 Hz) and limited pixel resolution which makes them unsuitable for high-speed communication applications. It is the MHz update rates and minimal pixelization problems of the AOM-based pulse shaper, which makes it very suitable candidate for the ultrafast communication applications. Major parts of the data-transmission problems also arise due to the inequality of the source channel signals. Built-in feedback-scheme would be a very attractive approach to overcome such non-ideality issues that exits in real systems. A real-time adaptive amplitude feedback on an AOM-based optical pulse shaping system implemented at 1550 nm targeting at new optical telecommunication applications [196]. Fig. 41 shows the schematic feedback algorithm and basic experimental set-up required in feedback-based computer-controlled AOM pulse shaping. Real-time amplitude feedback in an AOM-based pulse shaping system can modify any input spectrum, so that it is within 5% tolerance of the target shape in less than 10 iterations of the feedback loop, and can result in equalized channel signals (Fig. 42). Another important feature of the AOM pulse shaper is the simultaneous capability to impose phase modulation. Such phase modulation capabilities have been shown to generate precise ultrafine delay lines [126] (Fig. 43), which can be simultaneously transmitted to the receiver-end to act as a reference clock in decoding the transmitted data.

The concepts of full characterization of the amplitude and phase of the electronic wavefunction have also been extended to control the state of excitation in semiconductors including control of photocurrent direction [197] and charge oscillations leading to terahertz radiation [198]. Other control concepts in semiconductor structures include electron–phonon scattering, population and orientation

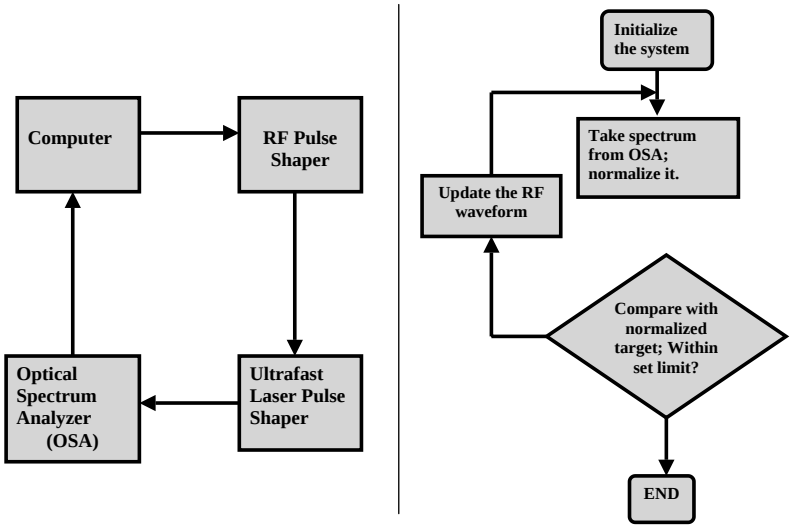

Fig. 41. Schematic of a simple feedback loop for a computer-controlled AOM pulse shaper. This particular schematic is shown for an amplitude only modulation where the measurement of wavelength is sufficient to characterize the pulse shape.

dynamics of excitons. Citrin [199] has discussed theoretical concepts of coherent control of excitons in quantum wells based on self-pulse shaping. Weiner [200] has discussed the application of pulse shaping to coherent control of charge oscillations in coupled quantum wells leading to terahertz emission. Focusing a short laser pulses onto a biased semiconductor wafer can produce terahertz radiation. If the photon energy exceeds the band gap, suddenly large amount electron–hole pair production takes place. The resulting transient current produces a terahertz radiation with duration of typically 1 ps. The interesting property of these terahertz pulses is that they may be shorter than a single cycle. These half-cycle pulses are of importance in studying Rydberg wavepackets. Unlike conventional radiation, which can ionize atom only when excited electron is near nuclear core, a nearly unipolar half-cycle pulse can eject an electron and track a wavepacket anywhere along its orbit. Quang et al. [201] have demonstrated the control of spontaneous emission from a three-level atom with one resonant frequency near the photonic band gap edge. Relative phase between pump and control laser has shown to control inversion, indicating the possibility of phase sensitive atomic scale optical memory device. Sanpera et al. [202] discuss the high harmonic generation in context of quantum interferences. They show that of superposition of bound states constituting the initial state, lead to scheme in which features of harmonic spectrum can be controlled. High harmonic generation is technologically important as the source of new coherent radiation source, all the way to the X-rays.

5.1. Terabit/s data communication applications

Yang et al. [126] demonstrated for the first time the rapid programmable ultrafast optical pulse shaping at 1550 nm wavelength, the important wavelength range for applications to optical

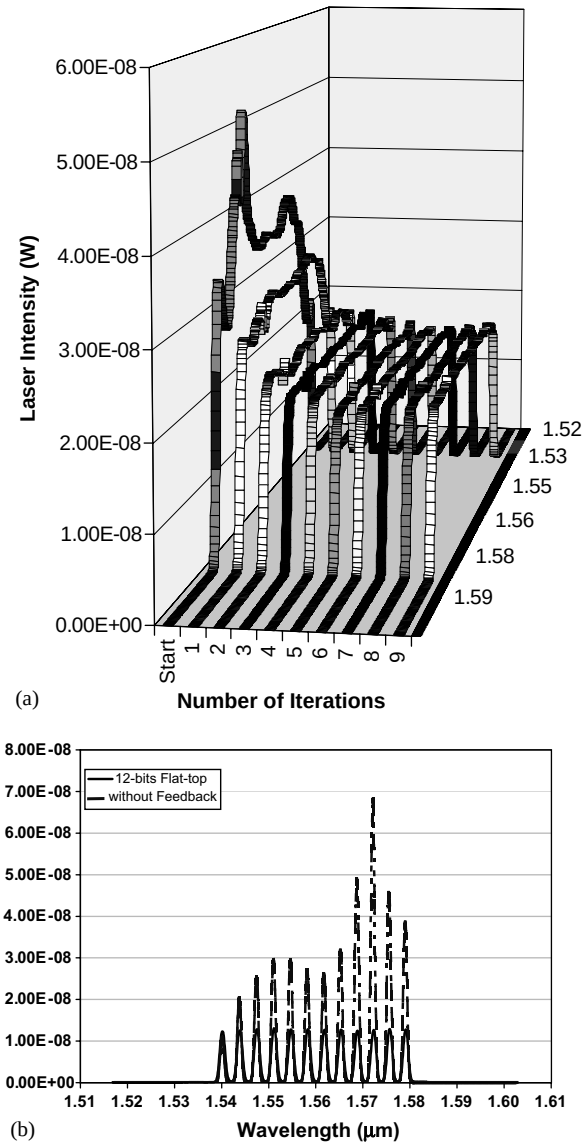

Fig. 42. Implementation of feedback loop to generate equalized channels. In (a), it is shown that even with a simple flowchart algorithm of Fig. 16, it is possible to overcome imperfect spectral features to generate a rectangular profile within 10 iterations. Once the transform is known, equalized channel generation shown in (b) is automatic.

communications. In particular to the optical information channel, what was achieved with ultrafast optical pulse shaping can be viewed as an optical spectral encoder with rapid update rate. One of important and promising applications of this spectral encoder is in high-speed optical communication. By definition, encoding information on an optical carrier requires pulse shaping; an unshaped optical wave (no amplitude, frequency, or phase modulation) is perfectly monochromatic, hence has no

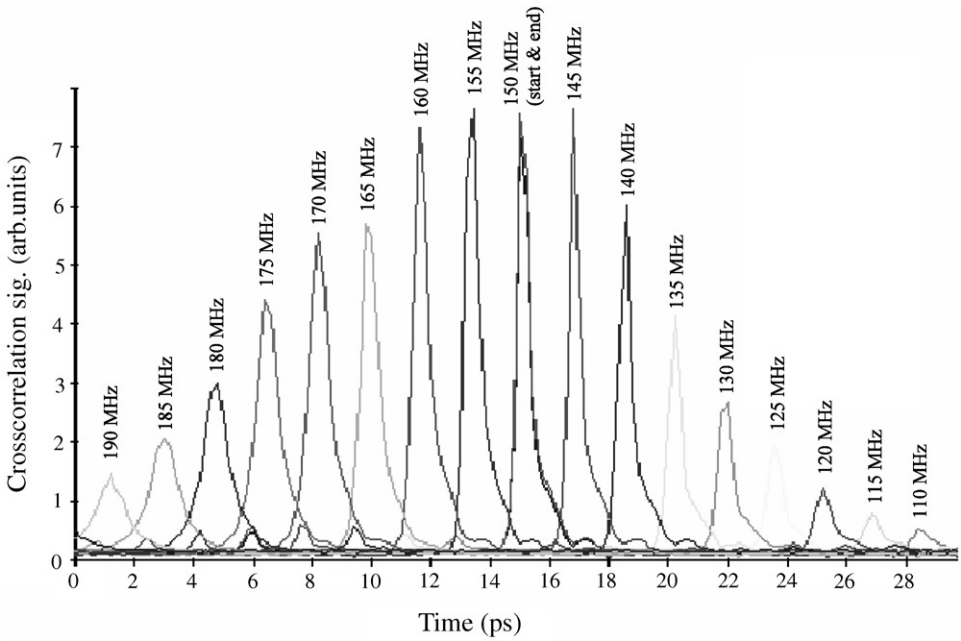

Fig. 43. Rapid tunable delay line generated from the AOM pulse shaper with the help of pure phase modulation. Such phase modulation could enable simultaneous transmission of an ultrafine delay line that could be used as a clock for a decoder at the receiver end.

bandwidth. Rapid information transmission (rise time Δt) implies large frequency bandwidths (Δv), in accord with the classical time-bandwidth uncertainty relation $\Delta v \Delta t \approx 1$. Thus advances in high-speed communications have historically been closely linked to developments of efficient modulators, and complex modulations have been commonly used in radio frequency and microwave communications applications for decades. In fact, commercially available "arbitrary waveform generators" (AWGs) can give any possible voltage waveform with ~ 1 ns rise-time. The rapid rise times of ultrafast laser pulses implies a far greater bandwidth than is conceivable at microwave frequencies. Mode-locked fibre lasers, optical fibres, and erbium-doped fibre amplifiers (EDFAs) operating at the minimum-loss fibre communications wavelength ($\lambda = 1.55$ μm) all have bandwidths in excess of 5 THz; yet the most advanced fibre-optical communications system currently in use operate at only approximately 10^9 bits per second (Gbps). This huge gap between the amount of optical bandwidth used and those of available indicates the extremely low bandwidth efficiency achievable in practical systems. Recently, huge amount of efforts are conducted by both university and industry researchers to develop dense WDM (DWDM) systems to narrow this gap.

The AOM spectral encoder can play many important roles in these DWDM systems by its flexibility of control over the optical signal [203]. At first glance this kind of sub-picosecond-resolution laser pulse shaping may sound both impossible and impractical, because no existing optical modulators have such rapid rise-times as mentioned before and even if you had a sub-picosecond modulator, where would you get THz voltage signal to drive it? The advantage of the spectrum encoder

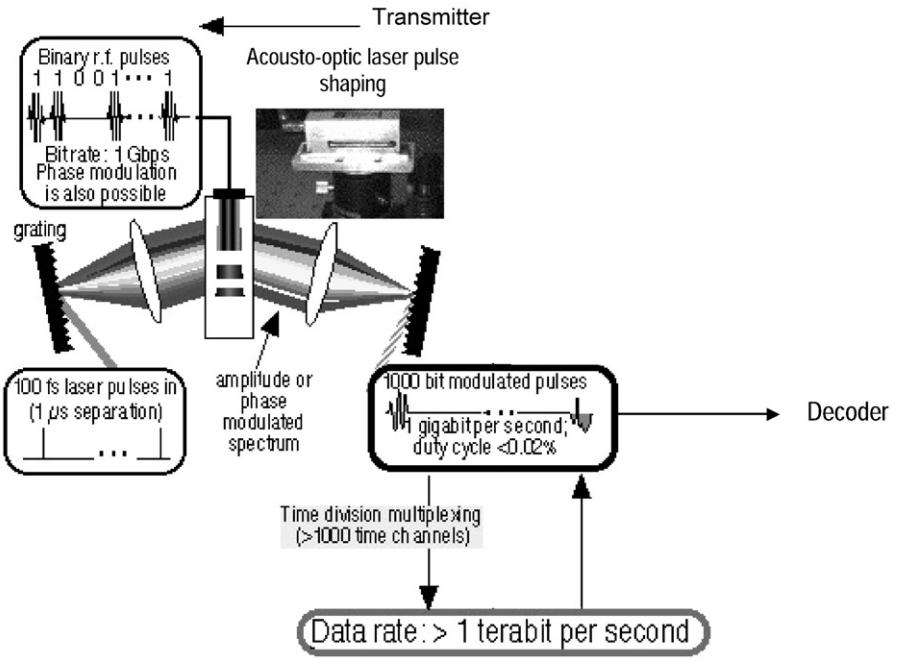

Fig. 44. An AOM ultrafast pulse shaping based proposal for a fibre optical link to achieve data throughput greater than 1 Tbps.

exploited to overcome the apparently formidable barrier is the huge difference between speed of sound and speed of light in AOM crystal. Since the ratio between two is about 1 to 1 million, one can use MHz electrical signal to achieve THz programmable modulation of an optical signal, yet still keep a reasonable update speed [30]. In practice, high resolution spectral encoding is a variation of DWDM by definition and can be used to significantly improve the bandwidth efficiency. The idea can be illustrated in the following way. Starting with a 100 fs FWHM optical pulse, for example, encoding 16 amplitude on–off-keying return-to-zero (RZ) format bits in its spectrum in the worst case broadens the pulse by a factor of 16—to about 1.6 ps FWHM ideally. The encoded pulses, therefore, can be well confined in a 4 ps optical switching window for example without significant distortion to the encoded spectrum. By doing this, the TDM system can benefit from spectrum encoding by a factor of 16 and achievable DTR can be as high as 4 Tbps. By increasing spectrum encoding density the slower TDM systems can also achieve DTR of or better than 1 Tbps. For example, for a TDM system with switching window of 40 ps, one can encode 160 bits in the spectrum to achieve the same transmission rate of 4 Tbps. Since the encoded pulses now are well confined in 40 ps time window, noticing that in worst cases the encoded pulses will be broadened up to 16 ps FWHM ideally. The limitation lies in the trade-off between the time resolution of TDM and the frequency resolution of spectrum encoding.

Fig. 44 shows the schematic of a proposed all-optical data transmitter with a throughput higher than 1 Tbps [204]. At the transmitter end, for a single TDM channel, a laser pulse source with 37 MHz repetition rate and 200 fs pulse width around 1.55 μm was sent into the AOM pulse shaper, which

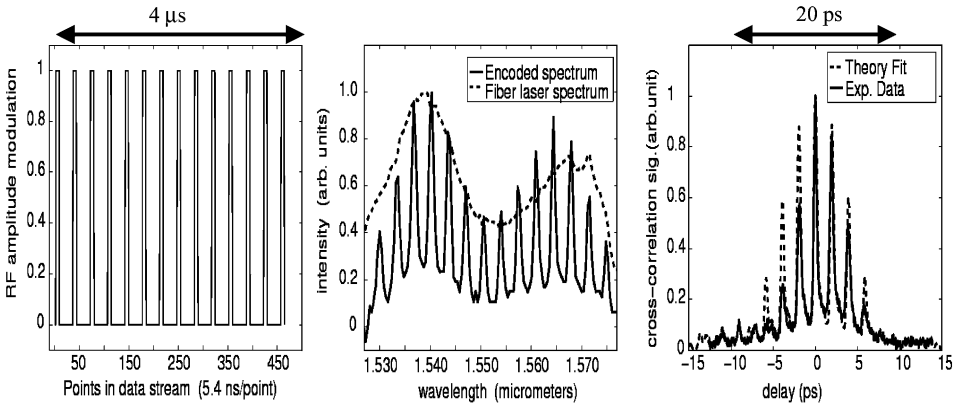

Fig. 45. 14-bit data frame with all-one pattern; the pulse shape in time domain shows the well confined temporal features; 3.5 Mbps electronic data stream shown in (a) is compressed into optical data bursts of more than 700 Gbit/s repeating every 4 μs, which allows optical TDM. (a) 3.5 Mbps electronic data frame of 4 μs. (b) Pulse spectra: solid curve shows the encoded spectrum while the dotted line shows the unshaped pulse spectrum. (c) Cross-correlation trace showing the temporal behaviour of the spectrally encoded pulse; solid curve is the measured data; the dotted curve is the theoretical prediction assuming the constant phase across the measured spectrum backbones. This compares favourably with most existing multiplexing technologies.

has been shown capable of encoding 14 RZ format amplitude modulation bits per pulse with the encoded pulse width restrained within a 20 ps time slot (Fig. 45). The spectrum-encoded pulses are then pulse picked at 250 kHz repetition rate and multiplexed in time domain by TDM techniques to be a single TDM channel. Since the time width of the TDM slot is 20 ps, a 100 GHz TDM switching is required to do a single TDM channel drop. At the receiver end, a WDM analyser could be used to decode the spectrum data. In the simplest form, a WDM analyser can be as simple as a spectrometer operating at 1.55 μm could be used. Since for a single TDM channel, the repetition rate is 250 kHz, and enhanced by the spectrum encoding technique, 14 bits can be encoded to a single pulse, the data transmission rate for a single TDM channel, therefore, achieves 3.5 Mbps. In the 4 μs repetition period, one can multiplexing up to 350 thousand TDM channels, therefore achieves a throughput of 1.4 Tbps for this single fibre data link. These current experiments [203] have showed the ability to encode 14 bits return-to-zero (RZ) data into the femtosecond pulse spectrum while keeping the time width of the encoded pulse within the 20 ps range. A time-domain multiplexing (TDM) network with switching window of 20 ps that is, in principle, capable of 100 Gbps communication rate can benefit from current spectrum encoding technology for a factor of 14 and will, therefore, achieve > 1 Tbps communication rate.

There is a trade-off between the TDM density and WDM density. For the particular AOM experimental set-up used by Yang et al. [205], the ultimate WDM density could be as high as 400 channels. This would trade for a 25 times less dense time-domain multiplexing. But either way, a throughput higher than 1 Tbps for one single fibre optical data link is achievable. Furthermore, since this spectrum modulation technique allows much more than just amplitude only modulation, it opens the door to many potential new optical communication architecture and protocols, incoherent or coherent. The flexibility that the AOM spectral encoder can achieve opens a vast opportunity

to new communication architectures. Some existing protocols can also take advantage of this new technique, like the CDMA and pulse shape coding (PSC) with entirely new appearance.

5.2. Novel laser technology and spectroscopy developments

Among the novel laser technology developments are issues such as efficient amplified laser source at various wavelengths ranging from X-rays to the far-IR. Thus, when high harmonic generation, which provides a tabletop source of soft X-rays that complements soft X-ray lasers, benefited from the application shaped pulses, the potential of feedback pulse shaping techniques to novel laser technology unravelled. High-harmonic generation also allows for tunability, by selecting a different harmonic or using a different input beam wavelength. High-harmonic generation typically yields only microwatts, with nanojoules per pulse, except with the use of feedback pulse shaping techniques [157]. The use of AOPDF schemes [120] and other pulse schemes to produce ultrashort amplified pulses at high efficiency demonstrates the importance of pulse shaping schemes for laser developments. Similarly, the use of optical parametric amplifier (OPA) and non-linear OPA's to transfer the shape of laser pulses from the fundamental wavelength regime to other wavelengths [206] has enhanced the laser technological developments. Thus, the generation of tunable UV–visible and IR programmable shaped pulses have become possible.

Extension of the NMR spectroscopic techniques, such as "two-dimensional optical spectroscopy" [207] is one of the most tantalizing analogues to the optical spectroscopists for the possible access to the further structural dynamical information content present in such experiments. In analogy to NMR, such techniques benefit immensely with the use of pulse shaping techniques by simplifying the observed spectra. Typically, couplings between transitions in an irradiated system (atom or molecule) can be detected through the presence of cross-terms in the two-dimensional spectrum. Additional unwanted cross-peaks arise from non-perfect pulse areas, simultaneous excitation of two transitions, and negative frequency components, but it has been shown by Keusters et al. [208] that a pulse shaping scheme that results in phase-cycling can simplify these spectra tremendously. Another recent approach [209] has shown great improvement in the spectral resolution with the introduction of new IR polarization conditions that completely eliminate diagonal peaks from the 2D IR spectra and leave only crosspeaks needed for structure determination. Thus, with the advent of the recent adaptive polarization control [168] and the capability of phase cycling [208] with pulse shaping techniques, realistic optical analogues of NMR are very promising.

6. Future prospects

Most of the issues on coherent control discussed in this review have been at the level of first demonstration or theoretical predictions that are yet to be demonstrated experimentally, which represent emerging areas where the future prospects are very high. Thus, with all the rapid technological developments, there is a big promise of experimental demonstrations of anharmonic ladder climbing, selective bond breaking that could realistically qualify as bond-selective chemistry, photon locking through adiabatic half-passage, etc. in the very near future. The very recent demonstrations of amplified tunable pulse shaping technology into the IR and visible wavelengths [206] are definite signs of

technology bottleneck issues becoming minimized. Nevertheless, let us discuss some more futuristic areas where the principles of coherent control promises to have significant impacts.

6.1. Quantum computing

One such important application of the concepts of coherent control is emerging in the area of quantum computing. The selectivity in excitation, which is offered by shaped laser techniques [14,49], may also serve as the building blocks for the development of the first practicable quantum computer. Optical schemes for quantum computing would require feedback-loop computer controlled pulse shaping, as has been demonstrated by Bucksbaum and coworkers [210] where they have discussed information storage and retrieval through quantum phase. They show that, in case of an eight-state Rydberg atom wavepacket, they can store information as a quantum phase in one or more flipped state, which could be subsequently retrieved in a single step in agreement with the Grover's algorithm. These experiments establish the promise on the applications of future of coherent control developments to practical quantum computing problems in the future. More recent experiments have shown the demonstration of Grover algorithm with classical Fourier optics [211].

Minimizing decoherence is an important challenge towards the realization of quantum computing (QC). While nuclear magnetic resonance (NMR) spectroscopy of molecules in liquid phase is an important approach to QC [212] and has long decoherence times, it suffers in terms of scalability to larger number of qubits [213]. Alternative approaches for QC are, therefore, being sought [214]. Optical spectroscopy of molecules and nanoparticles could potentially become a highly scalable approach, but for the intramolecular relaxation processes, such as intramolecular vibrational relaxation (IVR), which is the most important contributor to decoherence even in isolated molecules. Controlling IVR is also important for "coherent-control" due to its connection to "bond-selective" chemistry [36]. The prospect of QC can lead to a further resurgence of activity in this area. Restriction of IVR by optical schemes can be an attractive route towards selective excitation in large molecular systems. Albeit attractive, most of the photon-mediated approaches towards restricting IVR (also called "photon-locking") have used complicated pulse shapes that are yet to be demonstrated in the laboratory due to stringent requirements of intensity and precision.

Goswami [51] has proposed the use of simple chirped pulses for minimizing decoherence. In contrast to the complicated pulse shapes, simple chirped pulses have been produced routinely at very high intensities and at various different wavelengths for many applications, including selective excitation in coherent control [49]. Such selective optical control over molecules in an ensemble is as unique as addressing individual spins in a NMR spectrometer and lead to *quantum computing in bulk optical systems*. The main aim in coherent control has been controlling an observable, while in the case of QC individual logic gates would be implemented using the principle of controlling observables. The overall idea, therefore, is to use shaped-optical pulses, which, on interaction with a quantum system, would retain coherence for longer time so that a larger number of logic gates are implementable.

In terms of quantum computing, when a sequence of such experimentally achievable chirped-pulses act on a bulk system, and perform a series of quantum logic gates (e.g., AND, NOT, etc.), it would essentially constitute "ensemble quantum computing" [215]. Using the formalism of generalized chirped pulses discussed in Section 3.2, Goswami [51] discusses the construction of a CNOT gate as an example of experimentally implementable gate involving photon entanglement with quantum

Table 1
CNOT gate with simple chirped pulses

Shaped pulse	A	B	A ⊕ B
"Inverting" pulse	1	1	0
	1	0	1
"Dark" pulse	0	1	1
	0	0	0

system. The truth table for this CNOT gate is shown in Table 1 for a quantum mechanical ensemble B that can either be in the ground (state 0) or excited (state 1) interacting with the control pulse A, which provides robust chirped pulse inversion (condition 1) and the self-induced transparency or dark pulse (condition 0). Under the effect of inverting pulse, the ensemble undergoes population inversion while the dark pulse preserves the original state of the system. Shaped pulses are important for implementing such an ensemble gate since such coupled systems preclude the use of simple pulse area approaches of $\pi/2$ and π sequences for controlling coherence or inducing inversion. The dark pulses are also essential in restoring the system to its initial state without being limited by the natural lifetime of the system, which ensures speeding up the subsequent steps. An important point to note, however, is that this ensemble CNOT gate is constructed with one input wire as the classical light beam while the other one is the quantum two-level system. Thus it is not a fully quantum CNOT gate.

6.2. *Biomedical application*

General applications of lasers for biomedical purposes are well known for diagnostic tools, surgical tools and for imaging purposes [216]. The immediate extension of ultrashort pulse shaping technology for biomedical applications holds lots of promises, to further necessitate looking into its domain of influence. Though very few applications for ultrafast pulse shaping technology are currently in use, there are very strong indications as to where it would lead.

One of the most commonly adopted methods, for imaging, in recent times for three-dimensional profile measurement is optical coherence tomography [217,218] or a white light interferometer, which uses a broadband, low coherence light source. Recently the principle of femtosecond pulse shaping by spectral modulation has been used in conjunction with the joint transform correlator to make a spatio-temporal joint transform correlator [217]. The advantage of such a technique has been that it essentially removed the need of 1-D depth scanning and thereby avoided the long measurement times involved. Consequently, this eliminates the electronic computation needed to obtain the object image, and so it can be implemented as an all-optical set-up. Initially, this was demonstrated as a surface measurement set-up, however, as a natural extension, it was easily extended for providing tomographic sectioning of biological samples. In fact, with the use of principles of pulse shaping, a depth resolution of 70 μm was achieved [217]. Furthermore since there is no contact between the probe and the tissue, it is a useful non-invasive technique, which provides the physician with near-histological resolution imaging of sub-surface tissue morphology, potentially aiding in biopsy site selection and thus approaching the goal of "optical biopsy" [219].

Optical trapping and manipulation of viruses and bacteria [220] have been demonstrated in the late 1980s. Such optical tweezers are now used for localizing larger cells and observing the biomechanics [33] of each individual constituent of such a cell. It is possible to manipulate the activity of a particular molecule, which responds to the incident light with the help of the pulse-shaping technology. As this technology has proved its potential in chemistry in the coherent control of the chemical reaction, it is not very difficult to visualize that in near future similar attempt would be possible with the use of optical tweezers to isolate a particular constituent of the cell and induce some reaction or regulate a activity of this constituent [36]. Using a broadband source of light it has been possible to identify the pre-cancerous cells [221], especially the one which are epithelial in origin. This approach essentially looks at the abnormal size of the nucleus to identify whether it is cancerous or not. Once identification process is complete then one could use shaped pulses to trigger some photoreaction in the nucleus, which prevents the pre-cancerous cells from becoming cancerous ones. Thus, it is possible to foresee that ultrafast pulse shaping may not only be of use for diagnostic purposes, but also for therapeutic use.

Attempts are also on-way that are trying to combine the manipulation of the centre-of-mass or internal degrees of freedom of the target to achieve molecule specific coherent control in liquids that is of relevance to biology [36]. Experiments like, picosecond chirped pulse induced inversion, stimulated emission pumping and chirped femtosecond three-pulse four wave mixing have demonstrated that laser chirp can be used to control coherence transfer between the ground and excited states in gas phase molecules, like I_2. Typically, as the system becomes more and more complex, it is increasingly difficult to predict the outcome. Feedback closed-loop experiments have addressed this very successfully and recently, coherent control experiments have become possible in the liquid phase [192,195]. In condensed phase, an additional control that one might like to achieve (e.g. bio-molecular reactions in the liquid phase) is localization of active reactant. Optical tweezers have been shown to have the capability of localizing cells and even large molecules in the liquid phase. Since optical tweezers use light field to hold the large molecules, it is conceivable that the same light field can be used to manipulate the activity of the particular molecule of choice. In fact, we can perhaps say that the use of optical tweezers along with pulse shaping techniques could perhaps be a new window to attempting molecule-specific coherent control in liquids that is of relevance to biology.

All these discussions of using shaped pulses for inducing specific coherent controlled processes in biological samples essentially rely on delivering such pulses through optical fibres. However, ultrashort pulses propagating through the optical fibre gets reshaped, which would be undesirable. Here again the pulse-shaping technology can come to rescue as discussed in the first section on optical communication issues. In fact, in all such applications where ultrashort pulses have to be delivered through the optical fibre this is a serious problem. Knowing the optical characteristics of the fibre through which it propagates so that one can shape the pulses at the input so that as it propagates it would compensate for the dispersive effects resulting in the desired pulse shape at the terminal end. This would enable the desired pulse to be delivered at the target without distortion.

6.3. Novel semiconductor devices

Semiconductor quantum dots are nano-sized quantum structures that allow electronic properties to be tailored through quantum confinement. These nano-structures are known to have atom like spectra

with discrete and sharp spectral lines. The similarities between atoms and quantum dots suggest the possibility of using coherent optical interactions for wave function engineering. In contrast to higher dimensional semiconductor systems, quantum dots suggest the possibility of using coherent optical interactions for wave function engineering in a similar way to that achieved in atoms but with the technological advantages of a solid-state system. Thus, the results of coherent control in atoms can well be applied to localized quantum states of quantum dots to enable wave function engineering of specific target states. In an experiment on similar lines, D.G. Steel and coworkers [222] used picosecond optical excitation to coherently control the excitation in a single quantum dot on a time scale that is shorter compared to the decoherence timescale. Two pulse sequences were applied to manipulate the excitonic wave function by using the polarization of laser and by controlling the optical phase through time delay between the pulses. Such experiments promise the future possibility to implement various schemes for quantum computation and coherent information processing and transfer, where it is important to address and coherently control individual quantum units.

Novel optoelectronic devices like optical switches based on undoped quantum well structures, using pulse-shaping techniques have been predicted. Neogi et al. [223] have demonstrated that besides the relaxation time of the system, tailoring the properties of the coupling pulsed laser fields via pulse shape, delay or peak power can also be used to manipulate the interband transitions of the undoped semiconductor quantum well to enhance the switching performance, which depends on the optical non-linearity. They have also shown how the optical non-linearities of the interband transitions of semiconductor quantum well are controlled by the induced optical inter-subband transitions with the coupling laser fields, which results in sharp resonances and ultrafast interband non-linear response.

7. Conclusions

Ultrafast pulse shaping technology has seen a phenomenal growth in the last decade. As discussed here, it has made some substantial contributions in the study of some of the fundamental issues in physics like light–matter interactions in controlling intramolecular vibration rotation problem in chemistry, to manipulating the cell constituents in biology, to holding the promise of achieving terabit/s data transmission in optical communications. Each of the applications would require a suitable scheme for pulse shaping according to the demands of the applications. The successful emergence of feedback-loop experimentation techniques have helped in fast-forwarding the development of this field. As the technology matures further, it is also showing the promise of opening up exciting new application avenues in areas as diverse as biomedical research to quantum computation. Our overall effort in this review has been to bring to light the fact that coherent control efforts with pulse shaping techniques have just become an established research area and many more new exciting and upcoming research is on the way.

Acknowledgements

I am indebted to Professor Joerg Eichler for offering me a chance to write this review article. I would also like to express my gratitude to Professors Warren S. Warren and Hershel Rabitz and their students for fruitful research collaborations. Special thanks are due to my graduate students and

post-docs to have proofread this document several times. Funding for this writing period has been partially provided the Ministry of Information Technology, Government of India.

References

[1] R.V. Ambartsumian, V.S. Letokhov, in: C.B. Moor (Ed.), Chemical and Biochemical Applications of Lasers, Vol. 3, Academic Press, New York, 1977 (Chapter 2);
V.S. Letokhov, Phys. Today 30 (1977) 23;
N. Bloembergen, E. Yablonovitch, Phys. Today 31 (1978) 23;
A.H. Zewail, Phys. Today 33 (1980) 27;
J. Jortner, R.D. Levine, S.A. Rice (Eds.), Adv. Chem. Phys. 47, Wiley, New York, 1981, Parts 1 and 2.
[2] N. Bloembergen, A.H. Zewail, J. Phys. Chem. 88 (1984) 5459;
T. Elsaesser, W. Keiser, Annu. Rev. Phys. Chem. 42 (1991) 83;
D.J. Nesbitt, R.W. Field, J. Phys. Chem. 100 (1996) 12735;
M. Gruebele, R. Bigwood, Int. Rev. Phys. Chem. 17 (1998) 91;
V. Wong, M. Gruebele, J. Phys. Chem. A 103 (1999) 10083.
[3] M. Hentschel, R. Kienberger, Ch. Spielmann, G.A. Reider, N. Milosevic, T. Brabec, P. Corkum, U. Heinzmann, M. Drescher, F. Krausz, Nature 414 (2001) 509;
N.A. Papadogiannis, B. Witzel, C. Kalpouzos, D. Charalambidis, Phys. Rev. Lett. 83 (1999) 4289;
S.E. Harris, A.V. Sokolov, Phys. Rev. Lett. 81 (1998) 2894.
[4] R.L. Fork, B.I. Greene, C.V. Shank, Appl. Phys. Lett. 38 (1981) 671.
[5] M. Nakazawa (Ed.), IEICE Trans. E81-C (1998) 93;
U. Keller (Ed.), Appl. Phys. B: Lasers Opt. 65 (1997) 113;
C.P.J. Barty, W. White, W. Sibbett, R. Trebino (Eds.), IEEE J. Sel. Top. Quantum Electron. 4 (1998) 157.
[6] W. Kaiser, Ultrashort Laser Pulses and Applications, Springer, Berlin, 1988;
J.C. Diels, W. Rudolf, Ultrashort Laser Pulse Phenomena, Academic, San Diego, 1996;
T. Elsaesser, J.G. Fujimoto, D.A. Weirsma, W. Zinth (Eds.), Ultrafast Phenomena XI, Springer, Berlin, Germany, 1998;
C. Rulliere, Femtosecond Laser Pulses, Springer, Berlin, 1998.
[7] S. Backus, C.G. Durfee III, M.M. Murnane, H.C. Kapteyn, Rev. Sci. Instrum. 69 (1998) 1207.
[8] J. Farger, J. Oberle, in: C. Rulliere (Ed.), Femtosecond Laser Pulses, Springer, Berlin, 1998.
[9] See for example, Appl. Phys. B 70 (Suppl.), (2000), which is a special issue covering the ultrafast optics conference 2001.
[10] T. Brixner, N.H. Damrauer, G. Gerber, in: B. Bederson, H. Walther (Eds.), Advances in Atomic, Molecular, and Optical Physics, Vol. 46, Academic Press, London, 2001, pp. 1–54.
[11] H. Rabitz, R. de Vivie-Riedle, M. Motzkus, K. Kompa, Science 288 (2000) 824.
[12] S.A. Rice, M. Zhao, Optical Control of Molecular Dynamics, Wiley, New York, 2000.
[13] R.J. Gordon, S.A. Rice, Annu. Rev. Phys. Chem. 48 (1997) 601.
[14] W.S. Warren, H. Rabitz, M. Dahleh, Science 259 (1993) 1581.
[15] P. Brumer, M. Shapiro, in: A.D. Bandrauk (Ed.), Molecules in Laser Fields, Marcel Dekker, New York, 1994.
[16] K. Bergmann, H. Theuer, B.W. Shore, Rev. Mod. Phys. 70 (1998) 1003.
[17] A.H. Zewail, J. Phys. Chem. 100 (1996) 12701.
[18] R.N. Zare, Science 279 (1998) 1875.
[19] R.P. Feynman, F.L. Vernon Jr., R.W. Hellwarth, J. Appl. Phys. 28 (1957) 49.
[20] L.J. Butler, E.J. Hintsa, S.F. Shane, Y.T. Lee, J. Chem. Phys. 86 (1986) 2051.
[21] E. Jensen, J.S. Keller, G.C.G. Waschewsky, J.E. Stevens, R.L. Graham, K.F. Freed, L.J. Butler, J. Chem. Phys. 98 (1993) 2882.
[22] F. Fleming Crim, J. Phys. Chem. 100 (1996) 12725 (Centennial Issue);
J.D. Thoemke, J.M. Pfeiffer, R.B. Metz, F.F. Crim, J. Phys. Chem. 99 (1995) 13748.
[23] M.J. Bronikowski, W.R. Simpson, R.N. Zare, J. Phys. Chem. 97 (1993) 2194;
M.J. Bronikowski, W.R. Simpson, R.N. Zare, J. Phys. Chem. 97 (1993) 2204.

[24] Y. Chiu, H. Fu, J. Huang, S.L. Anderson, J. Chem. Phys. 101 (1994) 5410;
Y. Chiu, H. Fu, J. Huang, S.L. Anderson, J. Chem. Phys. 102 (1995) 1199.
[25] J.D. Thoemke, J.M. Pfeiffer, R.B. Metz, F.F. Crim, J. Phys. Chem. 99 (1995) 13748.
[26] C. Cohen, Y.Y. Lin, D.S. Elliott, Phys. Rev. Lett. 64 (1990) 507.
[27] P. Brumer, M. Shapiro, Acc. Chem. Res. 22 (1989) 407.
[28] D.J. Tannor, S.A. Rice, Adv. Chem. Phys. 70 (1988) 441.
[29] S. Shi, A. Woody, H. Rabitz, J. Chem. Phys. 88 (1988) 6870;
A.P. Peirce, M.A. Dahleh, H. Rabitz, Phys. Rev. A 37 (1988) 4950.
[30] A.M. Weiner, in: T. Asakura (Ed.), Trends in Optics and Photonics, Springer, Berlin, 1999, pp. 233–246.
[31] J.X. Tull, M.A. Dugan, W.S. Warren, Adv. Mag. Opt. Res. 20 (1997) 1057.
[32] A. Ashkin, J.M. Dziedzic, Phys. Rev. Lett. 54 (1985) 1245;
A. Ashkin, J.M. Dziedzic, T. Yamane, Nature 330 (1987) 769;
A. Ashkin, K. Schutze, J.M. Dziedzic, U. Euteneuer, M. Schliwa, Nature 348 (1990) 346.
[33] A.D. Mehta, M. Rief, J.A. Spudich, D.A. Smith, R.M. Simmons, Science 283 (1999) 1689.
[34] C.N. Cohen-Tannoudji, W.D. Phillips, Phys. Today 43 (1990) 33;
G.B. Lubkin, Phys. Today (1996) 22;
S. Chu, Sci. Am. (1992) 71;
W.D. Phillips, Rev. Mod. Phys. 70 (1998) 721;
http://www.nobel.se/announcement-97/physics97.html.
[35] J.J. Larsen, I.W. Larsen, H. Stapelfeldt, Phys. Rev. Lett. 83 (1999) 1123.
[36] D. Goswami, A.S. Sandhu, in: Advances in Multiphoton Processes and Spectroscopy, Vol. 13, p. 131;
S.H. Lin, A.A. Villaeys, Y. Fujimura (Eds.), World Scientific, Singapore, 2001.
[37] C. Williams, S. Clearwater, Explorations in Quantum Computing, Springer, New York, 1998.
[38] A.M. Weiner, Rev. Sci. Instrum. 71 (2000) 1929.
[39] A.M. Weiner, J.P. Heritage, Rev. Phys. Appl. 22 (1987) 1619;
A.M. Weiner, A.M. Kanan, IEEE J. Sel. Top. Quantum Electron. 4 (1998) 317.
[40] C. Froehly, B. Colombeau, M. Vampouille, in: E. Wolf (Ed.), Progress in Optics, Vol. 20, North-Holland, Amsterdam, 1983, pp. 65–153.
[41] C.W. Hillegas, J.X. Tull, D. Goswami, D. Stricland, W.S. Warren, Opt. Lett. 19 (1994) 737.
[42] E. Zeek, K. Maginnis, S. Backus, U. Russek, M.M. Murnane, G. Mourou, H.C. Kapteyn, G. Vdovin, Opt. Lett. 24 (1999) 493.
[43] D. Brady, A.G.-S. Chen, G. Rodriguez, Opt. Lett. 17 (1991) 611.
[44] K. Ema, F. Shimizu, Jpn. J. Appl. Phys. Pt. 2, 29 (1990) 631;
A.M. Weiner, D.E. Leaird, D.H. Reitz, E.G. Paek, IEEE J. Quantum Electron. 28 (1992) 2251.
[45] C.J. Bardeen, V.V. Yakolev, K.R. Wilson, S.D. Carpenter, P.M. Weber, W.S. Warren, Chem. Phys. Lett. 280 (1997) 151.
[46] B.W. Shore, The Theory of Coherent Excitation, Vols. 1 and 2, Wiley, New York, 1990.
[47] J. Baum, R. Tyco, A. Pines, Phys. Rev. A 32 (1985) 3435.
[48] L. Allen, J.H. Eberly, Optical Resonance and Two Level Atoms, Dover, New York, 1975.
[49] J.S. Melinger, S.R. Gandhi, A. Hariharan, D. Goswami, W.S. Warren, J. Chem. Phys. 101 (1994) 6439.
[50] S. Chelkowski, A.D. Bandrauk, J. Chem. Phys. 99 (1992) 4279.
[51] D. Goswami, Phys. Rev. Lett. 88 (2002) 177901-1.
[52] M.M.T. Loy, Phys. Rev. Lett. 32 (1974) 814;
M.M.T. Loy, Phys. Rev. Lett. 41 (1978) 473.
[53] F.C. Spano, W.S. Warren, Phys. Rev. A 37 (1988) 1013;
J.S. Melinger, A. Hariharan, S.R. Gandhi, W.S. Warren, in: J.-L. Martin, A. Mingus, G.A. Mourou, A.H. Zewail (Eds.), Ultrafast Phenomena VIII, Springer, Berlin, 1993, p. 113;
J.S. Melinger, A. Hariharan, S.R. Gandhi, W.S. Warren, J. Chem. Phys. 95 (1991) 2210;
J.S. Melinger, D. McMorrow, C. Hillegas, W.S. Warren, Phys. Rev. A 51 (1995) 3366.
[54] J.S. Melinger, S.R. Gandhi, A. Hariharan, J.X. Tull, W.S. Warren, Phys. Rev. Lett. 68 (1992) 2000.
[55] J. Macomber, The Dynamics of Spectroscopic Transitions, Wiley, New York, 1976.
[56] C.P. Lin, J. Bates, J. Mayer, W.S. Warren, J. Chem. Phys. 86 (1987) 3750.

[57] M. Haner, W.S. Warren, Appl. Opt. 26 (1987) 3687.
[58] M. Fetterman, D. Goswami, D. Keusters, J.-K. Rhee, W.S. Warren, Ultrafast Phenomenon XI, Springer, Berlin, 1998, pp. 24–26.
[59] F.H.M. Faisal, Theory of Multiphoton Processes, Plenum, New York, 1987.
[60] D. Meshulach, Y. Silberberg, Nature 396 (1998) 239.
[61] S.A. Hosseini, D. Goswami, Phys. Rev. A 64 (2001) 033410.
[62] D. Goswami, W.S. Warren, Phys. Rev A 50 (1994) 5190.
[63] C. Cohen-Tannoudji, B. Dui, F. Laloe, Quantum Mechanics, Wiley, New York, 1978.
[64] C.H. Townes, A.L. Schawlow, Microwave Spectroscopy, Dover, New York, 1975.
[65] D. Goswami, W.S. Warren, J. Chem. Phys. 99 (1993) 4509.
[66] P.M. Felker, A.H. Zewail, J. Chem. Phys. 82 (1985) 2961;
P.M. Felker, A.H. Zewail, J. Chem. Phys. 82 (1985) 2975;
P.M. Felker, A.H. Zewail, J. Chem. Phys. 82 (1985) 2994;
P.M. Felker, A.H. Zewail, J. Chem. Phys. 82 (1985) 3003.
[67] See, for example, C.P. Slichter, Principles of Magnetic Resonance, Springer, Berlin, 1990, p. 244.
[68] P.L. Knight, P.W. Milloni, Phys. Rep. 66 (1980) 21;
C. Cohen-Tannoudji, S. Haroche, J. Phys. (Paris) 30 (1969) 125;
C. Cohen-Tannoudji, S. Haroche, J. Phys. (Paris) 30 (1969) 153.
[69] Y.S. Bai, A.G. Yodh, T.W. Mossberg, Phys. Rev. Lett. 55 (1985) 1277;
N. Lu, P.R. Berman, Y.S. Bai, J.E. Golub, T.W. Mosseberg, Phys. Rev. A 34 (1986) 319.
[70] S. Mukamel, K. Shan, Chem. Phys. Lett. 117 (1985) 489.
[71] E.T. Sleva, I.M. Xavier, A.H. Zewail, J. Opt. Soc. Am. B 3 (1986) 483;
W.S. Warren, A.H. Zewail, Laser Chem. 2 (1983) 37.
[72] S. Chelkowski, A.D. Bandrauk, P.B. Corkum, Phys. Rev. Lett. 65 (1990) 2355.
[73] See for example, H.-L. Dai, R.W. Field (Eds.), Molecular dynamics and spectroscopy by stimulated emission pumping, Advanced Series in Physical Chemistry, Vol. 4, World Scientific, Singapore, 1995.
[74] C.E. Carroll, F.T. Hioe, Phys. Rev. A 54 (1996) 5147.
[75] J.R. Kuklinski, U. Gaubatz, F.T. Hioe, K. Bergmann, Phys. Rev. A 40 (1989) 6741.
[76] S. Schiemann, A. Kuhn, S. Steuerwald, K. Bergmann, Phys. Rev. Lett. 71 (1993) 3637.
[77] B.W. Shore, K. Bergmann, A. Kuhn, S. Schiemann, J. Oreg, Phys. Rev. A 45 (1992) 5297.
[78] U. Gaubatz, P. Rudecki, S. Scheimann, M. Kulz, K. Bergmann, Chem. Phys. Lett. 149 (1988) 463;
S. Schemann, A. Kuhn, S. Steverwald, K. Bergmann, Phys. Rev. Lett. 71 (1993) 3637.
[79] B. Broers, H.B. van Linden van den Heuvell, L.D. Noordam, Phys. Rev. Lett. 69 (1992) 2062.
[80] R.B. Vrijen, D.I. Duncan, L.D. Noordam, Phys. Rev A 56 (1997) 2205.
[81] S. Chelkowski, G.N. Gibson, Phys. Rev. A 52 (1995) 3417.
[82] S. Chelkowski, A.D. Bandrauk, J. Raman Spectrsc. 28 (1997) 459.
[83] J.C. Davis, W.S. Warren, J. Chem. Phys. 110 (1999) 4229.
[84] E.J. Heller, Acc. Chem. Res. 14 (1981) 368;
E.J. Heller, J. Chem. Phys. 62 (1975) 1544.
[85] S. Shi, A. Woody, H. Rabitz, J. Chem. Phys. 88 (1990) 6870.
[86] C. Moler, C. Von Loan, SIAM Rev. 20 (1978) 801;
M.D. Feit, J.A. Fleck, A. Steiger, J. Comput. Phys. 47 (1982) 412;
R. Heather, H. Metiu, J. Chem. Phys. 86 (1987) 5009.
[87] W.H. Press, B.P. Flanerry, S.A. Teukolsky, W.T. Vetterling, Numerical Recipes: The Art of Scientific Computing, Cambridge University, Cambridge, 1986.
[88] V. Dubov, H. Rabitz, Chem. Phys. Lett. 235 (1995) 309;
V. Dubov, H. Rabitz, J. Chem. Phys. 103 (1995) 8412.
[89] S. Shi, H. Rabitz, J. Chem. Phys. 92 (1988) 364.
[90] M. Sugawara, Y. Fujimura, J. Chem. Phys. 100 (1994) 5646;
M. Sugawara, Y. Fujimura, J. Chem. Phys. 101 (1994) 6586;
M. Sugawara, Y. Fujimura, Chem. Phys. 196 (1995) 113;
Y. Ohtsuki, H. Kono, Y. Fujimura, J. Chem. Phys. 109 (1998) 9318.

[91] H. Rabitz, S. Shi, Adv. Mol. Vibrations Collision Dynamics IA (1991) 187;
R.S. Judson, H. Rabitz, Phys. Rev. Lett. 68 (1992) 1500;
B. Armstrup, G.J. Toth, G. Szabo, H. Rabitz, A. Lorincz, J. Phys. Chem. 101 (1994) 3715.
[92] J.L. Krause, R.M. Whitnell, K.R. Wilson, Y. Yan, S. Mukamel, J. Chem. Phys. 99 (1993) 6562.
[93] B. Kohler, V.Y. Yakovlev, J. Che, J.L. Krause, M. Messina, K.R. Wilson, N. Schwentner, R.M. Whitnell, Y. Yan, Phys. Rev. Lett. 74 (1995) 3360.
[94] J.L Krause, R.M. Whitnell, K.R. Wilson, Y. Yan, S. Mukamel, J. Chem. Phys. 99 (1993) 6562;
B. Kohler, V.V. Yakovlev, J. Che, J.L. Krause, M. Messina, K.R. Wilson, N. Schwentner, R.M. Whitnell, Y. Yan, Phys. Rev. Lett. 74 (1995) 3360.
[95] B.M. Goodson, D. Goswami, H. Rabitz, W.S. Warren, J. Chem. Phys. 112 (2000) 5081.
[96] A. Assion, T. Baumert, M. Bergt, T. Brixner, B. Kiefer, V. Seyfried, M. Strehle, G. Gerber, Science 282 (1999) 918;
R.S. Judson, H. Rabitz, Phys. Rev. Lett. 68 (1992) 1500;
T. Brixner, M. Strehle, G. Gerber, Appl. Phys. B 68 (1991) 281.
[97] L.E.E. de Araujo, I.A. Walmsley, J. Chem. Phys. 103 (1999) 10409.
[98] D.J. Tannor, R. Kosloff, S.A. Rice, J. Chem. Phys. 85 (1986) 5805;
D.J. Tannor, S.A. Rice, Adv. Chem. Phys. 70 (1988) 441.
[99] V. Blanchet, C. Nicole, M.A. Bouchene, B. Girard, Phys. Rev. Lett. 78 (1997) 2716.
[100] A. Abrashkevich, M. Shapiro, P. Brumer, Phys. Rev. Lett. 81 (1998) 3789.
[101] N.F. Sherer, R.J. Carlson, A. Matro, M. Du, A.J. Ruggiero, V. Romero-Rochin, J.A. Cina, G.R. Fleming, S.A. Rice, J. Chem. Phys. 95 (1991) 1487;
N.F. Scherer, A. Ruggiero, M. Du, G.R. Fleming, J. Chem. Phys. 93 (1990) 856.
[102] T. Baumert, M. Grosser, R. Thalweiser, G. Gerber, Phys. Rev. Lett. 67 (1991) 3753;
T. Baumert, G. Gerber, Adv. At. Mol. Opt. Phys. 35 (1995) 163.
[103] T. Baumert, T. Brixner, V. Seyfried, M. Strehle, G. Gerber, Appl. Phys. B 65 (1997) 779;
T. Baumert, R. Thalweiser, G. Gerber, Chem. Phys. Lett. 209 (1993) 29.
[104] E.D. Potter, J.L. Herek, S. Pedersen, Q. Liu, A.H. Zewail, Nature 355 (1992) 66.
[105] E.J. Brown, I. Pastirk, B.I. Grimberg, V.V. Lozovoy, M. Dantus, J. Chem. Phys. 111 (1999) 3779;
I. Pastirk, V.V. Lozovoy, B.I. Grimberg, E.J. Brown, M. Dantus, J. Phys. Chem. A 103 (1999) 10226.
[106] P. Brumer, M. Shapiro, Chem. Phys. Lett. 82 (1986) 177;
C. Asaro, P. Brumer, M. Shapiro, Phys. Rev. Lett. 60 (1988) 1634.
[107] L. Zhu, V. Kleiman, X. Li, S.P. Lu, K. Trentelman, R.J. Gordon, Science 270 (1995) 77.
[108] S. Lee, J. Chem. Phys. 108 (1998) 3903.
[109] J.A. Fiss, L. Zhu, R.J. Gordon, Phys. Rev. Lett. 82 (1999) 65.
[110] F. Wang, C. Chen, D.S. Elloitt, Phys. Rev. Lett. 77 (1996) 2416.
[111] Y. Dakhnovskii, R.D. Coalson, J. Chem. Phys. 103 (1995) 2908;
Y. Dakhnovskii, D.G. Evans, H.J. Kim, R.D. Coalson, J. Chem. Phys. 103 (1995) 5461, and the references therein.
[112] Y.R. Shen, The Principles of Nonlinear Optics, Wiley, New York, 1984 (Chapter 7).
[113] D. Goswami, C.W. Hillegas, J.X. Tull, W.S. Warren, in: D.A. Wiersma (Ed.), Femtosecond Reaction Dynamics, North-Holland, Amsterdam, 1994, p. 291;
J.X. Tull, C.W. Hillegas, D. Goswami, W.S. Warren, Ultrafast Phenomena IX, 1994 Technical Digest Series, Vol. 7, ThD 28-1/553, 1994.
[114] G. Stobrawa, M. Hacker, T. Feurer, D. Zeidler, M. Motzkus, F. Reichel, Appl. Phys. B 72 (2001) 627.
[115] A.M. Weiner, D.E. Leaird, D.H. Reitze, E.G. Paek, IEEE J. Quantum Electron. 28 (1992) 2251.
[116] M. Wefers, K. Nelson, Opt. Lett. 18 (1993) 2033.
[117] Y. Ding, R.M. Brubaker, D.D. Nolte, M.R. Melloch, A.M. Weiner, Opt. Lett. 22 (1997) 718.
[118] A. Yariv, P. Yeh, Optical Waves in Crystals, Wiley, New York, 1984.
[119] P. Tournois, Opt. Commun. 140 (1997) 245;
F. Verluise, V. Laude, Z. Cheng, Ch. Spielmann, P. Tournois, Opt. Lett. 25 (2000) 575.
[120] Product description from Fastlite Inc., http://www.fastlite.com/public/apnotes/apnotdaz01.pdf
[121] D. Kaplan, P. Tournois, in: R.J. Miller, M.M. Murnane, N.F. Scherer, A.M. Weiner (Eds.), Ultrafast Phenomena XIII, Springer, Berlin, 2003.

[122] M.B. Danailov, I.P. Christov, J. Mod. Opt. 36 (1989) 725–731.
[123] M.A. Dugan, J.X. Tull, W.S. Warren, J. Opt. Soc. Am. B 14 (1997) 1–11.
[124] A.M. Weiner, IEEE. J. Quantum Electron. 19 (1995) 161.
[125] W. Yang, D. Goswami, W.S. Warren, CISS Proc. 2 (1998) 618.
[126] W. Yang, D. Keusters, D. Goswami, W.S. Warren, Opt. Lett. 23 (1998) 1843.
[127] M.R. Fetterman, D. Goswami, D. Keusters, W. Yang, J.-K. Rhee, W.S. Warren, Opt. Express 3 (10) (1998) 366–375.
[128] Ronchi grating available from Edmund Scientific, http://www.edmundscientific.com
[129] B. Kohler, V.V. Yakovlev, K.R. Wilson, J. Squier, K.W. DeLong, Rick Trebino, Opt. Lett. 20 (1995) 483.
[130] J.-K. Rhee, T.S. Sosnowski, A.-C. Tien, T.B. Norris, J. Opt. Soc. Am. B 13 (1996) 1780;
J.-K. Rhee, T.S. Sosnowski, T.B. Norris, J.A. Arns, W.S. Colburn, Opt. Lett. 19 (1994) 1550.
[131] D.N. Fittinghoff, J.L. Bowie, J.N. Sweetser, R.T. Jennings, M.A. Krumbugel, K.W. DeLong, R. Trebino, I.A. Walmsley, Opt. Lett. 21 (1996) 884.
[132] C. Iaconis, I.A. Walmsley, Opt. Lett. 23 (1998) 792;
T.M. Shuman, M.E. Anderson, J. Bromage, C. Iaconis, L. Waxer, I.A. Walmsley, Opt. Express 5 (1999) 134.
[133] T.G. Walker, W. Happer, Rev. Mod. Phys. 69 (1997) 629.
[134] M. Fetterman, J.C. Davis, D. Goswami, W. Yang, W.S. Warren, Phys. Rev. Lett. 82 (1999) 3984.
[135] F.C. Spano, W.S. Warren, Phys. Rev. A 37 (1998) 1013.
[136] J.C. Davis, M.R. Fetterman, D. Goswami, W. Yang, D. Keusters, W.S. Warren, CLEO/QELS '99, QTuM7, Baltimore Convention Center, MD, USA, May 23–28, 1999;
J.C. Davis, Ph.D. Thesis, Princeton University, 2000.
[137] M. Haner, W.S. Warren, Appl. Phys. Lett. 52 (1998) 1458;
M. Haner, W.S. Warren, Phys. Rev. B 41 (1990) 5792.
[138] A.M. Weiner, D.E. Leaird, G.P. Wiederrecht, K.A. Nelson, Science 247 (1990) 1317.
[139] M. Saruwatari, IEEE/LEOS Summer Optical Meeting on Optical Networks and their Enabling Technologies, IEEE Lake Tahol, NV, 1994;
A.M. Weiner, D.E. Leaird, D.H. Reitz, E.G. Paeck, IEEE J. Quantum Electron. 28 (1992) 2251.
[140] A.M. Weiner, J.P. Heritage, E.M. Krischner, J. Opt. Soc. Am. B 5 (1988) 1563.
[141] M.C. Nuss, W.H. Knox, U. Koren, Electron. Lett. 32 (1996) 1311;
L. Boivin, M.C. Nuss, W.H. Knox, J.B. Stark, Electron. Lett. 33 (1997) 827;
W.H. Knox, IEEE J. Selected Topics Quantum Electron. 6 (2000) 1273.
[142] A.M. Weiner, J.A. Salehi Jr., in: J. Midwinter (Ed.), Photonics in Switching, Vol. II, Academic Press, San Diego, 1993, p. 73;
J.A. Salehi, IEEE Trans. Commun. 37 (1998) 824;
J.A. Salehi, IEEE Network 3 (1998) 31;
J.A. Salehi, C.A. Breckett, IEEE Trans. Commun. 37 (1989) 834.
[143] A.M. Weiner, J.P. Heritage, J.A. Salehi, Opt. Lett. 13 (1998) 300;
J.A. Salehi, A.M. Weiner, J.P. Heritage, J. Lightwave Technol. 8 (1990) 478;
A.M. Weiner, J.A. Salehi, J.P. Heritage, M. Stern, Encoding and decoding of femtosecond pulses for code-division multiple access, in: J.E. Midwinter, H.S. Hintons (Eds.), OSA, Proceeding on Photonic Switching, Vol. 3, Optical Society of America, Washington, DC, 1989, p. 263.
[144] L.F. Mollenaeuer, M.J. Neubelt, S.G. Evangalides, J.P. Gordon, J.R. Simpson, L.G. Cohen, Opt. Lett. 15 (1990) 1203.
[145] A. Hasegawa, F. Tappert, Appl. Phys. Lett. 23 (1973) 142.
[146] A. Hasegawa, F. Tappert, Appl. Phys. Lett. 23 (1973) 171.
[147] A.M. Weiner, J.P. Heritage, R.J. Hawkins, R.N. Thurston, E.M. Krischner, P.E. Leaird, W.J. Tomlinson, Phys. Rev. Lett. 61 (1988) 2445.
[148] A.M. Weiner, in: J.R. Taylor (Ed.), Optical Solitons Theory and Experiment, Cambridge University Press, Cambridge, 1992, p. 378.
[149] W.J. Tomlinson, R.J. Hawkins, A.M. Weiner, J.P. Heritage, R.N. Thurston, J. Opt. Soc. Am. B 6 (1989) 329.
[150] M.N. Islam, Ultrafast Fiber Switching Devices and Systems, Cambridge University Press, Cambridge, 1992.
[151] S.R. Friberg, A.M. Weiner, Y. Silberberg, B.G. Stag, P.W. Smith, Opt. Lett. 13 (1988) 904.

[152] S.R. Friberg, Y. Silberberg, M.K. Oliver, M.J. Adrejco, M.R. Saifi, P.W. Smith, Appl. Phys. Lett. 51 (1987) 1135.
[153] R. Hoffe, J. Chrostwoski, Opt. Commun. 57 (1986) 34.
[154] K. Kitayama, S. Wang, Appl. Phys. Lett. 43 (1983) 17.
[155] J.P. Heritage, R.N. Thurston, W.J. Tomlinson, A.M. Weiner, R.H. Stolen, Appl. Phys. Lett. 45 (1985) 87.
[156] J.J. Rocca, V.N. Shlyaptsev, F.G. Tomasel, O.D. Cortazar, D. Hartshorn, J.L.A. Chilla, Phys. Rev. Lett. 73 (1994) 2191.
[157] R. Barteels, S. Backus, E. Zeek, L. Misoguti, G. Vdovin, I.P. Christov, M.M. Murnane, H.C. Kateyn, Nature 406 (2000) 164.
[158] P. Miane, D. Strickland, D. Bado, M. Besgot, G. Mourou, IEEE J. Quantum Electron. 24 (1988) 398.
[159] M. Pessot, P. Maine, G. Mourou, Opt. Commun. 62 (1987) 459.
[160] C.P.J. Barty, C.L.I. Gordon, B.E. Lemott, Opt. Lett. 19 (1994) 1442.
[161] T. Kato, Y. Fujimura, Chem. Phys. 202 (1996) 95;
T. Watanabe, H. Umeda, Y. Fujimura, A.D. Bandrauk, J. Mol. Struct. (Theor. Chem.) 461 (1999) 317.
[162] A.S. Sandhu, S. Banerjee, D.r. Goswami, Opt. Commun. 181 (2000) 101.
[163] S. Baneerjee, G. RavindraKumar, D. Mathur, Phys. Rev. A 60 (1999) R3369;
S. Baneerjee, G. RavindraKumar, D. Mathur, Phys. Rev. A 60 (1999) R25.
[164] N.L. Manakov, V.D. Ovsiannikov, A.F. Starace, Phys. Rev. Lett. 82 (1999) 4791.
[165] N.P.M. Huck, W.F. Jager, B. deLange, B.L. Feringa, Science 273 (1996) 1686.
[166] E. Hertz, O. Faucher, B. Lavorel, F. Dalla Via, R. Chaux, Phys. Rev. A 61 (2000) 033816.
[167] S. Wielandy, A.L. Gaeta, Phys. Rev. Lett. 81 (1998) 3359.
[168] T. Brixner, G. Gerber, Opt. Lett. 26 (2001) 557;
T. Brixner, G. Krampert, P. Niklaus, G. Gerber, Appl. Phys. B 74 (2002) S133.
[169] T.C. Weinacht, J. Ahn, P.H. Bucksbaum, Nature 397 (1999) 233;
T.C. Weinacht, J. Ahn, P.H. Bucksbaum, Phys. Rev. Lett. 80 (1998) 5505.
[170] J.L. Krause, K.J. Schafer, M. Ben-Nun, K.R. Wilson, Phys. Rev. Lett. 79 (1997) 4978.
[171] M.W. Noel, C.R. Stroud Jr., Opt. Express 1 (1997) 176.
[172] J. Parker, C.R. Stroud Jr., Phys. Rev. Lett. 56 (1986) 716.
[173] D.W. Schumacher, J.H. Hoogenraad, Dan Pinkos, P.H. Bucksbaum, Phys. Rev. A 52 (1995) 4719.
[174] I. Broner, P.C.M. Planken, M.C. Nuss, Marie S.C. Luo, Shun Lien Chuang, L. Pfeiffer, D.E. Leaird, A.M. Weiner, J. Opt. Soc. Am. B 11 (1994) 2457.
[175] X. Chen, J.A. Yeazell, Phys. Rev. Lett. 81 (1998) 5772.
[176] R. Uberna, M. Khalil, R.M. Williams, J.M. Papanikolas, S.R. Leone, J. Chem. Phys. 108 (1998) 9259.
[177] F. Texier, F. Robicheaux, Phys. Rev. A 61 (2000) 043401.
[178] R. Kosloff, S.A. Rice, P. Gaspard, S. Tersigni, D.J. Tannor, Chem. Phys. 139 (1989) 201.
[179] S. Shi, A. Woody, H. Rabitz, J. Chem. Phys. 88 (1988) 6870.
[180] G.J. Toth, A. Lorincz, H. Rabitz, J. Chem. Phys. 101 (1994) 3715.
[181] A. Assion, T. Baumert, M. Bergt, T. Brixner, B. Kiefer, V. Seyfried, M. Strehle, G. Gerber, Science 282 (1999) 918.
[182] T. Baumert, T. Brixner, V. Seyfried, M. Strehle, G. Gerber, Appl. Phys. B 65 (1997) 799.
[183] S. Kirkpatrick, C.D. Gerlatt Jr., M.P. Vecchi, Science 220 (1983) 671.
[184] R.J. Levis, H.A. Rabitz, J. Phys. Chem. 106 (2002) 6427;
R.J. Levis, G.M. Meenkir, H. Rabitz, Science 292 (2001) 709.
[185] C. Daniel, J. Full, L. Gonzalez, C. Kaposta, M. Krenz, C. Lopulescu, J. Manz, S. Minemoto, M. Oppel, P. Rosendo-Francisco, S. Vajda, L. Woste, Chem. Phys. 267 (2001) 247.
[186] D. Yelin, D. Mashulach, Y. Silberberg, Opt. Lett. 22 (1997) 1793.
[187] T. Brixner, A. Oehrlein, M. Strehle, G. Gerber, Appl. Phys. B 70 (2000) S119.
[188] A. Efimov, M.D. Moores, N.M. Beach, J.L. Krause, D.H. Reitze, Opt. Lett. 23 (1998) 1915.
[189] R. Uberna, Z. Amitay, R.A. Loomis, S.R. Leone, Faraday Discuss. 385 (1999).
[190] T. Hornung, R. Meier, M. Motzkus, Chem. Phys. Lett. 326 (2000) 445.
[191] T. Hornung, R. Meier, D. Zeidler, K.L. Kompa, D. Proch, M. Motzkus, Appl. Phys. B 71 (2000) 277.
[192] T. Brixner, N.H. Damrauer, P. Niklaus, G. Gerber, Nature 414 (2001) 57.
[193] T.C. Weinacht, J.L. White, P.H. Bucksbaum, J. Phys. Chem. A 103 (1999) 10166.

[194] T. Hornung, R. Meier, R. de Vivie-Riedle, M. Motzkus, Chem. Phys. 267 (2001) 261.
[195] J.L. Herek, W. Wohlleben, R.J. Cogdell, D. Zeidler, M. Motzkus, Nature 417 (2002) 533.
[196] W. Yang, F. Huang, M.R. Fetterman, J.C. Davis, D. Goswami, W.S. Warren, IEEE Photonics Tech. Lett. 12 (1999) 1665–1667.
[197] A. Hatche, Y. Kostoulas, R. Atanasov, J.L.P. Hughes, J.E. Sipe, H.M. van Driel, Phys. Rev. Lett. 78 (1997) 306.
[198] P.C.M. Planken, I. Brener, M.C. Nuss, Phys. Rev. B 48 (1993) 4903.
[199] D.S. Critin, Phys. Rev. Lett. 77 (1996) 4596.
[200] A.M. Weiner, J. Opt. Soc. Am. B 11 (1994) 2480.
[201] T. Quang, M. Woldeyohannes, S. John, G.S. Agarwal, Phys. Rev. Lett. 79 (1997) 5238.
[202] A. Sanpera, J.B. Watson, M. Lewenstein, K. Burnett, Phys. Rev. A 54 (1996) 4320.
[203] W. Yang, M.R. Fetterman, D. Goswami, W.S. Warren, J. Opt. Commun. 22 (2001) 15.
[204] H. Kobayashi, P.R. Prucnal, W.S. Warren, Performance and Control of Network Systems, Proc. SPIE 3231 (1997) 75.
[205] W. Yang, M.R. Fetterman, D. Goswami, W.S. Warren, J. Opt. Commun. 21 (2000) 7.
[206] H.-S. Tan, W.S. Warren, E. Schreiber, Opt. Lett. 26 (2001) 1812;
H.-S. Tan, E. Schreiber, W.S. Warren, Opt. Lett. 27 (2002) 439.
[207] O. Golonzka, M. Khalil, N. Demirdoven, A. Tokmakoff, J. Chem. Phys. 115 (2001) 10814.
[208] D. Keusters, H.-S. Tan, W.S. Warren, J. Phys. Chem. A 103 (1999) 10369.
[209] M.T. Zanni, N.-H. Ge, Y.S. Kim, R.M. Hochstrasser, Proc. Natl. Acad. Sci. 98 (2001) 11265.
[210] J. Ahn, T.C. Weinacht, P.H. Bucksbaum, Science 287 (2000) 463.
[211] N. Bhattacharya, H.B. van Linden van den Heuvell, R.J.C. Spreeuw, Phys. Rev. Lett. 88 (2002) 137901-1.
[212] N.A. Gershenfeld, I.L. Chuang, Science 275 (1997) 350.
[213] W.S. Warren, Science 277 (1997) 1688.
[214] H.E. Brandt, Prog. Quantum Electron. 22 (1998) 257;
D.P. DiVincenzo, D. Loss, J. Magn. Magn. Mater. 200 (1999) 202.
[215] M.A. Nielsen, I.L. Chuang, Quantum Computing and Quantum Information, Cambridge University Press, Cambridge, UK, 2000.
[216] D.A. Benaron, W.-F. Cheong, D.K. Stevenson, Science 276 (1997) 2002.
[217] Y. Yasuno, M. Nakama, Y. Sutoh, M. Ith, M. Mori, T. Yatagai, Opt. Commun. 186 (2000) 51.
[218] A.M. Rollins, M.D. Kulkarni, S. Yazdanfar, R. Ung-Aunyawee, J.A. Izatt, Opt. Express 3 (1988) 219.
[219] G.J. Tearney, M.E. Brezinski, B.E. Bouma, S.A. Boppart, C. Pitris, J.F. Southern, J.G. Fujimoto, Science 276 (1997) 2037.
[220] A. Ashkin, J.M. Dziedzic, Science 235 (1987) 1517.
[221] V. Backman, R. Gurjar, K. Badizadegan, I. Itzkan, R.R. Dasari, L.T. Perelman, M.S. Feld, IEEE J. Sel. Top. Quantum Electron. 5 (1999) 1019.
[222] N.H. Bonade, J. Erland, D. Gammon, D. Park, D.S. Katzer, D.G. Steel, Science 282 (1998) 1473.
[223] A. Neogi, H. Yoshida, T. Mozume, O. Wada, Opt. Commun. 159 (1999) 225.